T. AL-MSRHAD

ATILIM UNIVERSITY 2021

INVESTIGATION OF HYDROGEN PRODUCTION FROM SODIUM BOROHYDRIDE HYDROLYSIS WITH SUPPORTED METAL CATALYST

THE GRADUATE SCHOOL OF NATURAL AND APPLIED SCIENCES
OF
ATILIM UNIVERSITY

TUQA MAJEED HAMEED AL-MSRHAD

A MASTER OF SCIENCE
THESIS
IN
THE DEPARTMENT OF CHEMICAL ENGINEERING

FEBRUARY 2021

INVESTIGATION OF HYDROGEN PRODUCTION FROM SODIUM BOROHYDRIDE HYDROLYSIS WITH SUPPORTED METAL CATALYST

A THESIS SUBMITTED TO
THE GRADUATE SCHOOL OF NATURAL AND APPLIED SCIENCES
OF
ATILIM UNIVERSITY

BY

TUQA MAJEED HAMEED AL-MSRHAD

IN PARTIAL FULFILLMENT OF THE REQUIREMENTS
FOR
THE DEGREE OF MASTER OF SCIENCE
IN
THE DEPARTMENT OF CHEMICAL ENGINEERING

FEBRUARY 2021

Approval of the Graduate School of Natural and Applied Sciences, Atilim University

Prof. Dr. Ali Kara
Director

I certify that this thesis satisfies all the requirements as a thesis for the degree of **Master of Science in Chemical Engineering, Atılım University.**

Prof. Dr. Şeniz Özalp Yaman
Head of Department

This is to certify that we have read the thesis INVESTIGATION OF HYDROGEN PRODUCTION FROM SODIUM BORON HYDRIDE ($NABH_4$) HYDROLYSIS WITH SUPPORTED METAL CATALYST" submitted by TUQA MAJEED HAMEED AL-MSRHAD and that in our opinion it is fully adequate, in scope and quality, as a thesis for the degree of Master of Science.

Assoc. Prof. Dr. Yılser Devrim
Supervisor

Examining Committee Members:

Prof. Dr. Can Özgür Çolpan
Mechanical Engineering Dept., Dokuz Eylül University

Assoc. Prof. Dr. Yılser Devrim
Energy Systems Engineering Dept., Atilim University

Asst. Prof. Dr. Enver Güler
Chemical Engineering Dept., Atilim University

Date: *01.02.2021*

I hereby declare that all information in this document has been obtained and presented in accordance with academic rules and ethical conduct. I also declare that, as required by these rules and conduct, I have fully cited and referenced all material and results that are not original to this work.

Name, Last Name: Tuqa Majeed Hameed Al-MSRHAD

Signature:

ABSTRACT

INVESTIGATION OF HYDROGEN PRODUCTION FROM SODIUM BOROHYDRIDE HYDROLYSIS WITH SUPPORTED METAL CATALYST

Al-Msrhad, Tuqa Majeed Hameed
M.S., Department of Chemical Engineering
Supervisor: Assoc. Prof. Dr. Yılser Devrim

FEBRUARY 2021, 71 pages

In recent years, the decrease in fossil fuel resources and the increase in environmental pollution has increased the interest in alternative energy sources. Among alternative energy sources, Hydrogen (H_2) energy is of great importance due to its high energy density. The most important benefit in using H_2 energy is the clean and easy production and storage. When H_2 production methods are examined, sodium borohydride ($NaBH_4$) based H_2 production is of great significance, and the particular reason for this circumstance is that it is renewable, reliable, and efficient and can easily be integrated into proton exchange membrane fuel cells (PEMFC).

In this thesis, Palladium-Ruthenium (Pd:Ru) bimetallic catalyst supported on Multi-walled Carbon Nanotubes (MWCNT) and Multiwall Carbon Nanotube Doped Graphene Nanoplatelets (MWCNT-GNP) has been developed for H_2 production from hydrolysis of $NaBH_4$ for PEMFC application. These catalysts were synthesized by the microwave assisted synthesis approach. The prepared catalysts were characterized by Thermogravimetric Analysis (TGA), X-ray diffraction (XRD), Transmission Electron Microscopy (TEM) and cyclic voltammetry analysis (CV). The electrochemical surface area (ECSA) of the PdRu/MWCNT and PdRu/MWCNT-GNP catalysts were determined as 12.36 m^2/g and 20.74 m^2/g, respectively. PdRu/MWCNT showed a faintly lower ECSA loss as 34%.

The catalysts were tested to investigate the H_2 production from the chemical hydrolysis of $NaBH_4$. Hydrolysis reactions were examined under various experimental conditions. Kinetic studies were executed for PdRu/MWCNT and PdRu/MWCNT-GNP, and the activation energies were found as 18.90 kJ/mol and 22.33 kJ/mol, respectively. The reusability experiments with PdRu/MWCNT-GNP revealed that GDL supported catalysts maintained its 89 % efficiency better than the powder catalyst.

The PEMFC test performed at 65^oC showed that the H_2 generation system based on solid $NaBH_4$ hydrolysis and pure H_2 have similar performance. The obtained results showed that the PdRu/MWCNT-GNP bimetallic catalyst is an appropriate catalyst to produce H_2 from hydrolysis of $NaBH_4$ for PEMFC application.

Keywords: Bimetallic catalyst, Microwave Synthesis, Hydrogen generation, Sodium borohydride, Hydrolysis, Catalyst, Fuel Cell, Proton Exchange Membrane Fuel Cell, PdRu/MWCNT, PdRu/MWCNT-GNP.

ÖZ...

DESTEKLENİŞ METAL KATALİZÖR İLE SODYUM BOROHİDRİT ($NABH_4$) HİDROLİZİNDEN HİDROJEN ÜRETİMİNİN İNCELENMESİ

Tuqa Majeed Hameed Al-Msrhad
Yüksek Lisans, Kimya Mühendisliği ve Uygulamalı Kimya
Tez Yöneticisi: Doç. Dr. Yılser Devrim

Şubat 2021, 71 sayfa

Son yıllarda fosil yakıt kaynaklarının azalması ve çevre kirliliğinin artması alternatif enerji kaynaklarına olan ilgiyi artırmıştır. Alternatif enerji kaynakları arasında Hidrojen (H_2) enerjisi, yüksek enerji yoğunluğu nedeniyle büyük önem taşımaktadır. H_2 enerji kullanımındaki en önemli sorun temiz ve kolay üretim ve depolamadır. H_2 üretim yöntemleri incelendiğinde, Sodyum bor hidrür ($NaBH_4$) temelli H_2 üretimi, güvenilir, verimli ve proton değişimli membran yakıt pillerine (PEMFC) kolayca entegre edilebilmesi nedeniyle büyük önem taşımaktadır.

Bu tez çalışmasında, PEMFC uygulaması için $NaBH_4$'ten H_2 üretimi için çok duvarlı karbon nanotüp (MWCNT) ve çok duvarlı karbon nanotüp-grafen nano tabaka (MWCNT-GNP) destekli Palladyum-Rutenyum (Pd: Ru) bimetalik katalizörler geliştirilmiştir. Bu katalizörler mikrodalga sentez yöntemi ile hazırlanmıştır. Hazırlanan katalizörler Termogravimetrik Analizi (TGA), X-ışını kırınımı (XRD), transmisyon elektron mikroskobu (TEM) ve döngüsel voltametri (CV) analizleri ile karakterize edilmişlerdir. PdRu/MWCNT ve PdRu/MWCNT-GNP katalizörlerinin elektrokimyasal yüzey alanı (ECSA) sırasıyla 12.36 m^2/g ve 20.74 m^2/g olarak belirlenmiştir. Analizler sonucunda PdRu/MWCNT katalizörünün % 34 olarak düşük bir ECSA kaybı gösterdiği saptanmıştır.

Sentezlenen katalizörler, $NaBH_4$'ün kimyasal hidrolizinden H_2 üretimini araştırmak için farklı koşullarda test edilmiştir. PdRu/MWCNT ve PdRu/MWCNT-GNP katalizörleri için yapılan kinetik çalışmalar sonucunda aktivasyon enerjileri sırasıyla 18.90 kJ/mol ve 22.33 kJ/mol olarak bulunmuştur. PdRu/MWCNT-GNP katalizörü ile yapılan yeniden kullanılabilirlik deneyleri, GDL destekli katalizörlerin verimliliğini toz katalizörden daha iyi koruduğunu göstermiştir.

65 ^oC'de gerçekleştirilen PEMFC testleri sonucunda katı $NaBH_4$ temelli H_2 üretim sisteminin ve saf H_2'nin benzer performansa sahip olduğunu belirlenmiştir. Elde edilen sonuçlar, PdRu/MWCNT-GNP bimetalik katalizörün, PEMFC uygulaması için $NaBH_4$'ten H_2 üretmek için uygun bir katalizör olduğunu göstermektedir.

Anahtar Kelimeler: Bimetallik katalizör, Mikrodalga Sentezi, Hidrojen Üretimi, Sodyum Bor Hidrür, Hidroliz, Katalizör, Yakıt Pili, Proton Değişim Membran Yakıt Pili, PdRu/MWCNT, PdRu/MWCNT-GNP.

To my beloved parents, my father Majeed and my mother Ibtisam, who persistently supported me and never gave up on me.

To my sisters and brother, Shahad, Ruqaya and Ahmed.

To my treasured deceased grandfather Mousa, my grandmother Suad and my aunt Qabila.

To my friends Basim Ahmed and Shaymaa Abdulhafedh.

I will forever be grateful.

ACKNOWLEDGMENTS

Foremost, I would like to express my sincere gratitude to my supervisor, Assoc. Prof. Dr. Yılser DEVRİM for the continuous support of my master study and research, for her guidance, criticism, motivation, enthusiasm, patience, and immense knowledge that helped throughout the research period. I could not have asked for a better supervisor as she gave me the chance to learn so much about the hydrogen industry and fuel cells.

Moreover, a huge thanks to my parents, sisters, and brother for their prayers, patience, and support throughout my master's studies and my whole life in general.

TABLE OF CONTENTS

LIST OF FIGURES

FIGURES

LIST OF TABLES

TABLES

LIST OF ABBREVIATIONS

AFC	Alkaline Fuel Cell
Ag	Silver
AgCl	Silver Chloride
BL	Backing Layer
BPP	Bipolar Plates
CB	Carbon Black
CC	Carbon Cloth
CCM	Catalyst Coated Membrane
CE	Counter Electrode
CFP	Carbon Fiber Paper
CHP	Combine Heat and Power
CL	Catalyst Layer
CNT	Carbon Nanotube
CO	Carbon Monoxide
CO_2	Carbon Dioxide
CO_{3}^{-2}	Carbonate
CTAB	Cationic Cetyltrimethylammonium Bromide
CV	Cyclic Voltammetry
DI	Deionized Water
DL	Diffusion Layer
DMAc	N-N dimethylacetamide
DMFC	Direct Methanol Fuel Cell
E	Potential (Volt)
ECSA	Electrochemical Surface Areas
EG	Ethylene Glycol
EPDM	Ethylene-Propylene-Diene-Monomer
F	Faraday Constant (A.s/mole)
FC	Fuel Cell
FCC	Face-Centered Cubic
FWHM	Full Width Half Maximum
GC	Glassy Carbon
GDE	Gas Diffusion Electrode
GDL	Gas Diffusion Layer
G-MWCNT	Graphene-Multiwall Carbon Nano-tube
GNP	Graphene Nanoplatelet
H_2	Hydrogen
H_2O	Water
$H_2PtCl_6.6H_2O$	Hexachloroplatinic Acid Hexahdrate
H_2SO_4	Sulfuric Acid
H_3PO_4	Phosphoric Acid
HCL	Hydrochloric Acid
HER	Hydrogen Evolution Reaction

hf	Heat Formation of Reactants and Products
HOR	Hydrogen Oxidation Reaction
HT-PEMFC	High Temperature PEMFC
$HClO_4$	Perchloric Acid
HNO_3	Nitric Acid
ICP-MS	Inductively Coupled Plasma-Mass Spectroscopy
IPA	Isopropyl Alcohol
IRR	Butyl Rubber
K	Potassium
KOH	Potassium Hydroxide
Li	Lithium
$LiAlO_2$	Lithium Aluminum Oxide
LT-PEMFC	Low Temperature PEMFC
$m_{(PdRu)}$	The Weight of PdRu Catalyst
MCFC	Molten Carbonate Cell Fuel
MEA	Membrane Electrode Assembly
MFC	Mass Flow Controller
MPL	Microporous layer
MWCNT	Multiwall Carbon Nanotube
MWCNT-GNP	Graphene Doped Multiwall Carbon Nanotube
n	Number of Electrons Transferred
NaCl	Sodium Chloride
NaOH	Sodium Hydroxide
$NaBH_4$	Sodium borohydride
Ni	Nickel
NPG	Nitrogen-rich Graphene Nanopores
N_2 rich G	Nitrogen Rich Graphene
N_2_MWCNT	Nitrogen Doped MWCNT
N_{Avg}	The Avogadro Number (6.02 x 1023)
O_2	Oxygen
OCV	Open Circuit Voltage
OH^-	Hydroxide
ORR	Oxygen Reduction Reaction
PA doped PBI	Phosphoric Acid Doped Polybenzi-dazole
PAFC	Phosphoric Acid Fuel Cell
PBI	Polybenzimidazole
$Pd(acac)_2$	Palladium (II) bis(acetylacetonate)
$PdCl_2$	Palladium (II) Chloride
PDMS	Polydimethylsiloxane
PdPc	Palladium Phthalocyanine
PEMFC	Proton Exchange Membrane Fuel Cell
PFSA	Perfluorosulfonic acid
PI	Pressure Indicator

PIC	Pressure Indicator and Controller
ppm	Parts Per Million
PR	Pressure Regulator for Hydrogen
Pd	Palladium
PTFE	Polytetrafluoroethylene
PVDF	Polyvinylidene Difluoride
q	The Charge (Coulombs mol^{-1})
Ru	Ruthenium
RDE	Rotating Disk Electrode
RE	Reference Electrode
RH	Relative Humidity
rpm	Revolutions Per Minute
Rs	Raman Spectroscopy
$RuCl_3.XH_2O$	Ruthenium (III) Chloride
SAED	Selected Area Electronic Diffraction
$scCO_2$	Supercritical Carbon Dioxide Method
SDS	Anionic Sodium Dodecyl Sulfate
SEM	Scanning Electron Microscopy
sf	The Entropy of Products and Reactants
SOFC	Solid Oxide Fuel Cell
SPE	Solid Polymer Electrolyte
SSA	Specific Surface Area (m_2/g)
STEM	Scanning Transmission Electron Microscopy
SV	Selenoid Valve
SV2	Purge Selenoid Valve
SWCNT	Single wall Carbon Nanotube
T	Temperature (K)
TEM	Transmission Electron Microscopy
Tg	Glass Transition Temperature
TGA	Thermogravimetric Analysis
TIC	Temperature Indicator and Controller
TPB	Three-Phase Boundary
U_{PdRu}	Utilization Efficiency (%)
W	The Electrical Work ($J\ mol_{-1}$)
WE	Working Electrode
XPS	X-ray Photoelectron Spectroscopy
XRD	X-ray Diffraction
ZrO_2	Zirconium Oxide
H^+	Hydrogen Ion
q_{el}	The Charge of an Electron (Columbus/electron)
$E^0{}_\alpha$	Potential of Anode
$E^0{}_c$	Potential of Cathode
Q_H	The Charge of Hydrogen Adsorption/Desorption

ΔG	Gibbs Free Energy
ΔH	Enthalpy of the Chemical Reaction
ΔS	The Entropy Change of the Reaction
2D	Two-Dimensional
η	Efficiency
$\boldsymbol{\theta}$	The Angle at The Maximum of the Peak
ρ	The density of Pt metal
$\boldsymbol{\lambda}$	Wavelength of X-ray diffraction

CHAPTER 1

INTRODUCTION

1.1 Hydrogen Energy Storage

On account of the accelerated depletion of fossil fuel resources, developing an ecological, sustainable and renewable energy alternative holds extreme importance to satisfy the global energy demand [1]. Thus, hydrogen (H_2) as an energy carrier is deemed an attractive choice as it offers remarkable efficiencies and near-zero-emission for transportation and stationary power applications [2]. However, H_2 is not feasible as a direct energy source. It holds an energy density of 142 MJ/kg (three times higher than the energy density of petroleum, 47 MJ/kg) [3]. Additionally, fuel cells joined with H_2 would offer exceptional efficiencies (50-60%) in contrast to combustion engines (<25%). All those characteristics signify H_2 as a model candidate to replace petroleum in automotive applications [4].

1.2 Hydrogen Storage Technologies

1.2.1 Compressed Hydrogen Gas Tank

This technology is straightforward as it does not require numerous devices. However, it is not entirely secure because of the high pressure used in the tanks (350-700 bar) to store the compressed H_2 gas [5].

1.2.2 Liquid Hydrogen

Cooling down the H_2 gas to 20 K (-253.1°C) at atmospheric pressure changes the H_2 gas into the liquid state. Liquid H_2 holds excellent potential for storing H_2 energy as it enjoys a higher energy density than compressed H_2 gas. Liquid H_2 tanks typically consist of a double wall structure to guarantee thermal isolation at a shallow temperature [6]. The volumetric capacity of compressed H_2 in a 10,000 psi (700 bar) tank is merely 0.03 kg/liter. In contrast, that of liquid H_2 is 0.07 kg/liter. Likewise, liquefying involves isolation. It is consequently causing a decrease in capacities [5].

1.2.3 Metal Hydrides

H_2 atoms are absorbed in the solid-state in this storing technology, providing larger volume densities than liquid systems. Metal hydrides represent a more reliable alternative than the compressed H_2 gas and contain an excellent volumetric density of 0.06 kg/liter [5].

1.2.4 Chemical Hydrides

Chemical hydrides inevitably generate H_2 once they interact with other substances like water, catalysts, etc. Various chemical hydrides are extensively investigated, such as sodium borohydride ($NaBH_4$), sodium hydride (NaH), ammonia borane (NH_3BH_3) and magnesium hydride (MgH_2) [7]. The hydrolysis reaction is dependent on the temperature, pH, catalyst mass and the hydride amount used in the reaction solution. Chemical hydrides store high amounts of H_2 and the hydrolysis reaction rate is equally high, addressing them an excellent H_2 source [5]. The H_2 storage technology and cost status compared to DOE targets are presented in Figure 1.1.

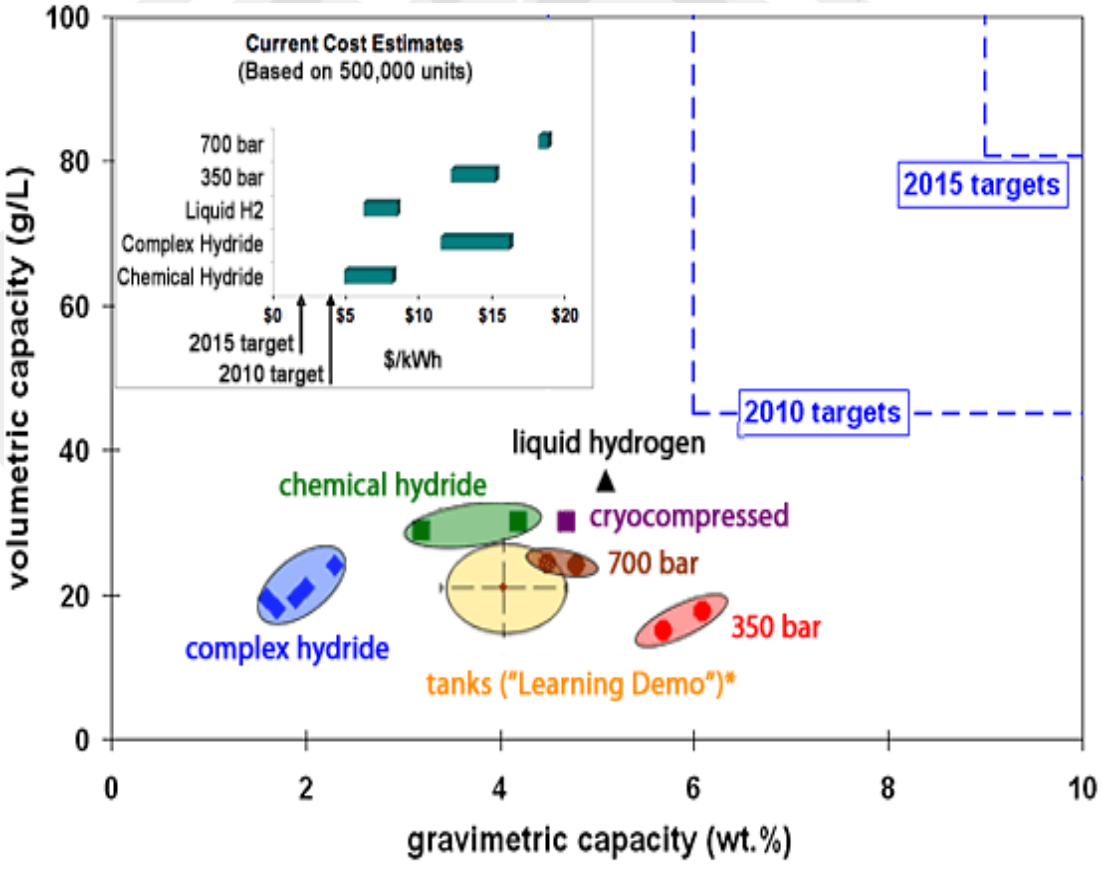

Figure 1.1 H_2 storage technology and cost status compared to DOE targets [8].

1.3 Sodium Borohydride

Also known as Sodium tetrahydridoborate and sodium tetrahydroborate. That is a white crystalline compound, as displayed in Figure 1.2. It is a profoundly stable compound and a potent reducing agent. Prof. H. C. Brown (1912-2004), Nobel Prize winner in Chemistry in 1972, is the first to prepare Sodium borohydride ($NaBH_4$) in 1942. Prof. H. I. Schlesinger investigated it, driven by the military interest for its potential as an H_2 storage material. For the next two decades, the matter of $NaBH_4$ remains the center of attention for several types of research. However, the research about $NaBH_4$ as a H_2 energy carrier laid low until the late 1990s [9]. $NaBH_4$ reacts with water (H_2O) to produce H_2 and heat in a process known as hydrolysis as shown in Equation (1).

$$NaBH_4 + 2H_2O \rightarrow NaBO_2 + 4H_2(g) + energy\ (heat) \quad (1)$$

The hydrolysis reaction of $NaBH_4$ is exothermic (-217 kJ mol^{-1}), spontaneous, and the proper use of an excellent metal-based catalyst considerably boosts up the reaction rate [3]. $NaBH_4$ consists of sodium and four hydrogen atoms attached to the boron atom, as shown in Figure 1.2. This chemical compound is safe, recyclable and grants good features to serve as an abundant H_2 source. Nevertheless, a considerable disadvantage here is that $NaBH_4$ is relatively expensive [4], $NaBH_4$ provides a fairly high theoretical H_2 storage capacity (10.8 wt. %) through hydrolysis reaction [5]. H_2 production from $NaBH_4$ solutions using a proper catalyst offers good characteristics, such as non-toxicity, non-flammability and stability. The H_2 generation rate of hydrolysis increases with the usage of a catalyst, H_2 generation can easily be controlled, H_2 storage efficiencies are rather high, and the products of the reaction are recyclable, in addition to the potential to generate H_2 even under low temperatures like 0°C [6].

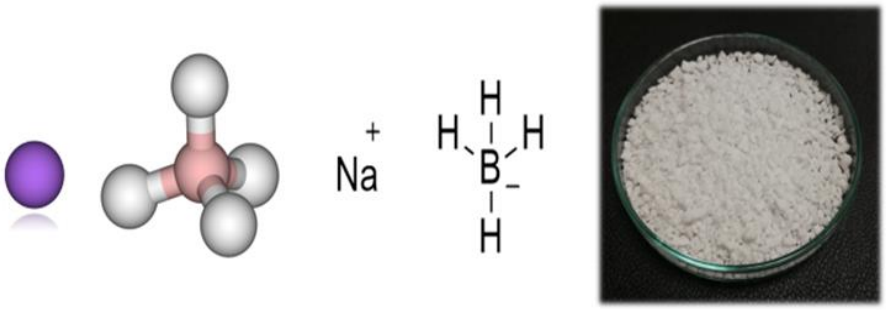

Figure 1.2 Sodium borohydride in molecular, chemical and physical form.

H_2 gravimetric capacity as a function of H_2 generators for several H_2 storage materials investigated by the Fuel Cell Technologies Office (FCTO) displayed in Figure 1.3.

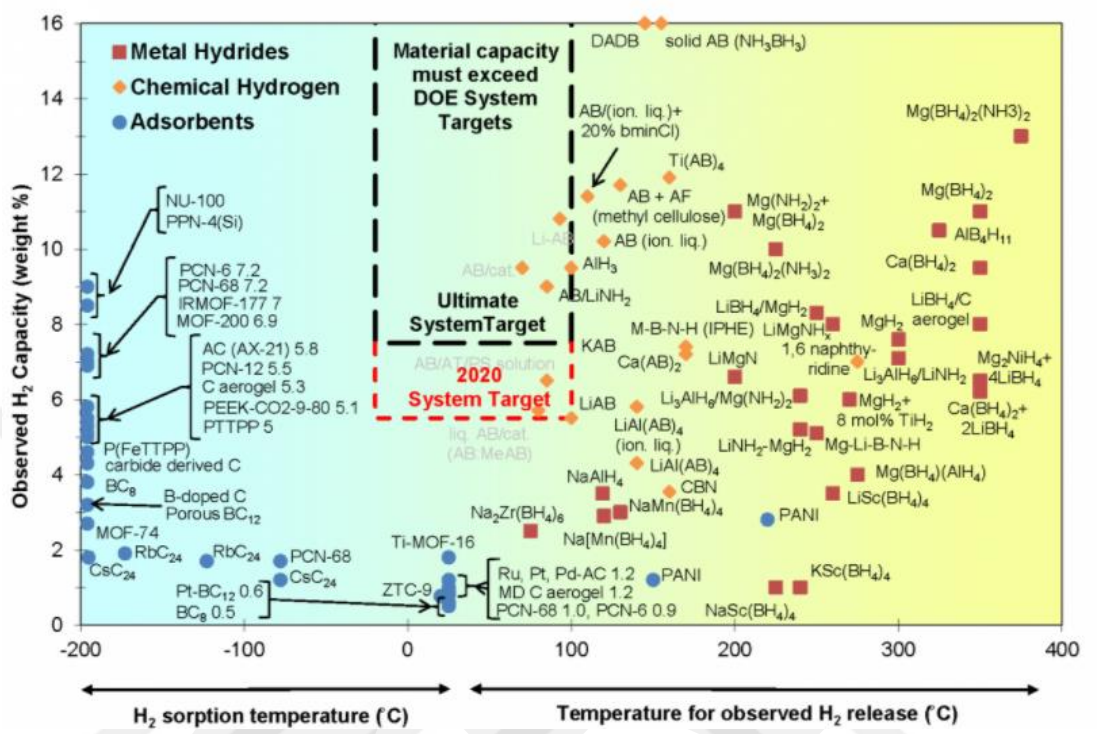

Figure 1.3 H_2 Storage Systems Compared to the 2020 DOE Targets [10].

1.4 Fuel Cell (FC)

A fuel cell is a device that converts chemical energy into electrical energy (electricity) via electrochemical reactions. A fuel cell consists of two electrodes, one named anode and the other named cathode and an electrolyte separating them. Oxidation takes place at the anode from where electrons travel through an external circuit, producing electricity. Electrons reach the cathode, causing a reduction reaction [11]. A sustained energy stream with a negligible number of contaminants in fuel cells reactions varies depending on the employed system. In fuel cells, the anode and cathode regularly need recharging (fuel to the anode and air to the cathode) to continue processing, unlike batteries storing energy and discharged after consumption. Fuel cells possess higher energy density, while batteries hold higher power density [12].

Fuel cells resemble combustion engines in being based on a chemical transformation throughout the oxidation of the fuel as in Equation (2)

$$H_2 + ½O_2 \leftrightarrow H_2O + energy\ (heat). \quad (2)$$

In the above general reaction, H_2 molecules are oxidized, generating water and heat in a controlled system; molecular transfer occurs by building molecular bonds and breaking others. This reaction is exothermic [13]. Figure 1.4 shows a diagram of a fuel cell and the electrochemical operation in the fuel cell.

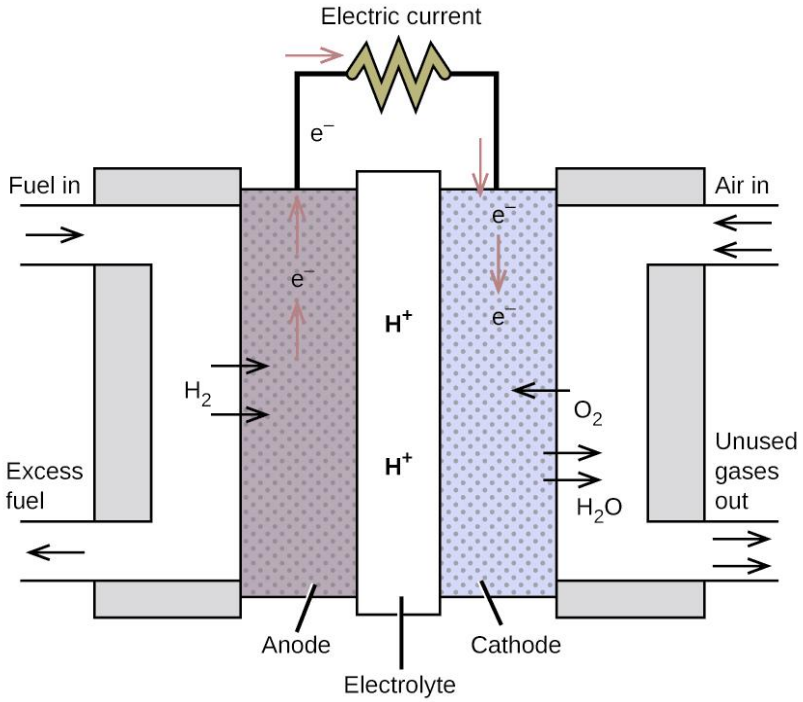

Figure 1.4 A diagram of a simple H_2 fuel cell (FC).

1.5 Characteristics of Fuel Cells

High Efficiency: Fuel cells are more efficient than combustion engines; even a small fuel cell system can perform as strongly as a massive system of combustion engines. In that manner, it is a primary focus in constructing small-scale fuel cell transportation systems [14].

Simplicity: The primary units of a fuel cell hold fixed system pieces. Retaining no mobile parts provides excellent reliability, durability and a silent operating system reducing noise pollution [15].

Scalability. Dissimilar to regular batteries, fuel cells are entirely scalable according to power and capacity. Large batteries malfunction when built in large sizes; they also last for brief periods and require discarding after being consumed. Nevertheless, fuel cells scale adequately from small energy consumption scales as in small transportable applications up to an enormous scale of energy consumption as in power plants [15].

Emissions. The fuel consumed in a fuel cell is H_2 and the products acquired from the electrochemical reaction are water, heat and electricity. Near-zero emissions are among the essential advantages since they reduce emission of contaminants in immobile and mobile applications [16].

1.6 History of Fuel Cells

Research developments that lead to a functional fuel cell design are credited to the chemist Sir William Grove. He substantiated In 1839 that the gases evolved by electrolysis at an electrode submerged in diluted sulphuric acid and made of platinum (electrolyte) can be utilized at the same electrodes to generate electrical current [17]. Fuel cells were firstly named gas batteries, and the name was later changed to fuel cells. Fuel cell development entered an extended period of sluggishness. In 1954, Cambridge University student Francis T. Bacon developed a functioning fuel cell. Bacon replaced the acid electrolyte with an alkaline electrolyte developing his system into the Bacon Cell or what is known today as the Alkaline Fuel Cell (AFC) [18]. In the late 1950s, the first proton exchange membrane fuel cell (PEMFC) was developed. NASA utilized PEMFC in the Gemini space project [19]; This was followed by the Apollo lunar mission, that was also carried out by NASA. The alkaline AFCs were chosen to generate electricity for life support, guidance and communications throughout the mission [20]. The efforts and research for the development were lethargic until the late 1980s when governments, numerous independent commercial companies, laboratories, and even universities started offering support to this field.

Nonetheless, the 1990s witnessed an outburst of activities with many companies growing in this fuel cell field [20]. In 1993, Energy Partners, a company that followed Perry Energy Systems, made the first passenger car entirely dependent on PEMFCs [21]. The organizations concerned with the fuel cell industry, such as Ballard and Plug

Power, enormously thrived in the 2000s for the great potential of having a new energy era. The number of fuel cell-related patents increased intensely; for example, there were around 5,000 FC-related patent applications in 2008 and around 6,000 in 2009 [22]. Figure 1.5 illustrates the milestones of the history of fuel cells.

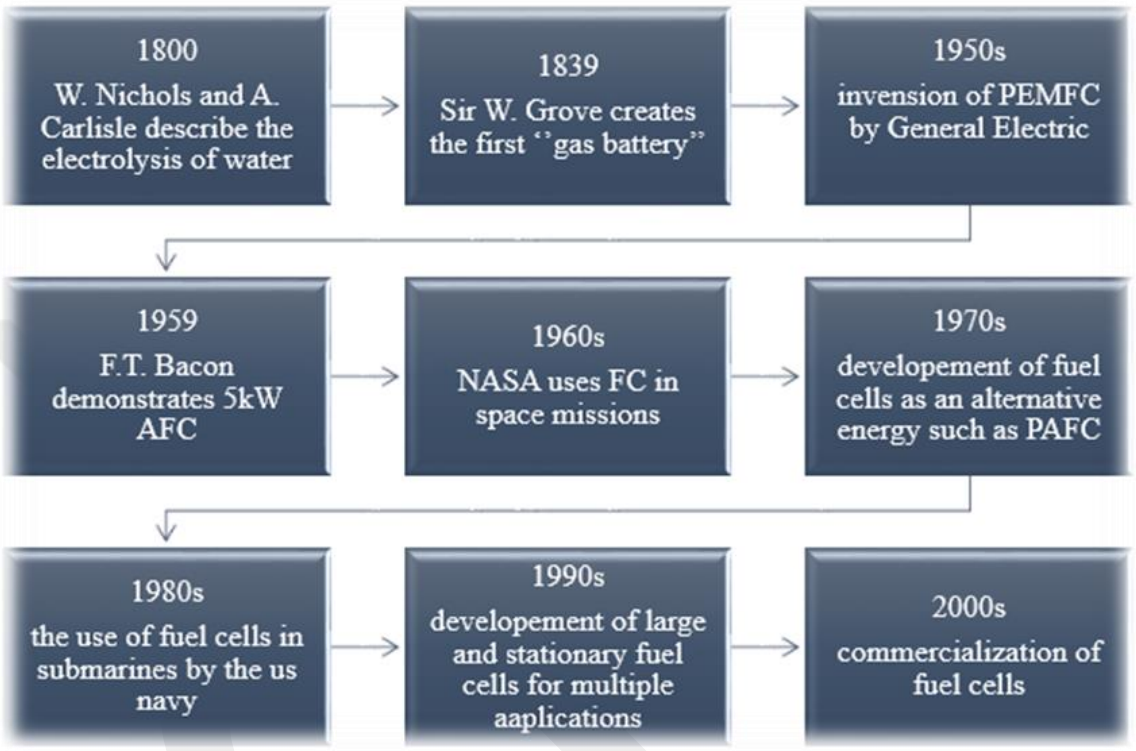

Figure 1.5 Main stages in the history of fuel cells [16], [23].

1.7 Types of Fuel Cells

Fuel cells are categorized according to type of electrolyte used in each type as shown in Table 1.1.

1.7.1 Alkaline Fuel Cell (AFC)

In AFCs, utilizing an alkaline electrolyte of potassium hydroxide (KOH) in an aqueous solution generates an electric current. The hydroxyl ions (OH^-) travel through the electrolyte to produce electrical energy [24]. One of the drawbacks of using AFCs is the potential to contain contamination due to the existence of CO_2. In the Cathode, CO_2 poisons the electrolyte, as time passes it can cause electrodes in some designs to become blocked with solid crystallized carbonate [25].

1.7.2 Phosphoric Acid Fuel Cell (PAFC)

PAFC employs Phosphoric acid (H_3PO_4) as the electrolyte. PAFC is stable and functions in relatively high temperatures up to 150-200ºC. It involves the electrode consisting of porous carbon paper and platinum, or platinum alloy, generally used as the catalyst. PAFC efficiency is typically 35-45%, and this efficiency advances with increasing pressure. PAFC holds unique qualities like high resistance to impurities, stability in a corrosive atmosphere and good conductivity [26].

1.7.3 Molten Carbonate Fuel Cell (MCFC)

The electrolyte in MCFC consists of a mixture of carbonate salts such as lithium carbonate (Li_2CO_3) and potassium carbonate (K_2CO_3). It will liquefy at an operating temperature of about 650ºC. Moreover, it attains the ability to conduct ions of Carbonate (CO_3^{-2}). The molten carbonate mixture is kept inside a porous solid matrix of lithium aluminum oxide ($LiAlO_2$). Furthermore, in the reaction of MCFC, H_2 is pumped to the anode it reacts with carbonate ions in the electrolyte to generate energy as an overall result, MCFC is one of the most complexes of all fuel cell types and the efficiency ranging between 47-60% in addition to its limited lifespan [27], [28].

1.7.4 Solid Oxide Fuel Cell (SOFC)

SOFC is extremely solid as it consists of a unique electrolyte made of solid zirconium oxide (ZrO_2), which is also called Zirconia. The water production in SOFC comes from H_2 and oxygen (O_2) as fuel, the anode in SOFC uses Nickel metal and to direct H_2 while cathode consists of a conductive oxide which does not react with O_2, the operating temperature of SOFC is ultra-high up to 1000ºC. SOFC does not need an electric catalyst because of its high operating temperature. The durability of the electrolyte in SOFC is great owing to the solidness it enjoys. SOFC is useful in many applications, such as generating electricity producing high power and has efficiency of about 60%. [27], [29].

1.7.5 Proton Exchange Membrane Fuel Cell (PEMFC)

The polymer membrane is used as an electrolyte in PEMFC. This electrolyte membrane consists of a compound known as poly perfluorocarbon sulphonate; it resembles

Teflon, but it has an acidic sulphonate bonded to the polymer support to obtain a conductive electrolyte. Typically, the electrolyte is not conductive, it becomes conductive when soaked with water as the acid groups that are bonded to the membrane producing the protons and generating conductivity. In PEMFC, porous carbon-containing platinum is employed to produce sufficient power, and cells are produced and joined in parallel groups and as a sequence. PEMFC operations include both H_2 and O_2.

The air provides O_2, while natural gas provides H_2. To avoid catalyst poisoning with CO and Sulphur compounds. Purification of H_2 gas is essential. Efficiency in PEMFC is about 60% when fed with pure H_2; this efficiency is considered an advantage in the automotive industry. Higher temperature can contribute to improve efficiency and reduce high sensitivity to catalyst poisoning [27]. PEMFC is more appealing than other fuel cell types. Depending on the operating temperature, there are two types. The one that functions in the range of 60-80°C is Low-Temperature PEMFC (LT-PEMFC), whereas the type that functions in temperatures higher than 100ºC is called High-Temperature PEMFC (HT-PEMFC) [30].

Table 1.1 Types of Fuel cells [20], [31].

Fuel cell	**Mobile Ion**	**Temp. (°C)**	**Power (kW)**	**Applications**
AFC	OH^-	70-120	20-100	Space stations and vehicles
PAFC	H^+	150-200	50-20000	On site steady energy systems
MCFC	CO_3^{2-}	650-800	300-3000	Cogeneration, power plants
SOFC	O^-	1000-1100	300-5000	Cogeneration, power plants
PEMFC	H^+	60-120	20-250	Transportation industry

CHAPTER 2

PEMFC

2.1 Operation of PEMFC

Proton Exchange Membrane Fuel Cell (PEMFC), also known as polymer membrane fuel cells is one of the most reliable types of fuel cells in the industrial field. The electrolyte material in PEMFC is polymeric membrane and it does not conduct electrons while transfers protons [32].

An electrochemical reaction of the PEM fuel cell that takes place on the external layer of the catalyst, as shown in Equations (3), (4) and (5).

$$Anode\ reaction: H_2 \rightarrow 2H^+ + 2e - \quad (3)$$

$$Cathode\ reaction\ \frac{1}{2}\ O_2 + 2H^+ + -2e^- \rightarrow H_2O \quad (4)$$

$$The\ overall\ reaction: H_2 + \frac{1}{2}\ O_2 \rightarrow H_2O + heat \quad (5)$$

The overall reaction enthalpy is the change between the products formation heat and the reactants heat, as Equation (6) illustrates:

$$\Delta H = (hf)H_2O - [(hf)H_2 - \frac{1}{2}(hf)O_2] \qquad \text{-286 kJ.mol}^{-1} \quad (6)$$

At room temperature, the heat of water formation equal to -286 kJ.mol^{-1} at the same time, the heat of H_2 and O_2 is equal to zero, which gives the overall enthalpy equal to -286 kJ.mol^{-1}. Entropy accompanies every reaction, and every charge must top the obstacle of activation energy to produce energy through the PEMFC. The released energy is equivalent to the Gibbs free energy change between the products and the reactants [33], [22].

The potential of a fuel cell is equal to 1.23 V it can be determined by using Equation (7):

$$\Delta G = \Delta H - T\Delta S \tag{7}$$

ΔG is the Gibbs free energy change, ΔH is the enthalpy change, T represent the temperature in kelvin (K) units and ΔS is the change in entropy. There are some irreversible losses in the energy conversion because of the entropy as in Equation (8):

$$\Delta S = (sf)_{H_2O} - [(sf)_{H_2} + 1/2(sf)_{O_2}] \tag{8}$$

Where (sf) is the entropy of the formation of a specific component. The electrical work is acquired from the transportation of electrons through a potential difference as for the electricity work in Equation (9):

$$W = qE \tag{9}$$

Where W represents the electrical work (J/mol), q is the total charge in (C/mol), and E is the cell voltage in volts units (V). In the reaction of the fuel cell unit, a total charge transferred in one mole of H_2 used up can be expressed as follows:

$$q = nN_{ave}q_{el} - nF \tag{10}$$

Where n is the number of electrons transported, N_{avg} is Avogadro's number (6.02 x 10^{23}), q_{el} is the total charge of a single electron (1.602 x 10^{-19} C/electron) and F is Faraday's constant (96,485 C/mol.electron). Work can be calculated according to Equation (11):

$$W = nFE \tag{11}$$

The Gibbs free energy can specify the total work as follows:

$$W = -\Delta G \tag{12}$$

So, the total cell voltage of the fuel cell system can be represented as:

$$E = -\Delta G/nF \tag{13}$$

The efficiency of any energy conversion system is equivalent to the ratio between the energy output (electricity) and the energy input (H_2 enthalpy) [22]:

$$Effeciency = \Delta G/\Delta H \tag{14}$$

The theoretical efficiency of PEMFC is 83%, which is relatively sufficient in addition to the high-energy production, almost zero emissions and quick start up time, making it more preferable than other fuel cells in the energy industry [34].

2.2 Main Components of PEMFC

Traditionally, a PEMFC involves a proton exchange membrane, catalyst layers (CL), gas diffusion layers (GDL), bipolar plate (BPP), gasket, current collectors and end plates. As presented in Figure 2.1 [35].

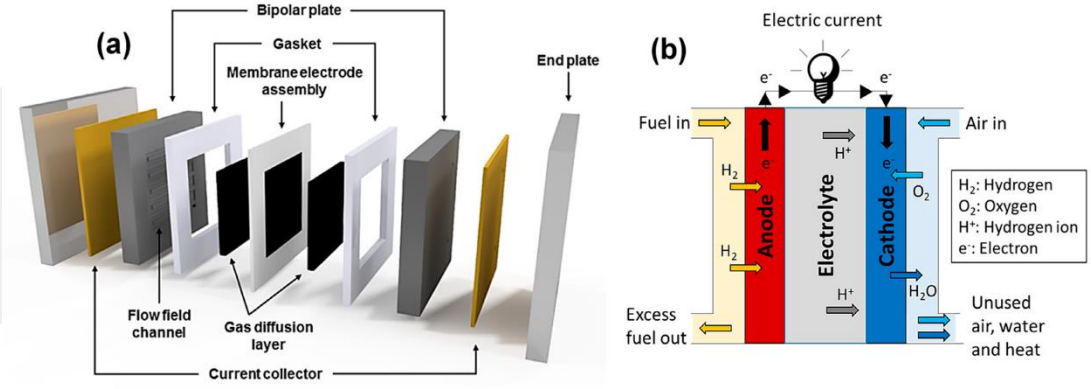

Figure 2.1 (a) Main components of a PEMFC (b) schematic of a typical membrane electrode assembly (MEA) [35].

2.2.1 Membrane

The membrane is the core of a PEMFC. Protons transport from the CL of the anode to the CL of the cathode through the membrane. The membrane works as an isolation layer between the H_2 and O_2. Hence, it electronically needs the insulating of the two

catalyst layers [36]. The membrane requires excellent conductivity to assist transference of protons in addition to the thermal and chemical stability in the fuel cell system [37]. Various membrane types were examined in PEMFC. Nafion® membrane is favorable in LT-PEMFC; it is a form of perfluorocarbon sulfonic acid membrane. DuPont prepared the Nafion family membranes [36]. Moreover, Membranes bond to the electrodes. Nafion membranes are made in different thicknesses, and the size can be controlled by cutting as they are obtainable in 254 μm (Nafion NE-1110), 183 μm (Nafion 117), 127 μm (Nafion 115), 50.8 μm (Nafion NRE-212) and 25.4 μm (Nafion NRE-211) [33]. The chemical structure of the Nafion membrane is apparent in Figure 2.2.

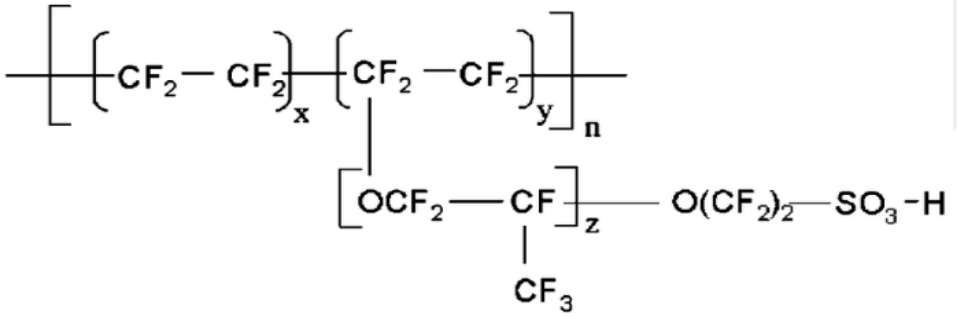

Figure 2.2 Chemical structure of Nafion membrane (PFSA) [38].

The Nafion membrane suffers multiple limitations, like maintaining low humidity at high temperatures leading to the dryness of the membrane and low ionic conductivity. Various researches focused on finding alternative membranes [39], such as poly(2,2-(m-phenylene)-5,5-bibenzimidazole (PBI) membrane doped in strong acids possessing the ability to endure higher temperatures [40], m-PBI is an aromatic polymer that has a heterocyclic structure as illustrated in Figure 2.3.

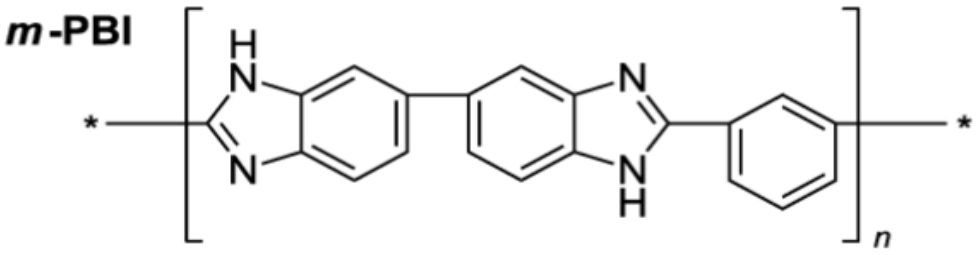

Figure 2.3 Chemical structure of m-PBI [41].

PBI doped in H_3PO_4 exhibits significant resistance to impurities. Additionally, it uses the waste heat released in the fuel cell system, decreasing the crossover and the absorptivity of the gas because of the dense feature it possesses [42], [43]. The chemical structure of the PBI/PA membrane is evident in Figure 2.4.

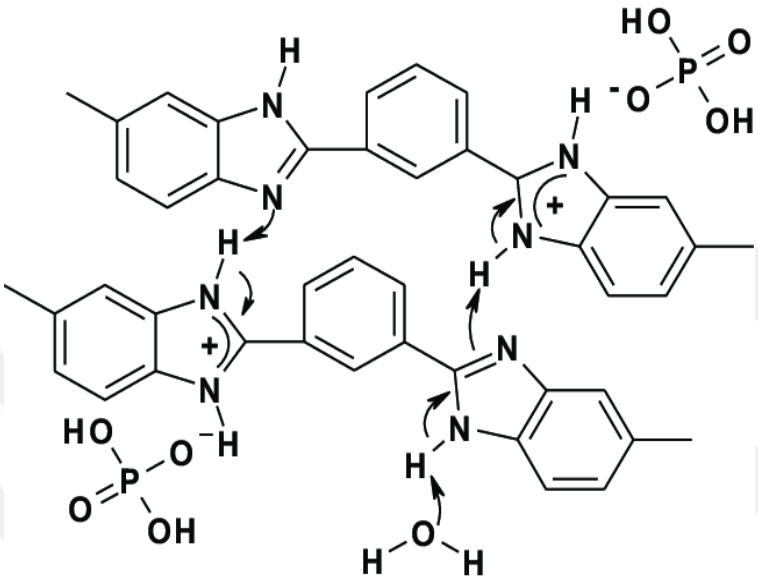

Figure 2.4 Chemical structure of PBI/PA [44].

2.2.2 Catalyst Layers (CLs)

The electrodes are the thin catalyst layers situated where the electrochemical reaction takes place. There are two catalyst layers attached to each side of the membrane located between the electrolyte and the gas diffusion layer at the anode and cathode, correspondingly [45]. CLs claim various features like possessing significant active surface areas, high porosity, high core activity, high electric, ionic conductivity and stability [46]. Generally, a Platinum catalyst is employed in PEMFCs because of various qualities it possesses like reactivity, stability and durability on the anode side [36]. Pt holds minimal diameters ranging from 2 to 8 nm supported on carbon units providing a high surface area to improve the catalyst dispersion offering a thermal and electrical track through the external circuit. Ionomers, which are materials utilized in the membrane are mixed in the CLs giving a proton exchange pathway. The mixture of the ionomer and the carbon particles provides enough porosity in the CL, gaining access for the reactant gas needed in the reaction [36].

2.2.3 Gas Diffusion Layers (GDLs)

The gas diffusion layer (GDL) is located on the sides of each CL in both anode and cathode. The porous structure it retains improves the dispersion of the reactants from the current flow channels into the active sites of the catalyst. GDL is a relatively thick layer to provide mechanical strength and protection for the CL. It is commonly produced of carbon cloth or carbon paper to guarantee structural strength [47]. Furthermore, GDLs transfer electrons from the CL of the electrodes to the electrons in bipolar plates.

2.2.4 Bipolar Plates (BPP)

The flow field plates are gathered on both sides of the GDLs. The overall unit is consisting of the stacked unit of the fuel cells. BPPs are typically produced from graphite or carbon-polymer composite resources or metals [36]. The functions of BPPs are:

(a) Facilitation of water controlling in the cell.
(b) Distribution of the fuel and oxidant inside the cell.
(c) To ease the management of heat.
(d) To detach separate cells in the stack from each other.
(e) To prevent the loss of reactants from the system [48].

Chemical stability, thermal conductivity, electrical conductivity and mechanical strength are essential under the conditions of the fuel cell system process in the bipolar plates [36].

2.2.5 Gaskets

Gaskets are between bipolar plates and the MEA in PEMFC. The fuel cell gaskets should retain superior thermal stability, electrical insulation, mechanical strength at low and high temperatures and enough rigidity with suitable processing capability. The primary function of gaskets is to prevent the gas leakage of reactant gases inside the fuel cell system [49].

2.2.6 End Plates

The end plates require mechanical strength to support a fuel cell stack and homogeneously distribute the forces. The material choice for end plates is moderately extensive

for the stacks of low temperature. However, there are some limitations as the stacks of a fuel cell grow bigger and bigger. There are various requirements in choosing the appropriate end plate material like mechanical strength, durability, thermal stability and economic availability. Many materials utilized in making fuel cell end plates like Titanium, Graphite, Aluminum, Stainless steel, Metal foams, Nickel, Polycarbonate, PVC, Polyethylene and various other polymers [33].

2.3 Types of the PEMFC

2.3.1 High Temperature Proton Exchange Membrane Fuel Cell (HT-PEMFC)

HT-PEMFC usually operates in the temperature range between 100-200ºC [50]. The safest temperature range for HT-PEMFC operations is between 120-180ºC because of the occurrence of degradation at temperatures higher than 180ºC [51]. HT-PEMFC holds good characteristics, such as having high tolerance towards CO poisoning [35], and enhanced reaction kinetics leading to the replacement of platinum with a less expensive catalysts, in addition to the easy control over water and heat as reactants [52]. The high operating temperature of HT-PEMFC causes the Nafion membrane to dry and lose its proton conductivity. Many researchers established a membrane that can operate in temperatures higher than 100ºC, possesses high conductivity at dry conditions, more durable and economically available [53]. One significant membrane that fulfills the required conditions is Phosphoric acid (H_3PO_4) doped Polybenzimidazole (PBI) membrane as it has low-cost, chemical and thermal stability, mechanical strength, durability and conductivity to protons in dry conditions, so H_3PO_4 serves as a medium to carry the protons in the chemical process [54], [55]. The high temperature of HT-PEMFC causes proton transfer resistance to decrease. Hence, increasing the temperature increases the reaction rate achieving an increase in the efficiency of the electrochemical reaction. To maintain a consistent temperature, remove excess in fuel cells using cooling systems, HT-PEMFC is fed directly from a reformer system because HT-PEMFC maintains high resistance towards contaminations [56].

2.3.2 Low Temperature Proton Exchange Membrane Fuel Cell (LT-PEMFC)

LT-PEMFC generally operates in the temperature range of 60-80ºC [50]. A LT-PEMFC enjoys numerous benefits like high efficiency, high power density, simplicity, short start-up time since the operating temperature is effortlessly achieved, reaction to

varying loads, etc. However, LT-PEMFC has the disadvantage of having a low tolerance to CO poisoning. LT-PEMFC would operate poorly if the CO quantity exceeds 30 ppm. Thus, CO must be converted into CO_2 [51]. Commonly, LT PEMFC power systems use high-pressure compressed gas (CGH2) in light-weight composite containers at a pressure range of 350-700 bar for storing H_2. Therefore, it possesses higher H_2 storage weight capability, shorter resupplying time and practically limitless H_2 flow rate as a supply to the fuel cell stack. However, the storage capacity volume of H_2 in the CGH2 systems is relatively low. In addition to having two fundamental difficulties, like the high costs of refueling and the low safety as they are connected to the high pressure of the H_2 storage [52]. The membrane used in the case of LT-PEMFC is PFSA (perfluorocarbon sulfonic acid) (Nafion), which provides an excellent proton conductivity, both thermal and chemical stability, elasticity and mechanical strength in low temperatures and in a high moistened medium since the lower presence of water molecules reduces the conductivity [53], [54], [55]. PFSA shows hydrophobic behavior. This phase works as the constant phase for the structural integrity of the membrane, and the sulfonic acid group performs as a hydrophilic side to the water tank [56]. Thus, the water management system is essential for the design of the LT-PEMFC stack. The existence of a minimal quantity of water molecules affects the whole power and the efficiency of the system. Because the water quantity is too low, the membrane would dry up leading to the reduction of proton conductivity and considerably increasesing the durability of the cell. However, large quantities of water on the cathode side result in overflowing and O_2 transference restriction through the porous gas diffusion layer [57], [58].

Temperature is essential to achieve a good reaction. However, excessive heat results in the dehydration of the membrane, and the Nafion membrane loses energy because of the increased transport resistance changes. One of the drawbacks of using PEM fuel cells is using pure H_2 because of the high operating cost [59]. Supplying H_2 in high purity was one of the chief obstacles for an extended time since the high purity H_2 is vital to avoid poisoning at the anode electro-catalyst in PEMFC [60]. In the H_2 oxidation reaction (HOR), there is a lot higher exchange current density at the anode side than that on the O_2 reduction reaction (ORR). This resulted in the slow pace of the electrochemical kinetics at the cathode side making it the determining factor in the overall reaction rate [61]. The electrical potential at the cathode is the cause of the

voltage loss in the cell [62]. High efficiency, high energy density and the short start-up time all marks LT-PEMFC as an attractive energy system [63].

2.4 Bimetallic Catalysts

Employing a proper catalyst is one of the best and most essential means to increase a specific reaction rate. Numerous studies have taken place in the literature investigating homogeneous and heterogeneous catalysts. Noble metals such as Pt, Pd, Au and Ru-based catalysts offer tremendous catalytic activity, high stability and represent ideal catalysts for H_2 generation reactions. The ruthenium (Ru) catalyst is relatively more affordable and effective in H_2 generation by the hydrolysis of $NaBH_4$ [64]. Multiple mono-metallic-based catalysts serve the same purpose, such as nickel (Ni) based catalysts [65], cobalt (Co) based catalysts [66], rhodium (Rh) [67] and ruthenium (Ru) catalysts [68].

Moreover, the bimetallic catalysts often have a synergistic effect due to the interaction between two metals to make a better catalyst. The synergistic effect results in offering better stability and activity compared to monometallic catalysts [69]. Furthermore, using these catalysts in supported catalyst form was proven to have an influential role in improving the durability of the catalyst and enhancing the activity by increasing the surface area of the reaction for these catalysts [65] [70].

Accordingly, many support materials went under investigation by scholars. Support materials play a vital role in improving catalyst utility by reducing catalyst loading. For instance, support materials have several forms, such as inorganic oxides [71], graphene structures [72], carbon nanotubes (CNTs) [73] and modified carbon structures [74], etc. Carbon black (CB) is commonly used as a support material in applications of PEMFCs [75]. However, the catalyst can get detached, accumulated and ruined on the CB support material. As a result, CB can suffer of corrosion, that is why it does not satisfy the requirements for the operating systems concerned with H_2 production in fuel cells [76].

Many studies took place regarding various carbon materials as support materials for catalysts because of their excellent electrical conductivity, high mechanical and thermal stability, high catalytic loadings and durability. Carbon nanotubes CNTs are a

much more desirable alternative as catalytic support than carbon black materials as they are stable not only in acidic but also in basic media [77] [78].

Over the past years, CNTs have attracted many researchers because of their mechanical, thermal and electrical properties [79]. CNTs consist of a one-dimensional structure in general. There are two types of CNTs, single-wall carbon nanotubes (SWCNTs) and multi-wall carbon nanotubes (MWCNTs). The difference between SWCNTs and MWNCTs is the number of wall layers [80]. The SWCNTs are made of a rolled up in a whole cylindrical shape of graphene, having a diameter of about 0.5-1.5 nm [81]. MWCNTs are made of more than a single cylindrical shell of graphene sheets, making a tree ring form organized surrounding a central hollow core with Vander Waals forces between neighboring sheets [82] as shown in Figure 2.5. The MWCNTs are more affordable for industrial applications, and possessing a lower particle size making them more dispersible [80].

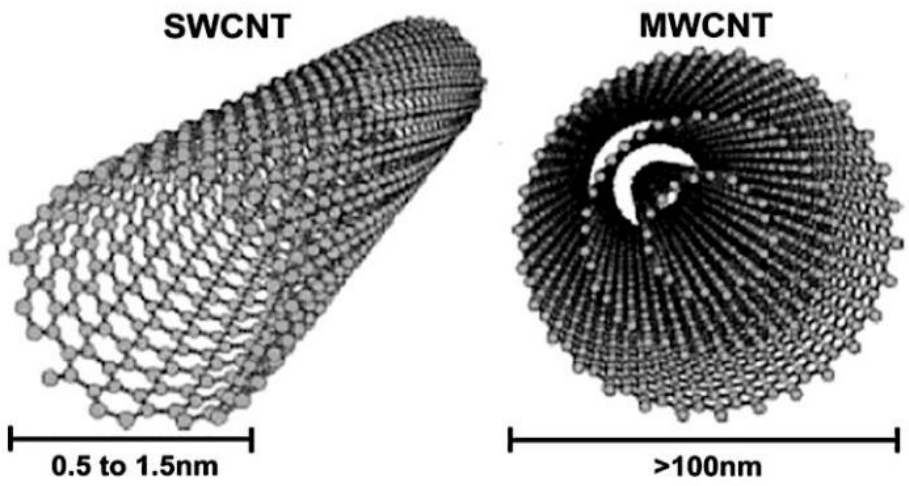

Figure 2.5 Single-walled carbon nanotube (SWCNT) and multi-walled carbon nanotube (MWCNT) [83].

The interaction between the support material and the metal catalyst enhances the activity, durability and efficiency of that catalyst. Furthermore, there is graphene (G) is important support material for PEMFC. The graphene structure is similar with CNTs. However, CNTs contain carbon atoms, so it has a one-dimensional profile (1D) whereas graphene possesses a plane form of two dimensions (2D) [84]. Graphene grew to become a desirable candidate as catalyst support as it is used for electrochemical

applications for having a colossal electrical conductivity, high surface area, exceptional catalytic activity, enhanced efficiency and high durability [42], [85], [86]. A graphene nano platelet (GNP) is a stack of graphene sheets with a thickness of 5 to 25 nm. It consists of 10-30 stack sheets in comparison to monolayer graphene. GNP has an even distribution in addition to the excellent interaction it enjoys with other materials [87], [88], [89]. However, GNP sheets undergo agglomeration caused by Van der Waals force. This obstacle can be avoided by incorporating two-dimensional (2D) GNP and one dimensional (1D) MWCNTs to make a single novel material that offers enhanced characteristics and creating a three dimensional (3D) hybrid MWCNT doped GNP (MWCNT-GNPs) [90], this hybrid support material (MWCNT-GNP) shows an excellent dispersion compared to MWCNTs and GNPs separately [91]. The interaction between MWCNTs and GNPs gives this 3D conductive network offering a significant electrical conductivity [92]. The addition of CNTs decreases the re-stacking concern of GNPs by inserting the gap between the G sheets [93]. However, the GNPs are likely to wrap around the CNTs to prevent the agglomeration of CNTs. Therefore, hybrid corroboration could offer a well-organized dispersion of CNTs and GNPs, and eventually, this mutual effect results in enhanced properties [94].

As for catalyst synthesis, it is essential to select an appropriate approach. In the synthesis of bimetallic catalysts, multiple approaches are available such as heterogeneous deposition-precipitation (HDP), impregnation, co-precipitation, incipient wetness, ion exchange, decomposition of metal clusters, activation after synthesis, calcination and reduction, plasma-assisted deposition, micro-emulsion and facile hydrothermal method [95], [96], [97], [98], [99], [100], [101], [102], [103].

Microwave-assisted synthesis is a fundamental technique in the preparation of a supported bimetallic catalyst as it permits the construction of controlled size colloidal nanoparticles (monometallic and bimetallic) in different morphologies and structures, it also provides a quick accomplishment of the preferred temperatures by offering homogenous heating for the catalyst synthesis [104]. The microwave-assisted preparation method offers an even spreading of the catalyst particles by stirring the water because of the presence of the electromagnetic field [105]. In microwave-assisted synthesis, the solvent is essential. Ethylene Glycol (EG) possesses a double role by acting as a solvent and a reducing agent simultaneously [106]. Microwave-assisted synthesis

is considered a promising technique as it gives a better distribution for the catalyst on the support material, increases catalytic activity, stability and durability, resulting in better performance for H_2 production and PEMFC applications.

Several studies in the literature given in Table 2.1 showing various bimetallic and monometallic catalysts, their synthesis methods, applications and characterization methods. Yong-Ting Li et al. studied the hydrolysis of NH_3BH_3 using PdRu catalyst encapsulated in g-C_3N_3. They found that PdRu/g-C_3N_3 showed higher catalytic activity than Pd/g-C_3N_3 and Ru/g-C_3N_3 with a turn over frequency (TOF) of 948.2 mol_{H2}/mol $_{cat}$.min and activation energy (Ea) of 24.2 KJ/mol [107]. M. Rakap explained the use of PdRu catalyst stabilized with the use of poly (N-vinyl-2-pyrrolidone) for the hydrolysis of $NaBH_4$ and NH_3BH_3 and found that this catalyst was recyclable and highly active, giving an average TOF of 762 mol_{H2}/mol $_{cat}$.min and Ea of about 52.4 KJ/mol from the hydrolysis of $NaBH_4$, and for the hydrolysis of NH_3BH_3 the average TOF values was 308 mol_{H2}/mol $_{cat}$.min and Ea was 54.5 KJ/mol [108]. Tang et al. studied PdRu alloy supported on N-Doped carbon as a catalyst for benzoic acid (BA) hydrogenation and found that the catalyst shows a considerably greater activity compared to the monometallic ones (Ru/CN and Pd/CN) [109]. Xiong et al. examined Pt-Pd nanodendrites supported on carbon as a catalyst for O_2 reduction in PEMFC and found that the catalyst improved the durability and the performance of PEMFC, improving the transfer of electrons, protons and O_2 enhancing the activity of ORR [110]. Fu et al. tested PtPd/G-MWCNT and found that it displays a great activity and enhanced durability towards ORR applications. They found that enhanced performance is credited to the synergistic effect in G-MWNT support [111]. A. Bharti and G. Cheruvally clarified that if the PtPd catalyst is supported on MWCNT with the existence or the absence of anionic (SDS) and cationic (CTAB) surfactant effect on ORR showed that SDS presence results in the desegregation of MWCNT that is quite similar to that support without the presence of a surfactant leading to the improvement of ORR performance [112] Zapata-Fernandez et al. studied PtPd/MWCNT for ORR in PEMFC applications, and they found that the catalyst gives a high electrocatalytic activity for PEMFC with a low concentration of Pt [113]. Chai et al. studied PdAu/GNs and found that the graphene-supported catalyst reveals outstanding electrocatalytic activities for applications in fuel cells [114]. Liu et al. studied PdAg/GNs and found that the PdAg nanorings

show better properties as a cathode electrocatalyst for O_2 reduction from the synergistic effect PdAg alloy showing a high catalytic performance for ORR for fuel cells. [115]. R. Awasthi and R. N. Singh studied the bimetallic catalyst PdSn/GNs optimization for enhanced methanol electrooxidation. They addressed that 18% Pd-2% Sn/GNS presents the highest electrocatalytic activity toward methanol electrooxidation (MOR) [116]. Zheng et al. studied RuSe/MWCNT with or without a citric acid catalyst for PEMFC applications and saw that the catalyst shows high catalytic performance and high durability [117]. Huff et al. studied Pd/MWCNTs composite as a catalyst for producing H_2 by the hydrolysis of $NaBH_4$, and they illustrated that the catalyst has an activation energy of 62.66 KJ/mol and gave H_2 at a rate of 23.0 $mLmin^{-1}g_{cat}^{-1}$ [118]. Kiyani et al. studied Pd/MWCNT for methanol oxidation reaction (MOR) and found a relatively lower activity than Pt/C. However, MWCNTs, as a support material for Pd showed better long-term stability in contrast to Pt/C, which is related to Pd particles being well dispersed on the support surface [119]. Seo et al. studied Pd supported on graphene catalyst for electrocatalysis and found that it is possible for the ORR Pd catalyst in alkaline solutions when supported on graphene compared to the Pt catalyst [120]. S. Akbayrak and S. Özkar studied Ru/MWCNT for H_2 generation from NH_3BH_3 hydrolysis and found an excellent catalytic activity with an activation energy of approximately 33 KJ/mol. The catalyst was characterized by showing that Ru nanoparticles of the size 1.4–3.0 nm were well dispersed on MWCNTs [68]. Liang et al. made a study about hydrolysis of $NaBH_4$ for H_2 generation with the use of ruthenium supported on graphite catalyst (Ru/GNs). The highest H_2 generation rate was 32.3 $mLmin^{-1}g_{cat}^{-1}$ in a 10 wt.% $NaBH_4$ and 5 wt.% NaOH solution, and they found that nanoparticles of Ru are chemically bonded on the graphite surface with sizes of approximately 10 nm [121].

In this study, PdRu/MWCNT and PdRu/MWCNT-GNP catalysts were synthesized with the microwave-assisted method to examine the effect of synthesized catalysts on $NaBH_4$ hydrolysis reaction. These two catalysts were characterized structurally by thermogravimetric analysis (TGA), X-ray diffraction (XRD), transmission electron microscope (TEM) analysis. The electrochemical characterization was performed by using the method of cyclic voltammetry (CV). The results showed that the catalyst supported with MWCNT-GNP had better durability and performance than the one supported with MWCNT, thanks to the excellent dispersion and the excellent interaction

between MWCNT and GNP, hence MWCNT-GNP possesses a higher specific surface area SSA. In addition to that, a kinetic study, reusability study, and a PEMFC performance tests were performed with PdRu/MWCNT-GNP catalyst.

Table 2.1 Comparison of the different catalysts in the literature for different applications.

Support	**Catalyst**	**Synthesis**	**Application**	**Characterization technique**	**Ref.**
g-C_3N_4	Pd-Ru	Polymerization	HER	TEM, SEM, XRD, ICP-OES, XPS, FT-IR	[107]
PVP-Stabilizer	Pd-Ru	Co-Reduction	HER	TEM, UV-Vis	[108]
CN	Pd-Ru	Co-Reduction	Hydrogenation of BA	ICP-AES, HRTEM, HRSTEM, XRD, XPS, H_2-TPR, TCD	[109]
C	Pt-Pd	Facile Solvothermal	ORR	XRD, TEM, HRTEM, XPS, ICP-AES, EDX, CV	[110]
G-MWCNTs	Pt-Pd	Electrochemical Reduction	ORR	SEM, TEM, EDS, XPS, XRD, CV	[111]
MWCNTs	Pt-Pd	Microwave assisted	ORR	XRD, ICP-AES, FESM, HRTEM, XPS, CV	[112]
MWCNTs	Pt-Pd	Galvanic displacement (GD)	ORR	TGA, TEM, ICP-OES, CV, EIS	[113]
GNs	Pd-Au	Galvanic displacement (GD)	FAOR	TEM, HRTEM, HAADF-STEM, EDS, FTIR, XRD, XPS, ICP, EIS, CV	[114]
GNs	Pd-Ag	Polyol reduction	ORR	XRD. XPS, TEM, HRTEM, EDX, HAADF, STEM, CV	[115]
GNs	Pd-Sn	Polyol reduction	MOR	XRD, SEM, TEM, CV	[116]
MWCNTs	Ru-Se	Microwave assisted	ORR	XRD, HRTEM, EDX, TEM, CV	[117]
MWCNTs	Pd	Chemical vapor deposition	HER	HRTEM, SEM, EDS	[118]
MWCNTs	Pd	Polyol reduction	MOR	SEM, TEM, CV	[119]
GNs	Pd	Chemical vapor deposition	ORR	SEM, TEM, XRD, CV	[120]
MWCNT	Ru	Chemical vapor deposition	HER	ICP-OES, XRD, TEM, SEM, EDX, XPS	[68]
GNs	Ru	Chemical vapor deposition	HER	TEM, XPS	[121]

CHAPTER 3

METHODOLOGY

3.1 Materials

Palladium (II) chloride ($PdCl_2$), Ruthenium (III) chloride ($RuCl_3 \cdot xH_2O$) were used as the fundamental metals, and they were purchased from Sigma-Aldrich. Ethylene glycol (EG) ($C_2H_6O_2$), Isopropyl alcohol (IPA) ($CH_3CHOHCH_3$), Deionized Water (DI), acetone (C_3H_6O), Sodium Hydroxide (NaOH), Sodium Borohydride ($NaBH_4$), Nitric Acid (HNO_3), Perchloric acid ($HClO_4$), were obtained from Sigma-Aldrich. Multi-Walled Carbon Nanotube (MWCNT) and Graphene doped Multi-Walled Carbon Nanotube (MWCNT–G) used as a support material for the metal catalysts were obtained from Nanografi (Turkey). Gases that were used in the experiments had a purity of (99.99 %), and they were purchased from Linde. The commercially available Pt/C (HiSPEC) catalysts were purchased from Alfa Aesar® (Karlsruhe, Germany). Nafion 212 membrane and 15 wt. % Nafion solution were purchased from Ion Power (USA). Sigracet 34 BC was selected as GDL (Germany).

3.2 Catalyst Preparation

The catalysts PdRu/MWCNT and PdRu/MWCNT-GNP were synthesized using microwave-assisted approach. In the beginning the support materials (50 mg), ethylene EG (24 ml) and IPA (6 ml) were mixed in a beaker. EG acts as an excellent reducing agent to transform metal ions into metal or alloy nanoparticles and serves as a colloidal metal stabilizing agent [122]. IPA is ecologically favored and helps in separating materials, solvents and catalysts in addition to adjusting the viscosity of the solution [123], [124]. Then, the prepared solution was mixed with ultrasonic bath for 60 minutes. The calculated amounts of $PdCl_2$ and $RuCl_3.xH_2O$ with the molar ratio of 50:50 was added to the solution, and then it was mixed in an ultrasonic bath for 10 minutes. Generally, pH should be 12 and above for high catalytic activity and small particle size for the supported catalyst prepared by microwave-assisted polyol synthesis [125]. Therefore, the pH of the solution was elevated to almost 12 by using

1 M of NaOH in EG solution. Then mixing the solution with magnetic stirring under the effect of nitrogen gas for 30 minutes, and after that, it was heated using the microwave at 600 W for 60 seconds. Those parameters were proven to give good results, according to a previous study [126]. After the microwave, the solution beaker was left to cool down to room temperature. The pH is decreased to approximately 2 by using 0.2 M of HNO_3 solution, and then the solution was mixed for a whole 30 minutes. The solution was separated and extracted by centrifugation and washed with acetone multiple times and was left in the oven at 100ºC to dry overnight. The catalysts preparation steps are illustrated in Figure 3.1.

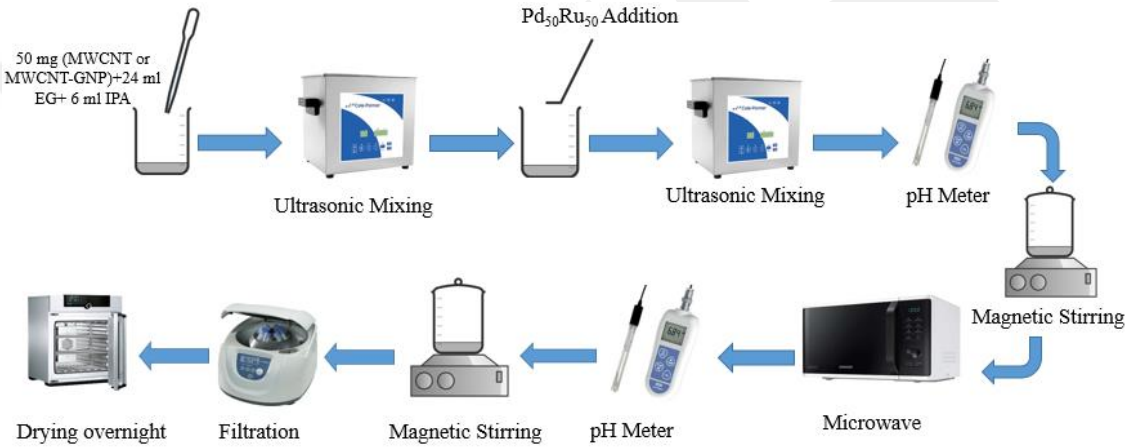

Figure 3.1 Experimental steps for catalyst synthesis.

3.3 Hydrogen Generation Tests

Figure 3.2 shows the experimental set up was prepared for the H_2 generation experiments. The setup consists of a round-bottomed flask that serves as the reaction vessel, graduated cylinder and conical flask. Initially, all equipment was cleaned very well. The setup system was well closed off to avoid any gas leakage, which might affect the H_2 generation process, all parts were connected and parafilm was used to seal all possible leakage points, and the setup was checked by a reference commercial catalyst Pt/C. Firstly, the appropriate amount of catalyst was placed in the round-bottomed flask and sodium hydroxide (NaOH) was also added in the solution to stabilize the reaction. After that, required amount of sodium borohydride ($NaBH_4$) was dissolved in 10 ml of deionized water (DI) and it was injected through the rubber stopper. The

flask was closed immediately and the change in the water level in the graduated cylinder was observed and registered with respect to the time passing to determine H_2 amount generated. This process was performed multiple times with changing various conditions and fixing the others such as amount of $NaBH_4$ and NaOH, temperature and catalyst mass to find the highest reaction rate and efficiency for the catalysts used in the experiments.

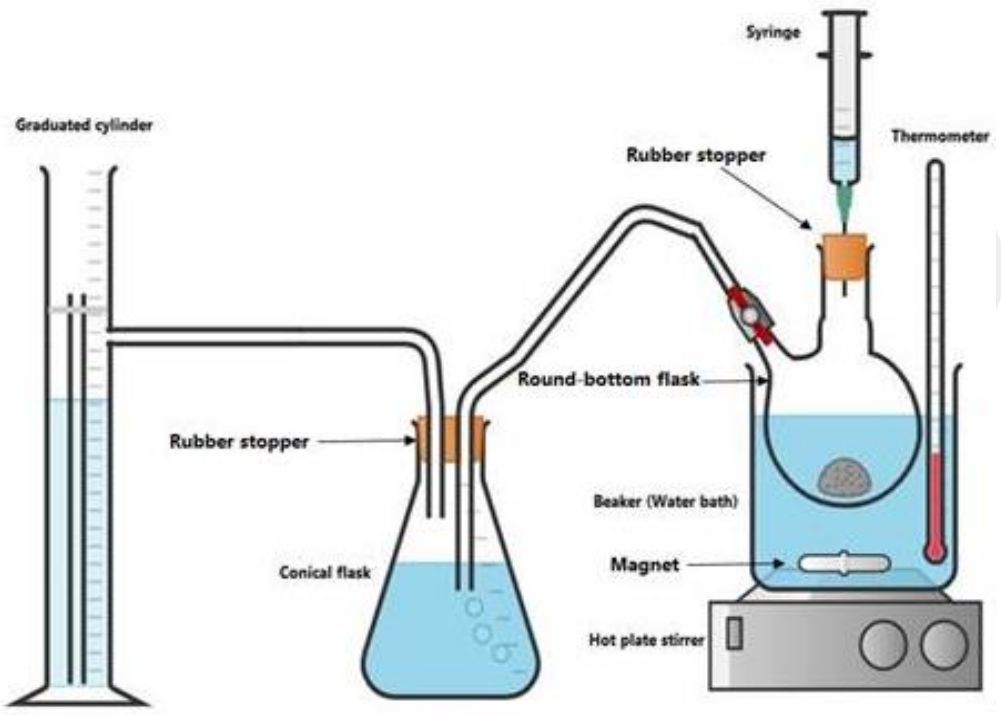

Figure 3.2 The $NaBH_4$ hydrolysis setup used in the laboratory for H_2 generation experiments.

3.4 Catalyst Characterization

3.4.1 Structural Characterization

The thermal behavior and metal loading of the prepared catalysts were examined by Thermal Analyzer (Perkin Elmer Pyris 1) in the range of 100-900 °C with a heating rate of 10 °C/min under air [127]. The crystalline structure of the catalysts was investigated with XRD (X-Ray Diffraction). The XRD experiments were performed with Rigaku Ultima-IV device using Cu Kα1 (λ = 1.5406 A) which is operating at 20–60 kV and 2–60 mA over the range of $10<2\theta<90°$ [127], [128], [129]. The distribution of the metal particles over the support materials were determined by JEOL 2100 JEM TEM instrument working at high-resolution (HR) mode.

3.4.2 Electrochemical Measurements

Cyclic voltammetry (CV) is a suitable characterization technique that is used to observe the Electrochemical Active Surface Area (ECSA), dissolution/agglomeration and carbon corrosion of the catalysts [130], [131]. CV measurements were examined with the Potentiostat (Wonatech ZIVE-SP2 Potentiostat/ Galvanostat/ FRA) as shown in Figure 3.3. CV system includes three electrodes, the working electrode (WE), the reference electrode (RE), in addition to the counter electrode (CE). A disc electrode (0.0707 cm^2) made of glassy carbon (GC), an electrode Ag/AgCl filled with saturated NaCl solution, and Pt's spiral was used as the WE, the RE and the CE correspondingly. The CV measurement was performed at 25^oC with 200 mV/s from 0.25 – 1.2 V in 0.1 M of $HClO_4$ as the electrolyte solution. The electrolyte solution was cleaned with N_2 gas for 30 minutes to eliminate O_2 residues before starting the CV experiments.

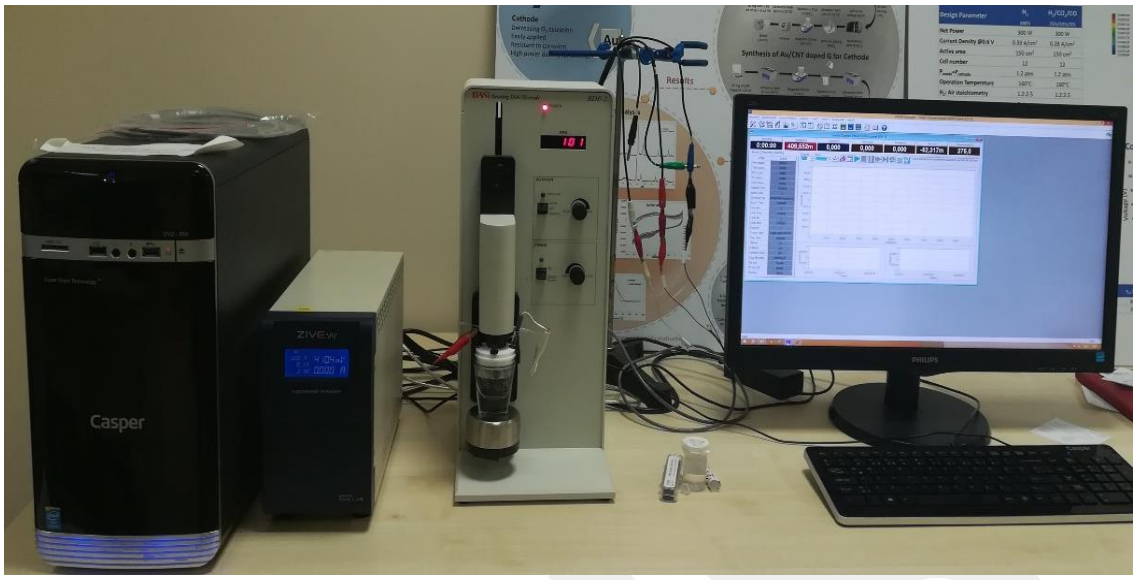

Figure 3.3 ZIVE SP2 Single Channel Potentiostat used for CV test.

3.4.3 Reusability Tests for Hydrogen Generation

In order to investigate the reproducibility of the prepared catalyst for H_2 generation, experiments were performed by using at constant reaction parameters (25^{o}C, 0.2 M $NaBH_4$, 0.2 M NaOH and 0.02 g of catalyst). The PdRu/MWCNT-GNP catalyst was used for reusability experiments. When the first experiment completed, the catalyst was separated from reaction solution by centrifugation for 4 minutes. Then the catalyst was washed and injected into the round-bottomed flask to start the 2nd experiment (1st reusability test). The same process was repeated for 3rd experiment (2nd reusability test) to observe the drop in the efficiency of the catalyst with continuous usage.

The supported catalyst was prepared for second part of reusability experiments. In this case powder catalyst was supported on the carbon-based gas diffusion layer (GDL) to observe the effect of a supported catalyst on reusability. Gas Diffusion Electrodes (GDE) were arranged by the coating of the catalysts on GDL. The catalyst ink solution was prepared with the same amount of catalysts used in the test of powder form catalyst. For supported catalyst preparation firstly, the appropriate amount of catalyst, Nafion solution as a binder, DI water and IPA were mixed with mechanical stirring. Then the solution was put in an ultrasonic bath for 1 hour. Afterward, the prepared catalyst solution was coated on GDL by a brushing technique up to the desired catalyst

loading. The prepared GDE was put in a round-bottomed flask and then appropriate amount of NaOH and $NaBH_4$ dissolved in 10 ml of DI water was injected into the flask with keeping the temperature at 25°C. After the 1st H_2 generation experiment was completed, the GDE was removed from the reaction medium and washed with DI water. Then 2nd H_2 generation experiment (1st reusability test) was performed using the same GDE. With the same method, the experiments are repeated until the GDE performance decreases.

3.5 PEMFC Performance Test

The $NaBH_4$ hydrolysis system was integrated into a single PEMFC with an active area of 5 cm^2 to determine the H_2 production performance of the PdRu/MWCNT-GNP catalyst. Firstly, MEA should be prepared to examine the H_2 generation performance of the PdRu/MWCNT-GNP catalyst in PEMFC. MEAs were prepared by ultrasonic coating technique, according to Devrim [132]. The catalyst ink was prepared by dispersing Pt/C catalysts (40 % wt.) into a mixture of isopropanol and Nafion dispersion (15% wt.). The resulted ink was sprayed onto the gas diffusion layer using the Sono-Tek 'Exacta Coat' ultrasonic coating machine that was operated at 120 kHz (Figure 3.4-a). The Pt catalyst loading of 0.5 mg/cm^2 was used for both the anode and the cathode side. Finally, the Nafion 212 membrane was sandwiched between two electrodes and hot-pressed at 130 °C and 172 N/cm^2 for 3 min (Figure 3.4-b). Before the performance test, MEA short circuit test was executed by measuring the resistance via multimeter.

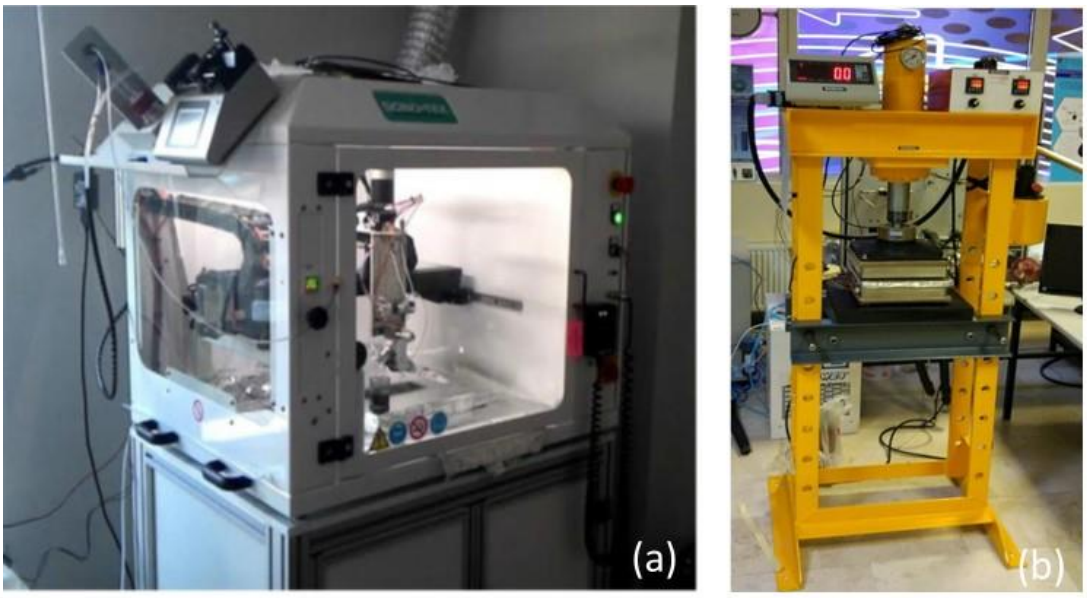

Figure 3.4 (a) Ultrasonic coating system, (b) Hot press.

Single-cell performance of MEA was evaluated by the $NaBH_4$ hydrolysis system integrated single-cell PEMFC test station. The temperature of the PEMFC was controlled by thermocouples placed in bipolar plates. Before the single-cell test, the leak test was conducted with the assistance of the USFCC leak check procedure. Pure H_2 and air were used for MEA stabilization during the PEMFC performance test. During the experiments, pure humidified H_2 (0.2 slpm) and air (0.25 slpm) were fed to the anode/cathode as fuel and oxidant, respectively. The PEMFC was operated for 2 h at 0.6 V for stabilization. Then, the performance test was carried out by H_2 produced from the $NaBH_4$ system. The current values were recorded through the stepwise switching of load from open circuit voltage (OCV) V to 0.4 V with an interval of 0.05 V. Schematic demonstration of the PEMFC test station is illustrated in Figure 3.5.

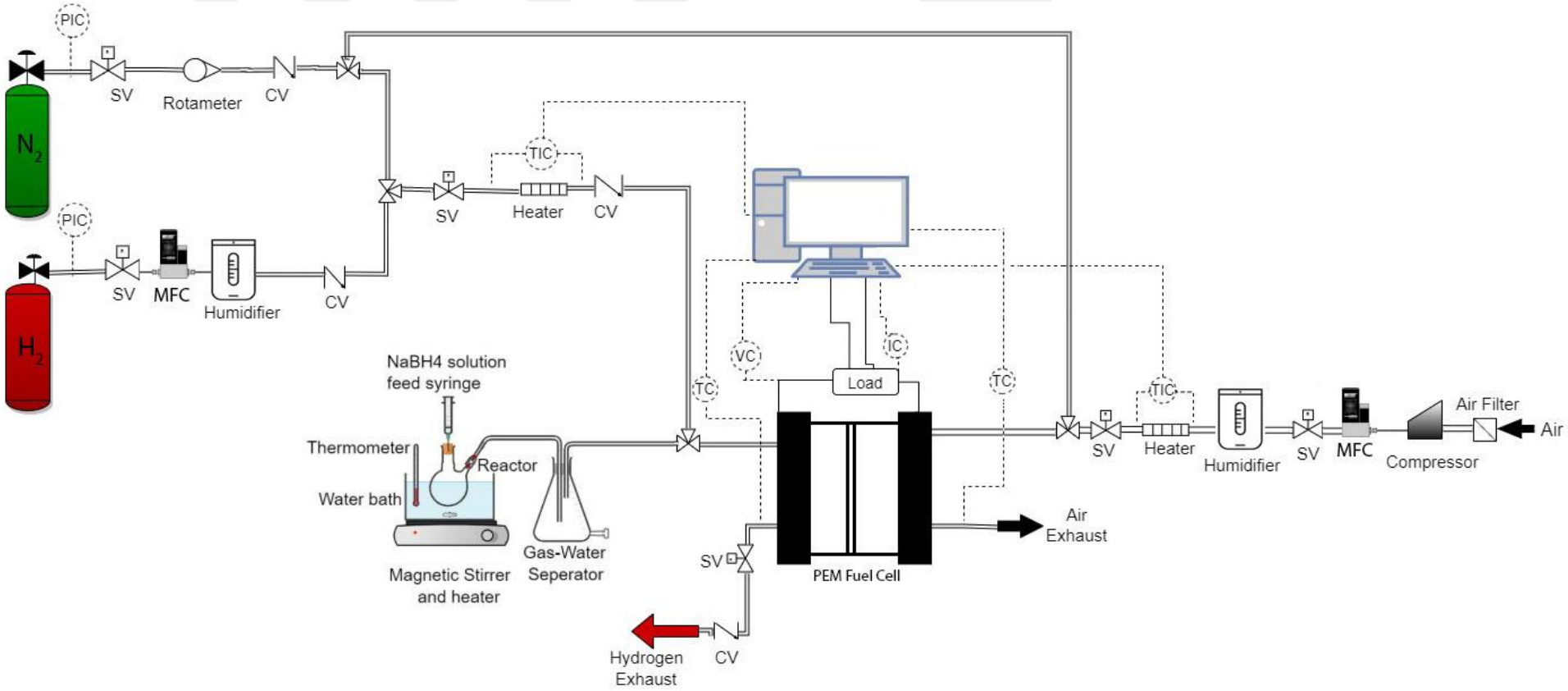

CV: Check valve, IC: Stack current controller, MFC: Mass flow controller, PIC: Pressure indicator and controller,
SV: solenoid valve , TC: Temperature controller, TIC: Temperature indicator and controller, VC: Voltage controller

Figure 3.5 $NaBH_4$ hydrolysis system integrated single-cell PEMFC test station.

CHAPTER 4

RESULTS AND DISCUSSION

4.1 Structural Characterization of the Catalysts

The TGA curves of the synthesized catalysts are illustrated in Figure 4.1. TGA curves show three distinct regions of mass loss for PdRu/MWCNT-GNP and two for PdRu/MWCNT.

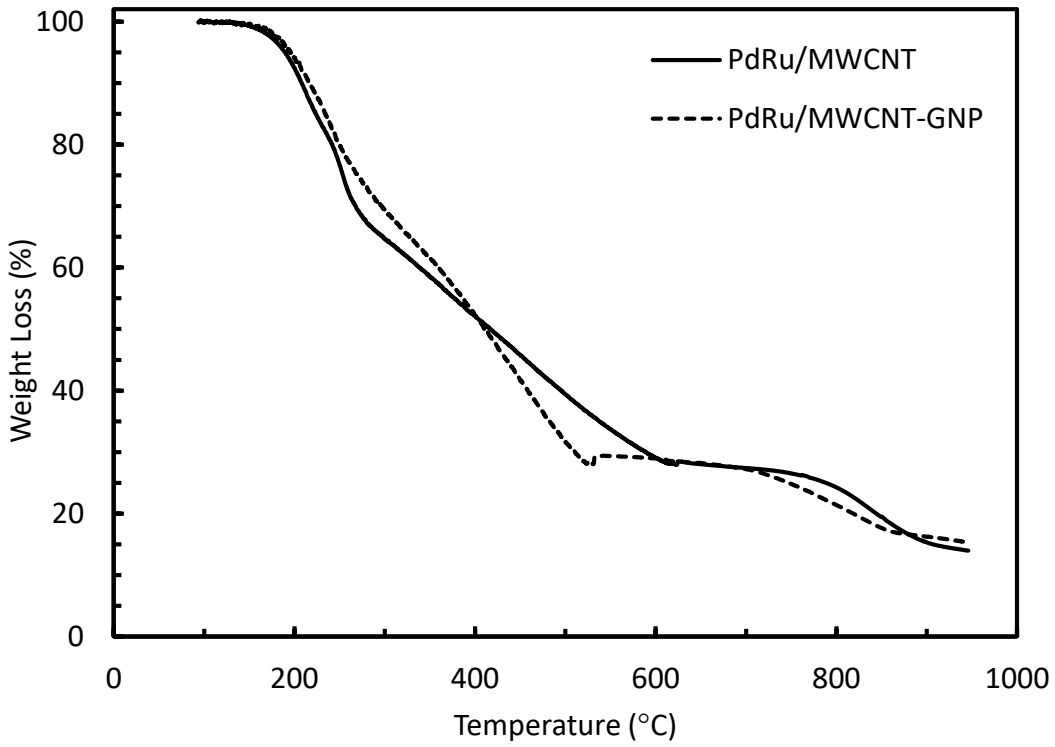

Figure 4.1 Thermal analysis of the PdRu/MWCNT and PdRu/MWCNT-GNP catalysts.

The first mass loss was observed in the range of 200-280ºC for PdRu/MWCNT and 200-240°C for PdRu/MWCNT-GNP, this is possibly attributed to the elimination of the volatile materials and absorbed water. The second mass loss region was obtained in the temperature range between 600-820ºC and 550-800ºC for PdRu/MWCNT and PdRu/MWCNT-GNP catalysts, respectively. Second mass loss region can be ascribed

to the thermal decomposition of the carbon support. And finally, the third mass loss region for PdRu/MWCNT-GNP ranges from 800-900^{o}C caused by the carbon oxidation of the catalyst. Consequently, the PdRu loadings were calculated for the two catalysts: 14.01 % and 15.39 % for PdRu/MWCNT and PdRu/MWCNT-GNP, respectively; therefore, both catalysts display excellent thermal stability.

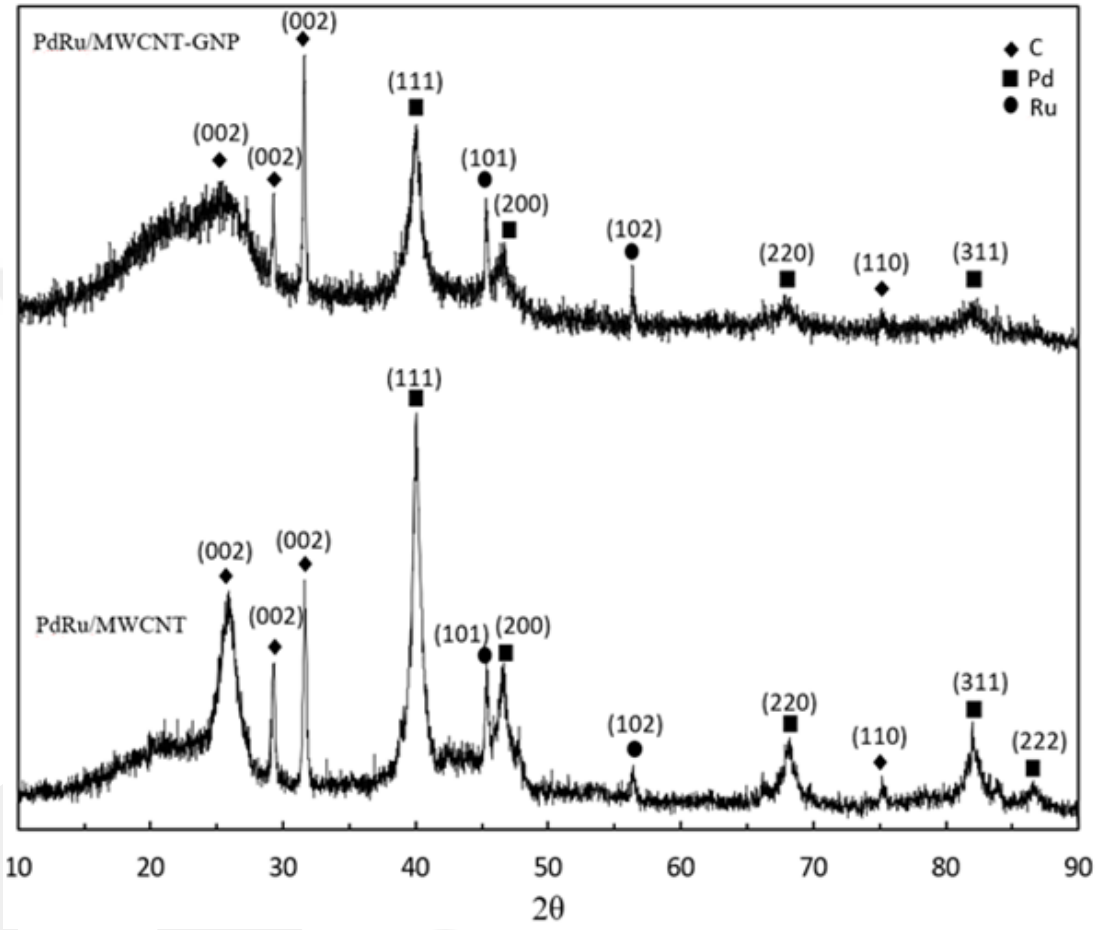

Figure 4.2 The XRD patterns of PdRu/MWCNT and PdRu/MWCNT-GNP catalysts.

XRD patterns are shown in Figure 4.2. For PdRu/MWCNT-GNP catalyst three peaks were observed at 2θ of 26.11º, 29.24º and 31.6º consistent to the C (002) characteristic diffraction peak [133], establishing the presence of MWCNT-GNP support material. The diffraction peaks were determined at 2θ of 39.99º, 46.65º, 68.07 º and 81.9º were related to the Pd (111), (200), (220), and (311) characteristic diffraction peaks, respectively, relatively close to previous studies in the literature [134], [135]. The 2θ peaks at about 45.34º and 56.415º can be attributed to the Ru (101) and (102) characteristic

diffraction peaks [136]. Similar peaks were obtained for PdRu/MWCNT catalyst. The diffraction peaks around 26.11°, 29.247° and 31.653° can be indexed as C (002), confirming the existence of MWCNT support. The peaks were located at 2θ of 39.953°, 46.68°, 68.08°, 82.2° and 86.62 are assigned to the Pd (111), (200), (220), (311) and (222) characteristic diffraction peaks, respectively. The diffraction peaks around 45.33° and 53.39° can be indexed as Ru (101) and (102) characteristic diffraction peaks.

The crystallite size of the electrocatalysts were determined from the XRD results with the use of (111) diffraction peaks using the Debye-Scherrer equation [137]:

$$D = \frac{0.9 \times \lambda}{B \times \cos\theta} \tag{15}$$

Where D is the crystallite size in (nm), λ represents the wavelength of the X-Ray Diffraction (0.154 nm), B is the full width at half maximum (FWHM) (radians), and θ is the angle at a maximum of the peak (radians). The metal catalyst particle size on the catalyst support material is vital for improving the efficiency and electrocatalytic activity of the electrocatalysts [42]. The peaks accuracy was determined using the Gaussian elimination technique to find FWHM to find the crystallites size. The crystallite sizes were found to be 2.01 nm and 1.55 nm for PdRu/MWCNT and PdRu/MWCNT-GNP catalysts, respectively.

The (111) and (200) planes of PdRu were faintly shifted to higher values of 2θ [138], this might be attributed to the content increase of Pd with the bimetallic catalyst at this point. To calculate the d-spacing (interplanar spacing between the atoms) for (111) planes for the two catalysts, Bragg's law was used as shown in Equation (16):

$$d = \frac{n \times \lambda}{2 \times \sin\theta} \tag{16}$$

Where d represents the space between the atomic layers in the crystal (Å), λ is the wavelength of X-ray (1.5406 Å), θ the peak angle, and n = 1 is the order of reflection, and the results for d-spacing were almost identical for both catalysts, the lattice constant for the diffraction peak (111) of PdRu bimetallic was measured from the equation (17) [139]:

$$\frac{1}{d^2} = \frac{h^2+k^2+l^2}{a^2} \quad (17)$$

Where d represents the distance between the atomic layers in a crystal, h, k, l are the miller indices, and a is the lattice constant. The calculated lattice constants (a) show that the values of all catalysts between in the Pd (3.89 Å) and Ru (3.83 Å) bimetallic catalyst constructs a firm structure when combined [140].

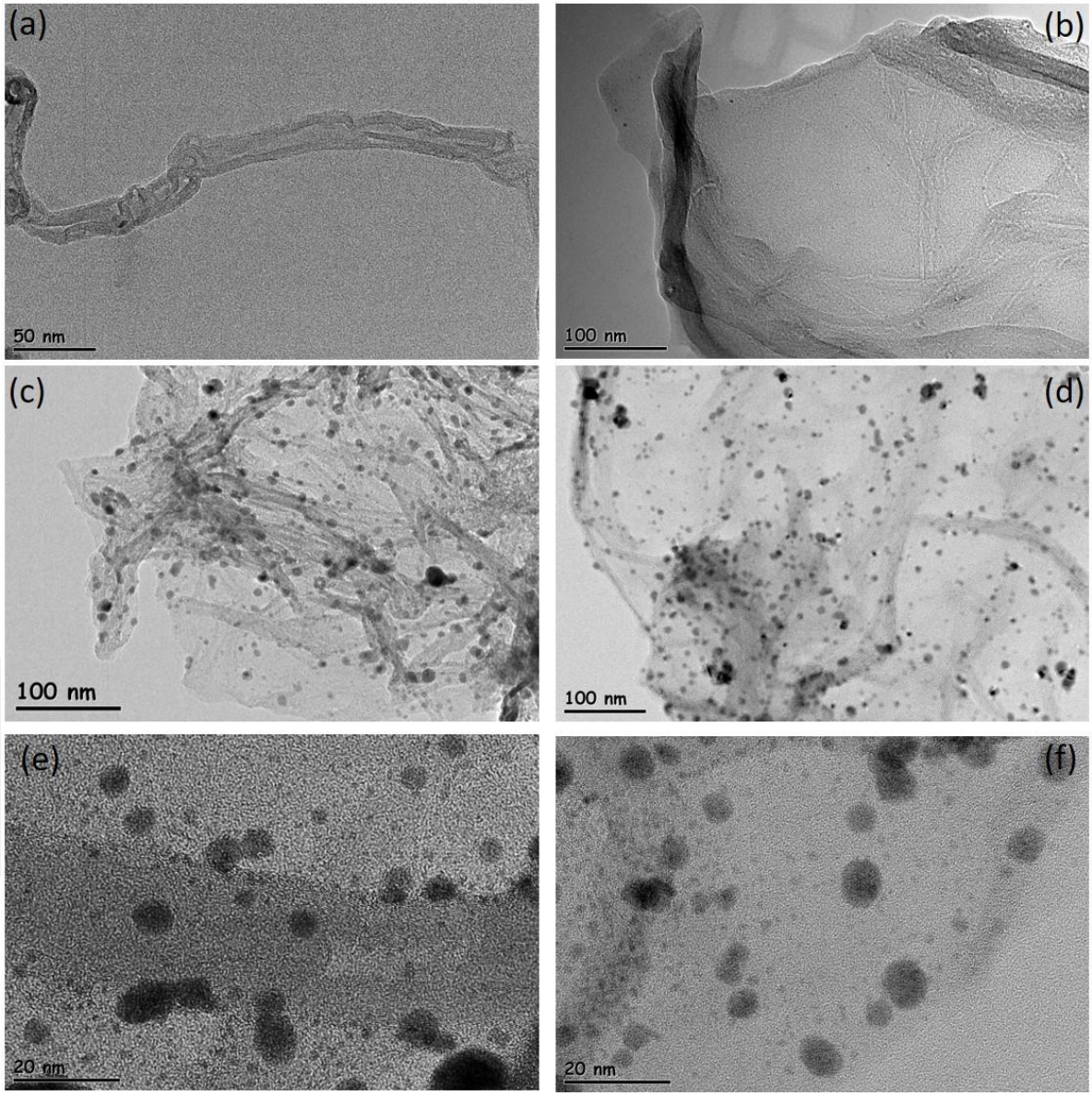

Figure 4.3 The TEM images of the a) MWCNT, b) MWCNT-GNP, c-d) PdRu/MWCNT-GNP and e-f) PdRu/MWCNT catalysts.

Figure 4.3 illustrates the TEM images of the MWCNT, MWCNT-GNP, PdRu/MWCNT and PdRu/MWCNT-GNP catalysts, respectively. As seen from Figure 4.3 the successful attachment of Pd and Ru on the MWCNT and MWCNT-GNP support materials. It was determined that Pd and Ru particles were almost homogeneously distributed on the support material. The sphere-like particles can clearly be seen in both images of the catalysts, which may be ascribed to the surface energy minimization, and very few particles can be seen in a single image because of the low loading quantity and high dispersion of the bimetallic catalysts on the support materials [141]. From (c) and (d) it can be seen that the PdRu particles were regularly distributed on the support materials. However, some agglomeration was observed in both catalysts. The average particle size of the pdRu/MWCNT and PdRu/MWCNT-GNP were determined as 6.1 nm and 5 nm, respectively. The catalyst with MWCNT-GNP have higher performance and conductivity in the microwave absorption than the GNP or MWCNT individually, because of the merging of the flaws and the simplicity of transmission of electrons in addition to the increase of the basal divergence [142]. Accordingly, the synergistic effect between GNP and MWCNT averts the re-stacking of G layers and offers more active sites.

4.2 Electrochemical Characterization

4.2.1 Cyclic Voltammetry (CV) Results

The CV tests results of the prepared catalysts are illustrated in Figure 4.4. CV curves have three distinct areas: the first one shows the H_2 adsorption/desorption peak region, the second region consists of the double layer, and finally the metal oxidation/reduction region. The stability of the synthesized catalysts was determined in each 100 scan cycles of the CV. Electrochemical chemical active surface area (ECSA) shows the active points for HER where triple-phase contact the membrane, the catalyst and the reactant gas to accomplish the electrochemical reaction [42].

ECSA is determined by calculating the dual charge in the H_2 adsorption/desorption area after adjusting the double-layer from the CV tests [143]. ECSA was calculated using Equation (18) [144]:

$$ECSA\left(\frac{cm^2}{g}\ of\ metal\right) = \frac{Q_H\left(\frac{\mu C}{cm^2}\right)}{K\left(\frac{\mu C}{cm^2}\right)\times m_L(g_{\ metal}/m^2)} \tag{18}$$

where $Q_{H\ is}$ the charge for H_2 adsorption/desorption, m_L (g) is the catalyst loading on CG electrode and K is the reference charge constant value [145].

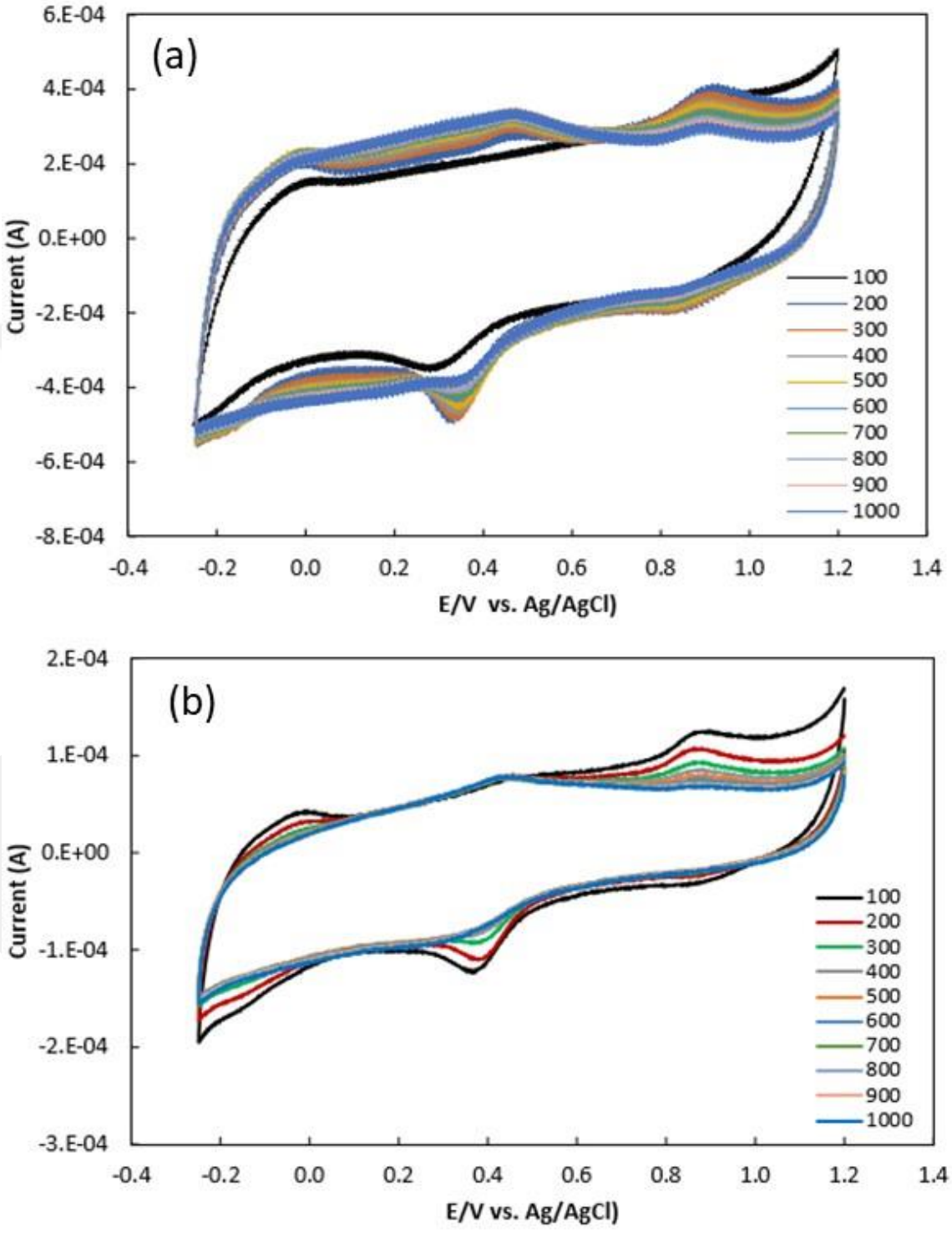

Figure 4.4 CV of (a) PdRu/MWCNT, (b) PdRu/MWCNT-GNP at room temperature in 0.1 M $HClO_4$ solution purged in N_2 for 1000 cycles.

The specific surface area (SSA) for the bimetallic catalysts is calculated using Equation (19) [146]:

$$SSA = \frac{6000}{\rho_{PdRu \times d}} \quad (19)$$

Where ρ represents the PdRu density, d (nm) is the diameter of PdRu, which are calculated from the XRD. The density of PdRu density was determined from Equation (20) [147]:

$$\rho_{PdRu} = \rho_{Pd}\chi_{Pd} + \rho_{Ru}\chi_{Ru} \quad (20)$$

Where ρ_{Pd} is the palladium density (12.02 g/cm^3) and ρ_{Ru} is the ruthenium density (12.37 g/cm^3) χ_{Pd} and χ_{Ru} are molar fractions of Pd and Ru in the bimetallic catalyst without the support material.

Table 4.1 ECSA and ECSA loss and SSA values of the catalysts.

Catalyst	$ECSA_{initial}$ (m^2/g)	$ECSA_{final}$ (m^2/g)	ECSA loss (%)	SSA (m^2/g)
PdRu/MWCNT-GNP	20.74	12.99	37	317
PdRu/MWCNT	12.36	8.12	34	245

Table 4.2 shows the ECSA and ECSA loss and SSA values of the catalysts. The ECSA values of the catalysts were calculated before and after the stability tests. The best initial ECSA was obtained with the PdRu/MWCNT-GNP catalyst as 20.7 m^2/g. At the end of 1000 cycles, the ECSA loss of the PdRu/MWCNT-GNP and PdRu/MWCNT catalysts were determined as 37% and 34 %, respectively. The highest value of SSA was obtained from the catalyst PdRu/MWCNT-GNP compared to the PdRu/MWCNT catalyst, which could be attributed to the smaller particle diameter.

4.3 Hydrogen Generation Experiments

It is commonly known that the reaction rate is significantly controlled by the type and the amount of the catalyst used in a specific reaction. However, other parameters can

considerably affect that specific reaction, such as the concentration of $NaBH_4$, the concentration of NaOH and the temperature. Those parameters were studied in this thesis, the results are discussed as follows.

4.3.1 Effect of the Concentration of $NaBH_4$ on H_2 Generation

The effect of $NaBH_4$ concentration on the H_2 generation rate was examined using three different concentrations of $NaBH_4$ (0.1, 0.2 and 0.3 M) with fixing the other factors (0.2 M NaOH, 0.02 g catalyst, 25ºC). Figure 4.5 illustrates the effect of $NaBH_4$ concentration on the H_2 generation for PdRu/MWCNT-GNP and PdRu/MWCNT catalysts. The amount of generated H_2 escalate with increasing $NaBH_4$ concentration up to a certain point because the decreasing of $NaBO_2$ solubility lead to an increase in the viscosity of the solution throughout reaction decreasing the reaction rates or with $NaBH_4$ conversion according to the literature [148].

The amount of H_2 generated, and the reaction rates of H_2 were calculated using the linear portions in both Figures using Equation (21) for the same concentration of $NaBH_4$.

$$r_{H_2} = \frac{Slope}{m_{cat.}} \tag{21}$$

According to the hydrolysis reaction of $NaBH_4$, the reaction rate of the $NaBH_4$, $NaBO_2$, H_2O and H_2 were found considering the stoichiometric ratio. The three experiments were performed to determine the H_2 generation rates of $NaBH_4$ hydrolysis reaction at 25ºC for PdRu/MWCNT catalyst were found as 27.3, 33.6 and 36.6 mmol/min.g_{cat} for 0.1, 0.2 and 0.3 M $NaBH_4$ respectively. In the case PdRu/MWCNT-GNP catalyst the H_2 generation rates was found as 40.50, 45.00 and 48.60 mmol/min.g_{cat} for 0.1, 0.2 and 0.3 M $NaBH_4$ respectively. According to the results acquired, the reaction rates for PdRu/MWCNT-GNP are higher compared to PdRu/MWCNT catalysts. The enhanced generation rate can be attributed to synergistic effects in MWCNT-GNP support, providing a better catalyst utilization and interaction.

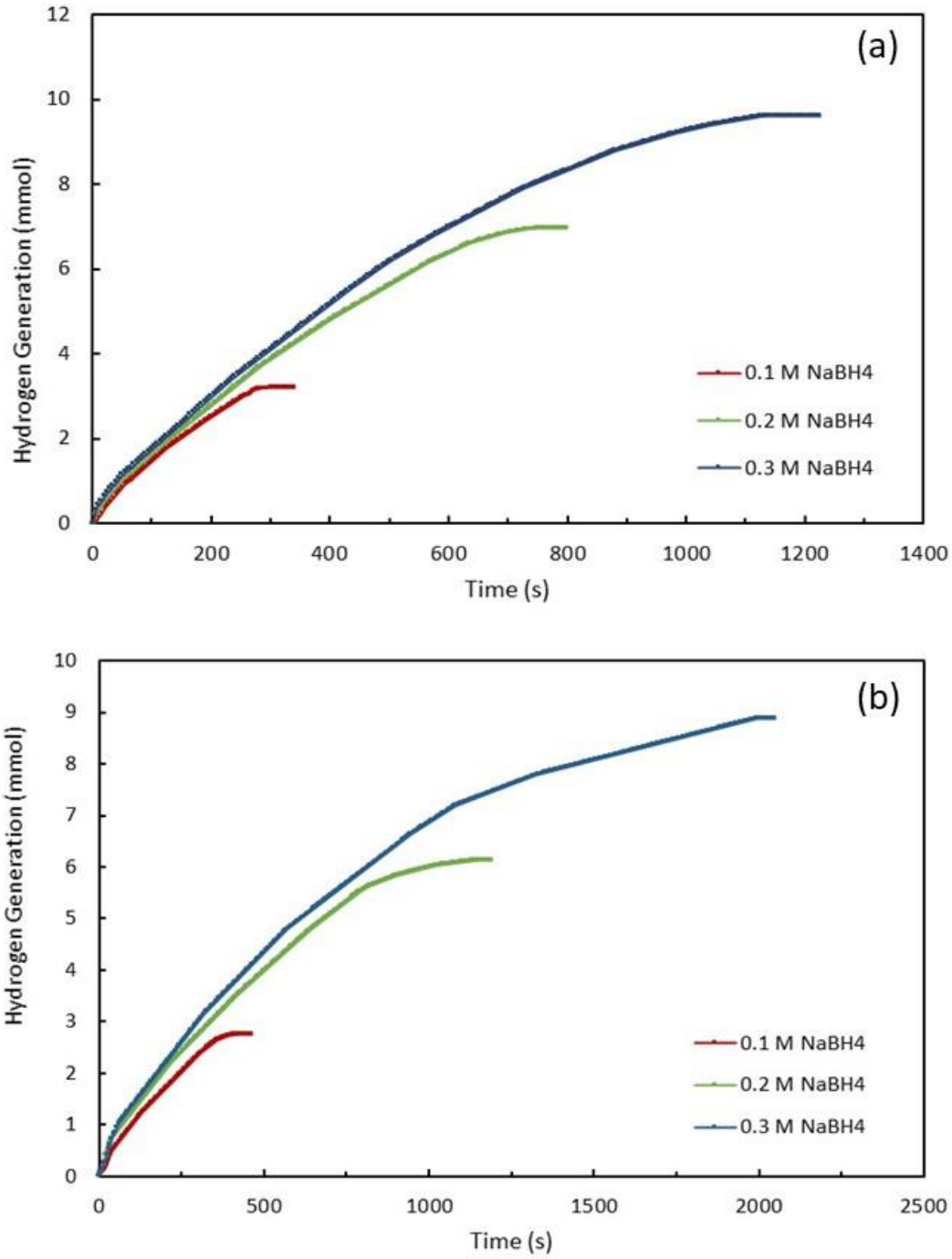

Figure 4.5 Effect of the concentration of $NaBH_4$ on H_2 generation using a) PdRu/MWCNT-GNP and b) PdRu/MWCNT catalyst at 25°C.

4.3.2 Effect of the Concentration NaOH on H_2 Generation

The $NaBH_4$ solution can be hydrolyze spontaneously when the pH value of the solution is lower than 9. The main reason for using NaOH in the solution medium is to increase the stability of a solution by preventing self-degradation of the $NaBH_4$. In addition,

NaOH concentration has a significant effect on the rate of hydrogen generation [149]. The kinetics of reactions vary from low to highly concentrated NaOH solutions. The rate is independent of NaOH concentration in highly basic (≥10 wt.% NaOH) aqueous solutions of $NaBH_4$, whereas the dependency decreases for lower-basic (< 10 wt.% NaOH) solutions, confirming the inhibition of NaOH hydrolysis kinetics [150].
Additionally

To examine the stabilization ability of NaOH on H_2 generation reactions, H_2 generation experiments were performed in the presence of different NaOH concentrations [151], [152]. Three experiments were performed in 0.2, 0.5 and 0.8 M NaOH for both catalysts with keeping the other parameters (0.2 M $NaBH_4$, 0.02 g catalyst, 25°C). Figure 4.6 and Figure 4.7 illustrate the effect of the NaOH concentration on H_2 generation for PdRu/MWCNT-GNP and PdRu/MWCNT catalysts, respectively.

According to the obtained results, the H_2 generation rates of the PdRu/MWCNT-GNP catalyst was obtained as 45, 40.8 and 36.0 mmol/min.g_{cat} for 0.2, 0.5 and 0.8 M NaOH, respectively. PdRu/MWCNT catalyst revealed reaction rates of 33.6, 29.1 and 18.3 mmol/min.g_{cat} for 0.2, 0.5 and 0.8 M NaOH, respectively. The highest reaction rate was achieved with 0.2 M NaOH for both catalysts. The pH of the solution increases with increasing NaOH concentration in the reaction, OH^- ions play an inhibitory role and cause a decrease in proton concentration. Using an excessive amount of NaOH also increases the basicity and consequently increases the viscosity of the reaction affecting the interaction between the catalyst and the chemical hydride [151]. By the increasing of the concentration of NaOH, OH^- is regarded as a reasonable adsorbate with BH_4^- for the catalyst surface. Thus the rate of hydrogen production decreases with escalation of OH^-, which occupies the adsorption sites, and interaction with the active components on the composite catalyst is unlikely for BH_4^- [149].

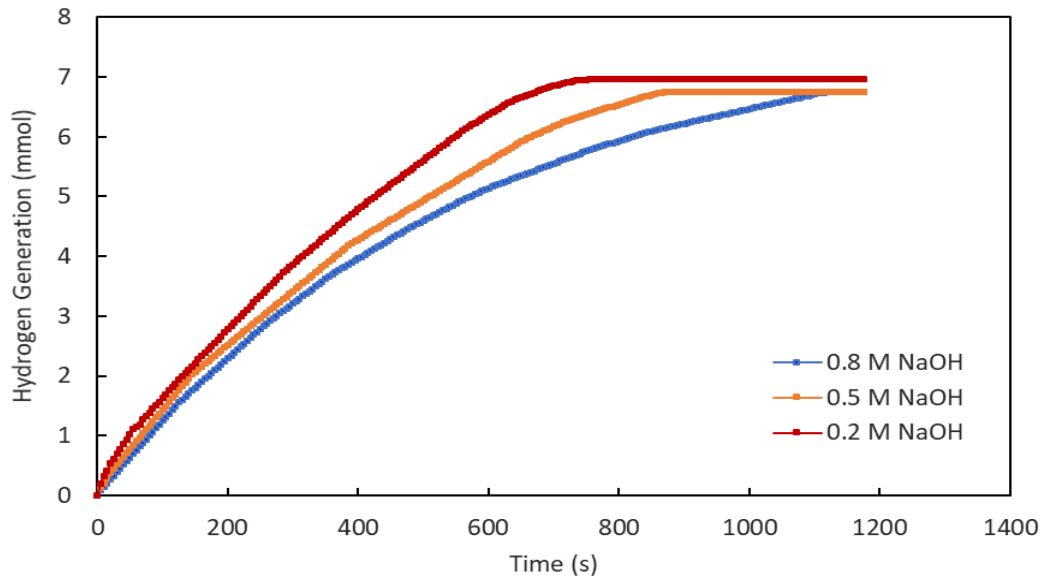

Figure 4.6 Effect of the NaOH concentration on H_2 generation for PdRu/MWCNT-GNP catalyst.

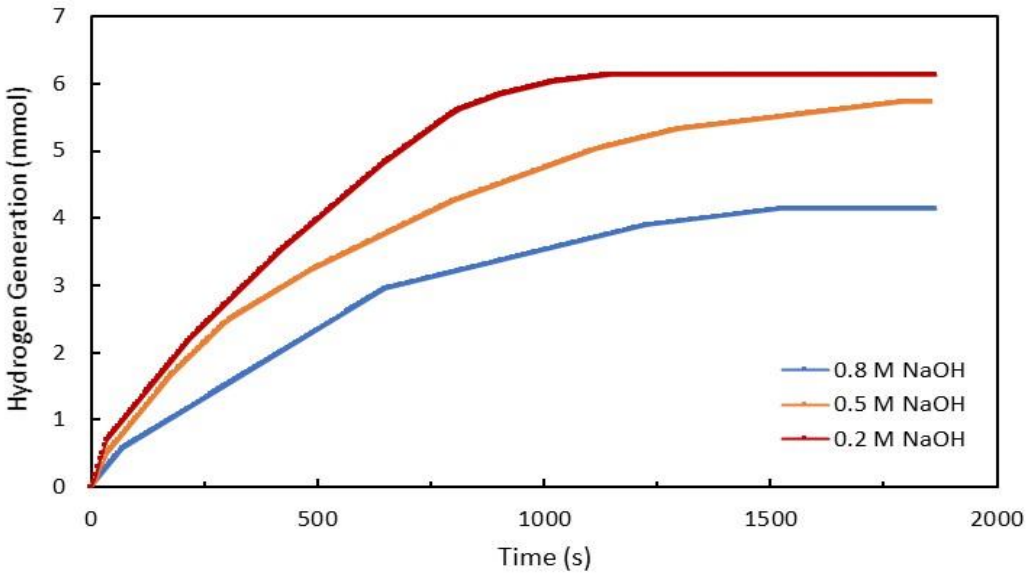

Figure 4.7 Effect of the NaOH concentration on H_2 generation for PdRu/MWCNT catalyst.

4.3.3 Effect of the Temperature on H_2 Generation

Three different temperatures (25, 35 and 45°C) were experimented to study the effect of the temperature on the H_2 generation and the reaction rate with fixing the other

experimental parameters (0.2 M $NaBH_4$, 0.2 M NaOH, 0.02 g catalyst). The effect of temperature on the H_2 generation is shown in Figure 4.8 and Figure 4.9 for PdRu/MWCNT-GNP and PdRu/MWCNT catalyst.

PdRu/MWCNT-GNP catalyst reaction rates were determined as 45, 65.1 and 79.2 mmol/min.g_{cat}. Besides, the reaction rates for the PdRu/MWCNT catalyst were determined as 33.6, 42.6 and 54.3 mmol/min.g_{cat} in 25, 35 and 45°C, respectively. Similar behavior was observed when changing the temperature for both catalysts. With increasing reaction temperature, the reaction viscosity of the solution decreases, so the flow resistance of the solution decreases causing an increase in the interaction between the reactant molecules increasing the reaction rates [153], [154]. Results also demonstrated that a superior H_2 generation rates were obtained from PdRu/MWCNT-GNP compared to PdRu/MWCNT. This behavior can be related to the higher surface area of the MWCNT-GNP support compared to the regular MWCNT [155].

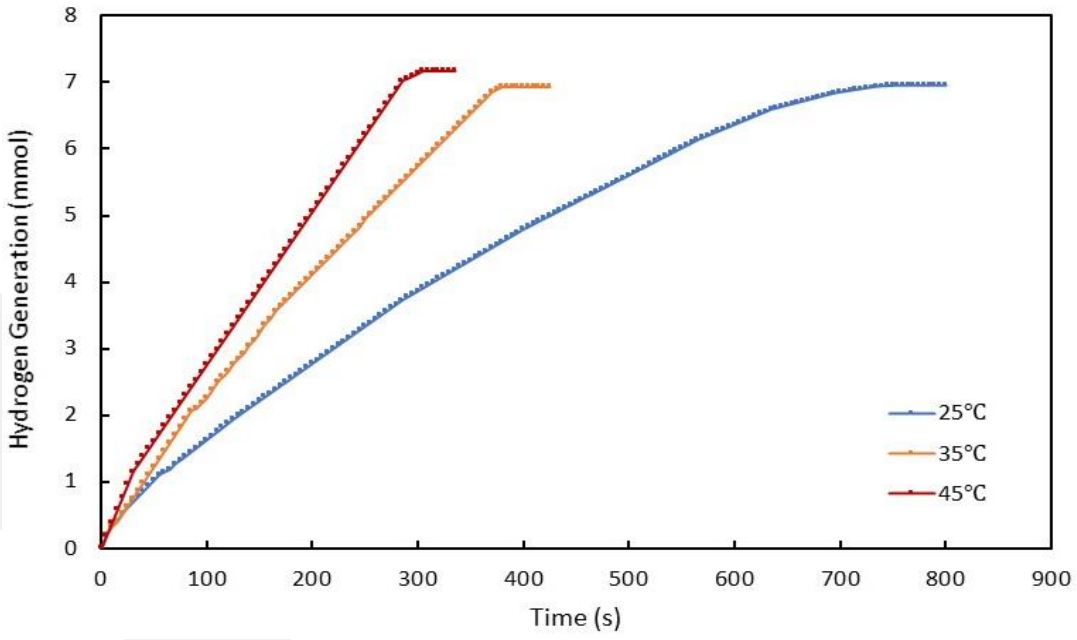

Figure 4.8 Effect of the reaction temperature on H_2 generation for PdRu/MWCNT-GNP catalyst.

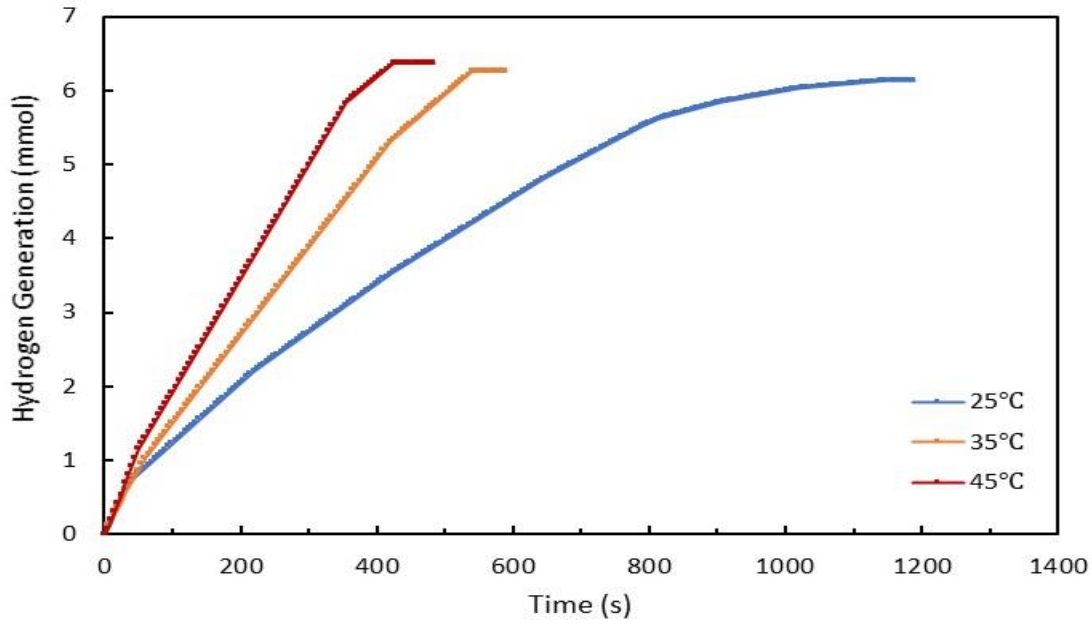

Figure 4.9 Effect of the reaction temperature on H_2 generation for PdRu/MWCNT catalyst.

4.3.4 Effect of the amount of the catalyst on H_2 Generation

Three different amounts of catalysts (0.01, 0.02 and 0.03 g) were examined to study the effect of the catalyst amount on the H_2 generation fixing the other reaction parameters (0.2 M $NaBH_4$, NaOH 0.2 M, 25^{o}C). The effect of catalyst amount on the H_2 generation for PdRu/MWCNT-GNP and PdRu/MWCNT catalysts is evident in Figure 4.10 and Figure 4.11, respectively.

The reaction rates were obtained as 21.3, 45, 51.3 mmol/min.g_{cat} for 0.01, 0.02, 0.03 g PdRu/MWCNT-GNP catalyst. In case of PdRu/MWCNT catalyst, the reaction rates were determined as 25.5, 33.6, 43.2 mmol/min.g_{cat} for 0.01, 0.02, 0.03 g catalyst. When the amount of the catalyst was increased, the H_2 generation and generation rate was increased. The increase can be related to the enhanced active sites presented by the higher amount of the catalyst.

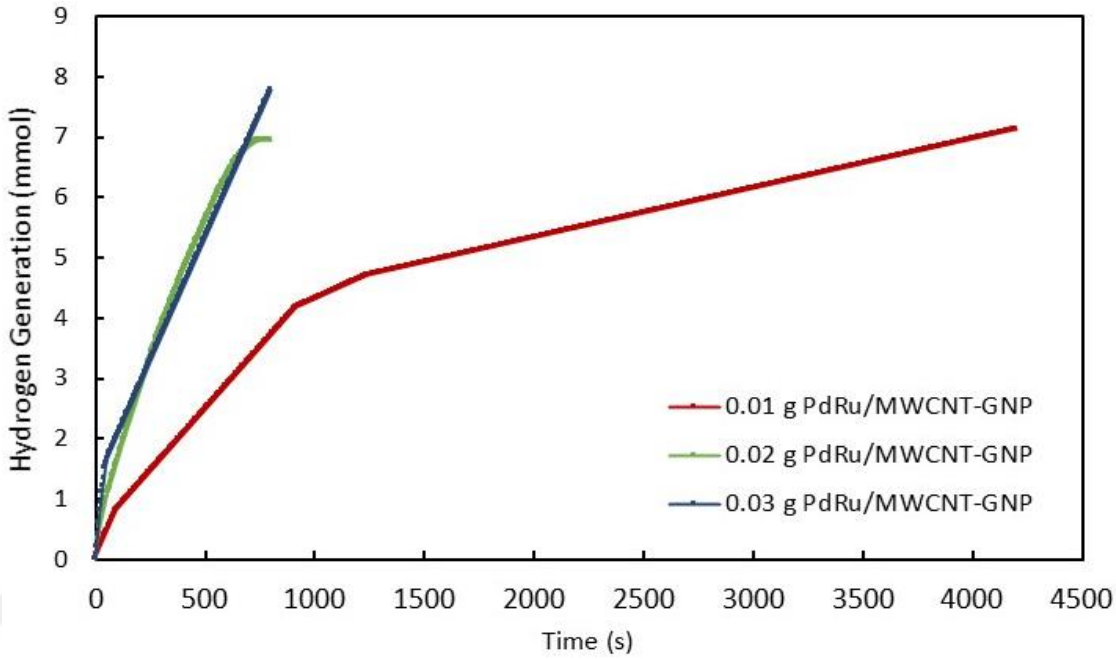

Figure 4.10 Effect of the catalyst mass on H_2 generation for PdRu/MWCNT-GNP catalyst.

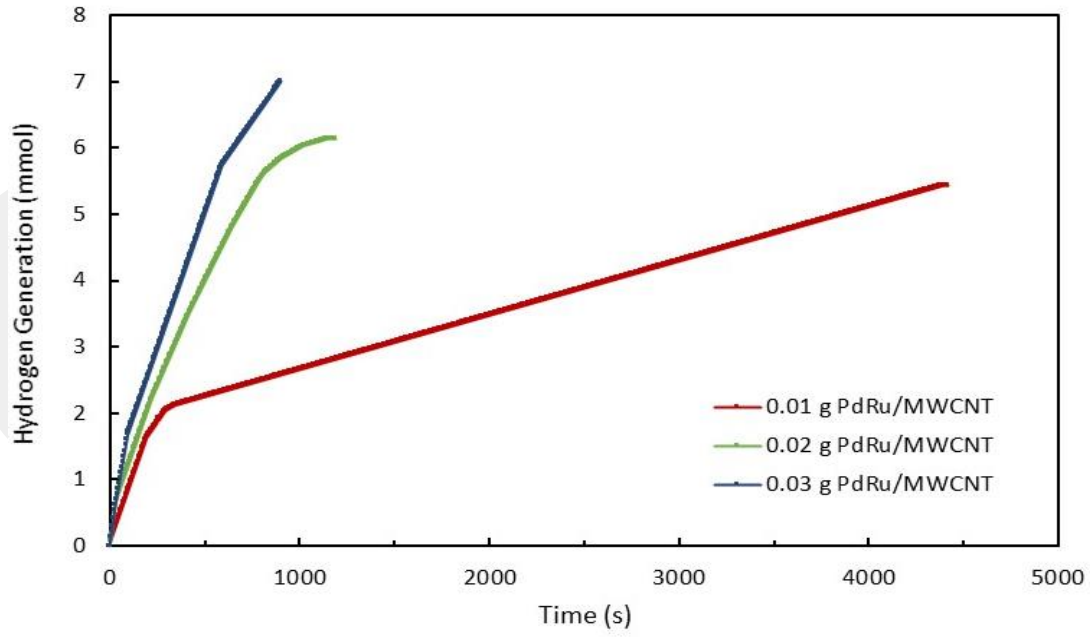

Figure 4.11 Effect of the catalyst mass on H_2 generation for PdRu/MWCNT catalyst.

4.4 Reusability Tests of the H_2 Generation Reaction

The powder catalyst and the catalyst supported on the gas diffusion layer were used to examine the reproducibility of the H_2 generation reaction. PdRu/MWCNT-GNP catalyst was selected for comparison experiments. The reaction parameters were kept during the experiments (25°C, 0.2 M $NaBH_4$, 0.2 M NaOH and 0.02 g of catalyst). The catalytic activity of PdRu/MWCNT-GNP catalyst was decreased at the end of four times of reusability test with approximately 87 % efficiency. The decrease in catalytic activity may be related to decreased activation at the catalyst surface and the reduced accessibility of active sites. Figures 4.12 and 4.13 illustrate the H_2 generation efficiencies of the powder PdRu/MWCNT-GNP and the GDL supported PdRu/MWCNT-GNP catalyst after reusability tests.

Compared with the powder catalyst, it appears that the PdRu/MWCNT-GNP catalyst supported on GLD retains its 89 % efficiency even after the 4th use. Correspondingly, the reusability efficiency was found to be better in the supported catalyst, as the catalytic loss was lower.

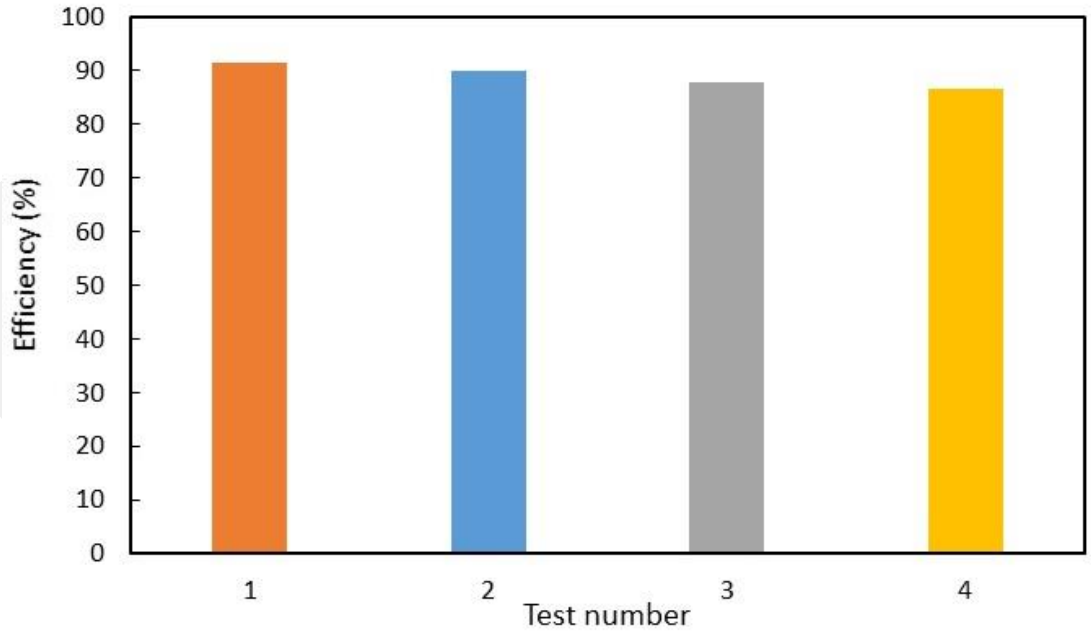

Figure 4.12 The efficiencies of reusability experiments of powder PdRu/MWCNT-GNP.

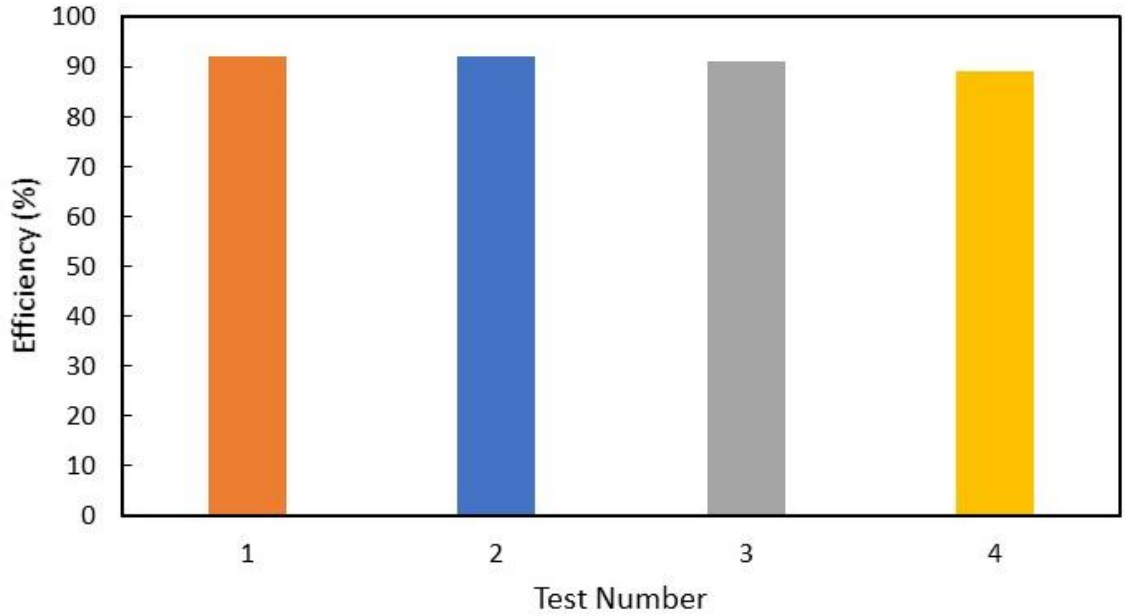

Figure 4.13 The efficiencies of reusability experiments of GDL PdRu/MWCNT-GNP.

4.5 Kinetic Studies

One of the objectives of this research is to examine the kinetic calculations for finding the Ea of the H_2 generation from the hydrolysis of $NaBH_4$ with the use of the PdRu/MWCNT and PdRu/MWCNT-GNP catalysts. The rate expression in terms of $NaBH_4$ concentration and temperature can be given as follows [151]:

$$r_{H_2} = kC_{NaBH_4}{}^{a} \tag{22}$$

Equation (23) was obtained when the natural logarithm is taken for both sides of Equation (22):

$$\ln(r_{H_2}) = lnk + \alpha lnC_{NaBH_4} \tag{23}$$

Figure 4.14 and 4.15 shows the $\ln(r_{H_2})$ versus lnC_{NaBH_4} for PdRu/MWCNT-GNP and PdRu/MWCNT catalysts, respectively. The activation energy of the PdRu/MWCNT-GNP and PdRu/MWCNT catalysts was determined by using Equation (24), which is derived from the Arrhenius Equation:

$$k = Ae^{E_a/RT} \tag{24}$$

$$lnk = lnA - \frac{E_a}{R}\frac{1}{T} \quad (25)$$

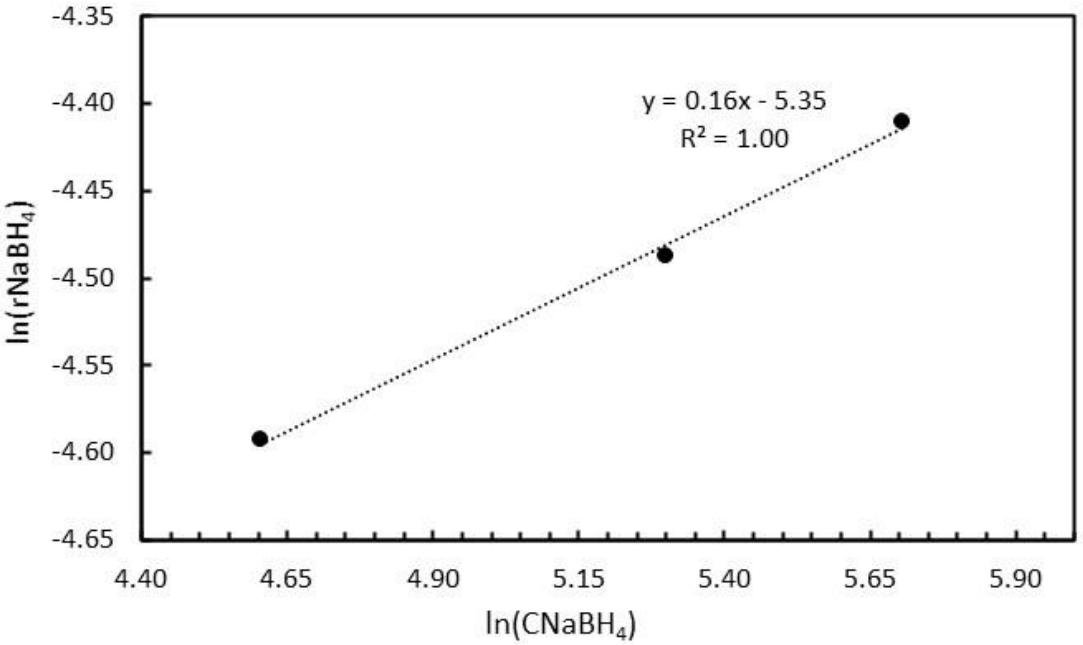

Figure 4.14 $\ln(r_{H_2})$ versus lnC_{NaBH_4} for PdRu/MWCNT-GNP catalyst.

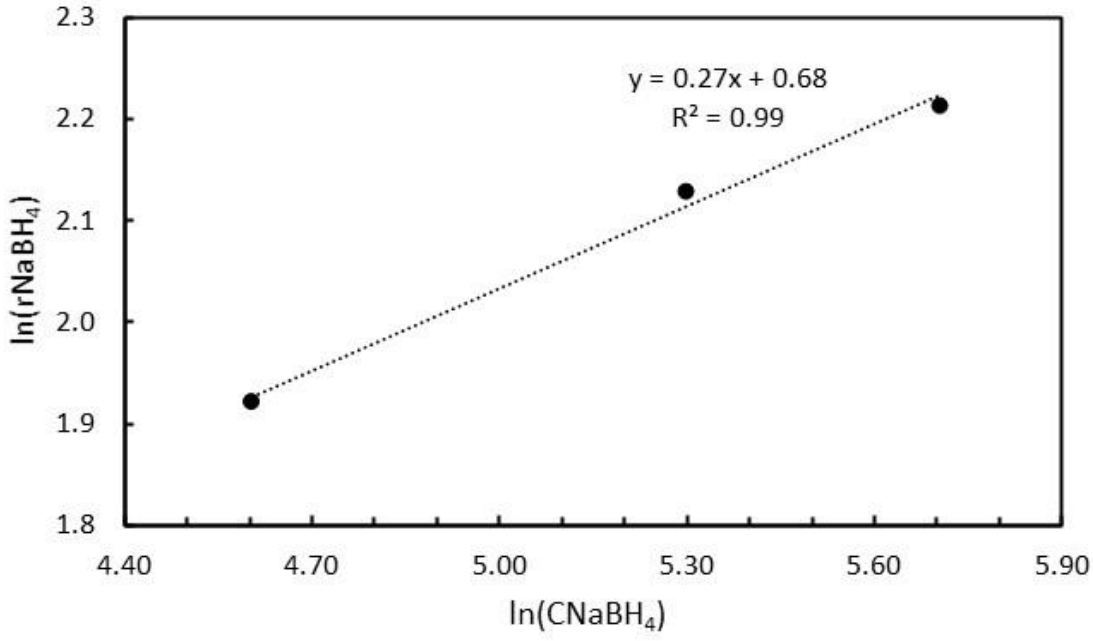

Figure 4.15 $\ln(r_{H_2})$ versus lnC_{NaBH_4} for PdRu/MWCNT catalyst.

Figure 4.16 and 4.17 illustrates the Arrhenius plot of ln(k) versus 1/T for PdRu/MWCNT-GNP and PdRu/MWCNT catalysts, respectively. The Ea and A of the PdRu/MWCNT-GNP and PdRu/MWCNT catalysts were calculated from the slope and the intercept points of the line.

By setting the R in Ea/R, the activation energies of catalytic hydrolysis of $NaBH_4$ reaction were calculated from the slope of the straight lines for PdRu/MWCNT-GNP and PdRu/MWCNT catalyst as 22.33 kJ/mol and 18.90 kJ/mol, respectively.

The reaction rate for H_2 generation reaction rate can be found from Equation (26) and Equation (27) according to the concentration of the $NaBH_4$ and temperature of the reaction showing the orders of 0.165 and 0.27 for PdRu/MWCNT-GNP catalyst and PdRu/MWCNT catalyst, respectively:

$$r_{H_2} = 15.87 \times 10^4 e^{-\frac{2686.5}{T}} C_{NaBH_4}^{0.165} \left(\frac{mmol}{min.g_{cat}}\right), R^2 = 0.98 \quad (26)$$

$$r_{H_2} = 16.43 \times 10^4 e^{-\frac{2273.3}{T}} C_{NaBH_4}^{0.270} \left(\frac{mmol}{min.g_{cat}}\right), R^2 = 0.99 \quad (27)$$

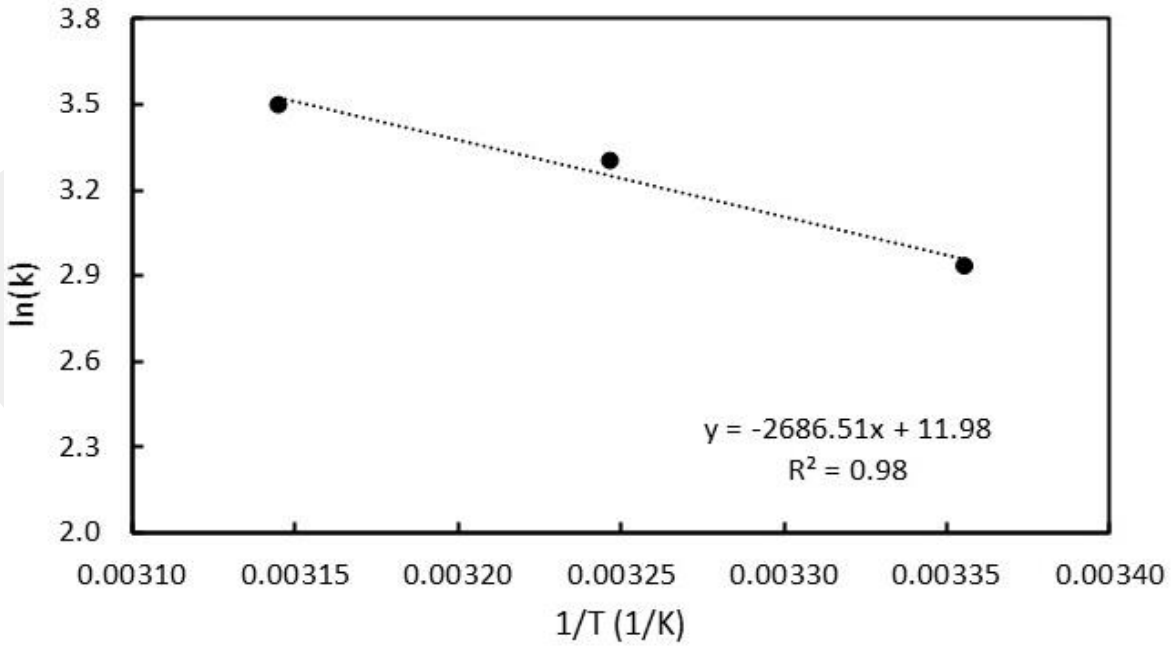

Figure 4.16 The slope of a straight line for PdRu/MWCNT-GNP catalyst.

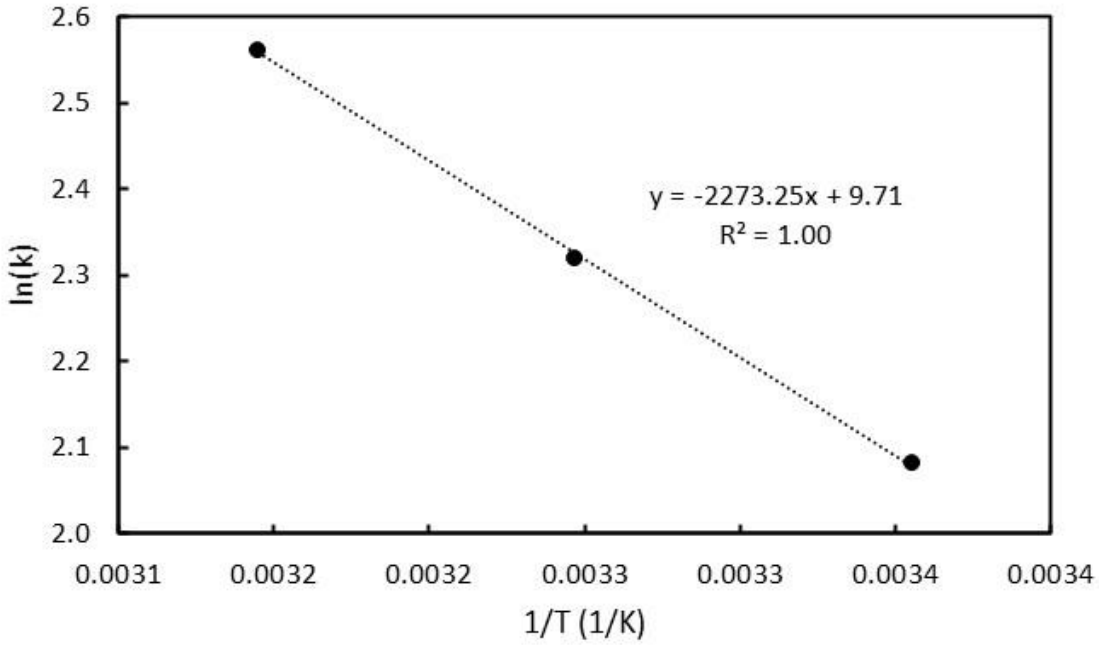

Figure 4.17 The slope of a straight line for PdRu/MWCNT catalyst.

According to those results, the hydrolysis reaction with PdRu/MWCNT-GNP catalyst is more efficient and controllable than PdRu/MWCNT catalyst. The activation energies are also on good terms. The PdRu/MWCNT-GNP catalyst exhibited higher catalytic activity in H_2 generation than PdRu/MWCNT catalyst, owing to the homogeneous dispersion of PdRu bimetallic particles on the support material MWCNT-GNP, in addition to MWCNT-GNP having a higher surface area, providing more active sites for the reaction.

Table 4.2 and Table 4.3 show the H_2 generation rates, efficiency and TOF values of the PdRu/MWCNT-GNP and PdRu/MWCNT catalysts at different experimental conditions, respectively. TOF (turnover frequency) is define as the number of moles of product per mole of catalyst per time. TOF values were calculated according to the volume of released H_2 in overall test period.

Table 4.2 Calculations for H_2 generation rates, efficiency and TOF values of the PdRu/MWCNT-GNP catalyst.

Exp. No.	**M_{NaBH4} (M)**	**M_{NaOH} (M)**	**Catalyst (g)**	**T (K)**	**r_{H2} (mmol/(min.g_{cat})**	**η (%)**	**TOF (mol $_{H2}$/mol_{cat}.min)**
1	0.1	0.2	0.02	298	40.5	80	44.1
2	0.2	0.2	0.02	298	45.0	87	38.2
3	0.3	0.2	0.02	298	48.6	80	35.0
4	0.2	0.8	0.02	298	36.0	82	30.9
5	0.2	0.5	0.02	298	40.8	87	25.5
6	0.2	0.2	0.02	308	65.1	87	75.6
7	0.2	0.2	0.02	318	79.2	90	97.5
8	0.2	0.2	0.01	298	21.3	90	7.1
9	0.2	0.2	0.03	298	51.3	91	37.6

Table 4.3 Calculations for H_2 generation rates, efficiency and TOF values of the PdRu/MWCNT catalyst.

Exp. No.	**M_{NaBH4} (M)**	**M_{NaOH} (M)**	**Catalyst (g)**	**T (K)**	**r_{H2} (mmol/(min.g_{cat})**	**η (%)**	**TOF (mol $_{H2}$/mol_{cat}.min)**
1	0.1	0.2	0.02	298	27.3	69	27.0
2	0.2	0.2	0.02	298	33.6	77	22.1
3	0.3	0.2	0.02	298	36.6	74	18.5
4	0.2	0.8	0.02	298	18.3	52	9.5
5	0.2	0.5	0.02	298	32.4	72	16.0
6	0.2	0.2	0.02	308	42.6	78	48.1
7	0.2	0.2	0.02	318	54.3	80	62.1
8	0.2	0.2	0.01	298	25.5	68	5.1
9	0.2	0.2	0.03	298	43.2	87	32.3

Activation energies and TOF values of different catalysts used for hydrolysis of NaBH4 in the literature are listed in Table 4.4. According to the obtained results, the PdRu/MWCNT and PdRu/MWCNT-GNP catalysts activation energies are in good agreement with the previously reported results. These catalysts can also be considered as a appreciate catalyst due to their low activation energy and high TOF values.

Table 4.4 Various catalyst types used mostly in literature for $NaBH_4$ hydrolysis reaction.

No.	Catalyst	Ea (kJ/mol)	TOF (mol $_{H2}$/mol$_{cat}$.min)	Ref.
1	PdRu/MWCNT	18.9	62.1	This study
2	PdRu/MWCNT-GNP	22.33	97.5	This study
3	Pd/PD-ZIF-67	58.5	495	[156]
4	Co-Ce-B/Chi-C	33.1	23.6	[157]
5	1.2-BE-p(VI)-Co	33.19	34.4	[158]
6	Ru(0) Nanocluster	28.5	474	[159]
7	HPO_4^{2-}/Ni(0) nanoclusters	54.5	6.04	[160]
8	Ru(0)/X-NW	75	305	[161]
9	Poly(vinylidene fluoride)-Ni	49.3	55.6	[162]
10	Pt-Ru@PVP NPs	63.2	549	[163]
11	p(HEMA)-Co	37.01	3.84	[164]
12	Co–Cu–B(5%(wt))/rGO	36.76	66.88	[165]
13	Mn/CeO_2	43	6.95	[166]
14	CHNA/Ti	39.78	3.03	[167]

4.6 PEMFC Test Performance Tests

$NaBH_4$ based H_2 generation system integrated to the PEMFC. Before $NaBH_4$ system integration to the PEMFC, tests were performed with pure H_2 for comparison. PEMFC test was examined in a PEMFC fixture which has the active area of 5 cm^2, working temperature is 65°C. For PEMFC tests, air flow rate of was kept constant at 0.25 L/min for all experiments. H_2 was humidified during the PEMFC test. Figure 4.18 shows the PEMFC performance test results with pure H_2 and Air as a reactant gas at 65°C oper-

ating temperature. According to the obtained results, the current density was determined as 0.38 A/cm^2 @ 0.6 V working voltage. Additionally, maximum power density was obtained as 0.33 W/cm^2 at 0.82 A/cm^2 current density. After the PEMFC had stabilized, it was kept constant at 0.6 V operating voltage for $NaBH_4$ hydrolysis system integration.

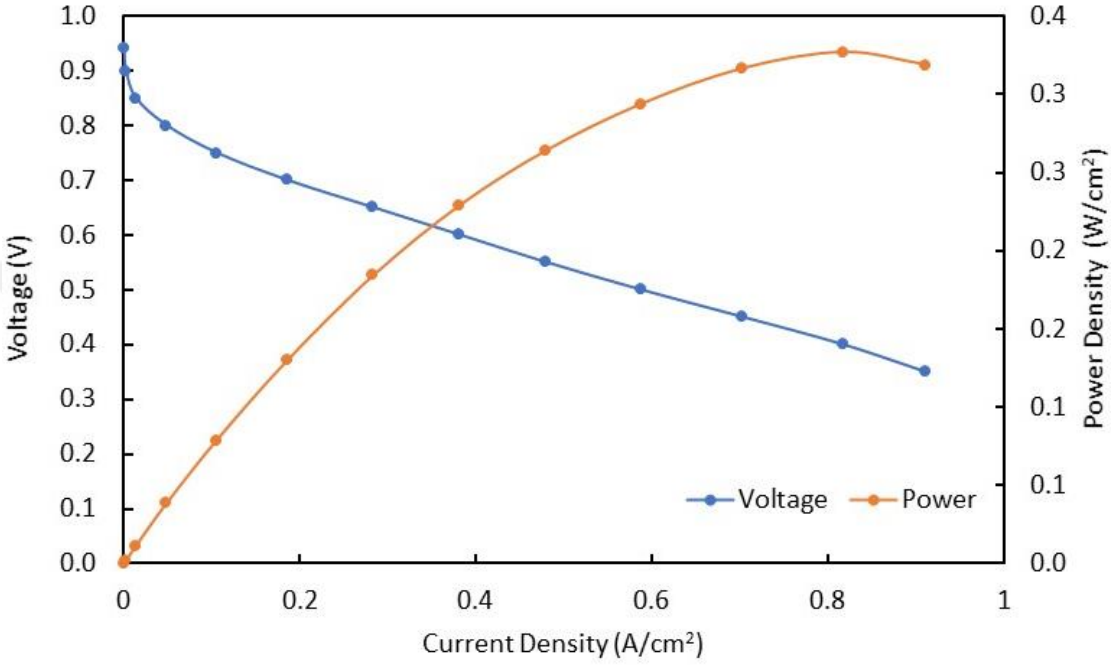

Figure 4.18 PEMFC performance at 65ºC with pure H_2 and Air as a reactant gas.

For $NaBH_4$ integration the required amount of H_2 was calculated from Faraday's law according to Equation (28) as shown in below:

$$\dot{n}_{H_2} = S_{H_2} \times \frac{i \times A}{n \times F} \times N_{cell} \tag{28}$$

Where, $\dot{n}_{H_2}$ is the H_2 molar flow rate, S_{H_2} is stoichiometric ratio, i is current density (A/cm^2), A is the active area (cm^2), N_{cell} is number of cells, n is electron number (for H_2 n=2) and and F is Faraday constant (96485 C/mol). S_{H_2} is given as 4 due to the single cell operation. For 15 min PEMFC working; 0.123 mol H_2 is required in PEMFC to obtain 0.38 A/cm^2 @0.6 V. 1.335 g of $NaBH_4$ was placed in the reactor with 0.48 g PdRu/MWCNT-GNP catalyst. The efficiency of the reaction was given as 87 % according to the Table 4.2.

Figure 4.19 illustrates the PEMFC operation of the $NaBH_4$ hydrolysis system that was composed of PdRu/MWCNT-GNP catalyst. When the $NaBH_4$ hydrolysis system was integrated into PEMFC, the same performance was obtained as pure H_2 PEMFC performance, it did not change due to the moisture content of the hydrogen obtained from the hydrolysis reaction. As a result of the tests, 0.38 A/cm^2 constant current density was obtained with H_2 gas fed from the $NaBH_4$ system for 15 minutes. After 15 min the PEMFC performance was decreased suddenly due to the lack of H_2.

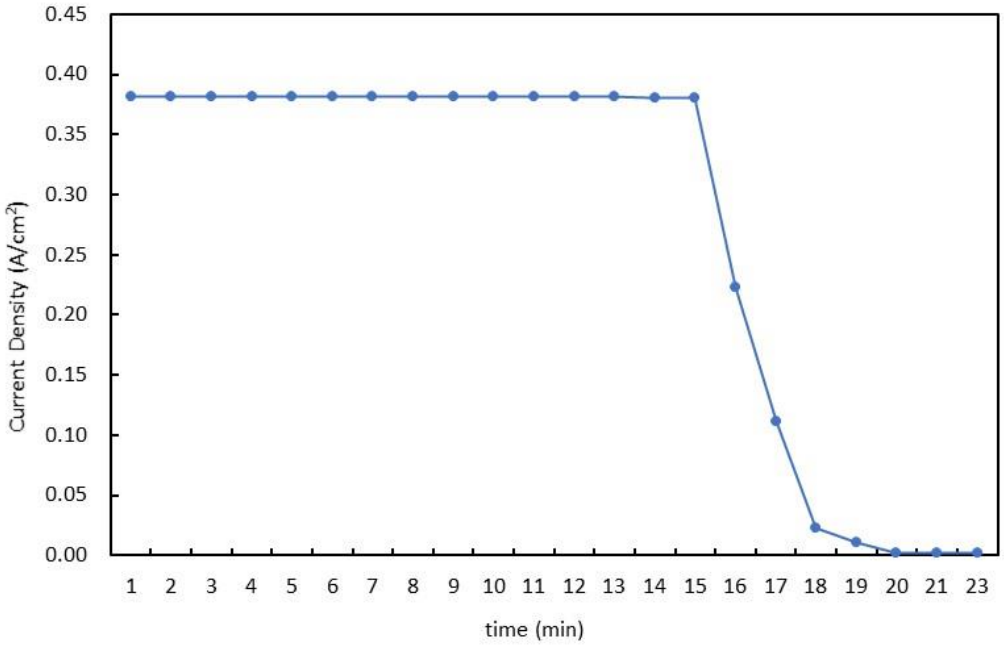

Figure 4.19 PEMFC performance at 65ºC with $NaBH_4$ based H_2 and Air as a reactant gas for PdRu/MWCNT-GNP catalyst (0.2 M $NaBH_4$, 0.2 M NaOH and 0.027 g catalyst).

CHAPTER 5

CONCLUSIONS

This study investigated the H_2 production from the hydrolysis of solid $NaBH_4$ using MWCNT-GNP and MWCNT as support materials for Pd:Ru nanoparticles. The catalysts were synthesized via the microwave-assisted approach at 600 W, 60 s.

Various parameters like concentration of $NaBH_4$, concentration of NaOH, temperature of the reaction and catalyst amount were investigated for the hydrolysis of $NaBH_4$. It was concluded that the increasing of $NaBH_4$ concentration increases the H_2 production rates for PdRu/MWCNT-GNP and PdRu/MWCNT catalysts. Increasing NaOH concentration raises the viscosity of the reaction downgrading the catalytic activity by blocking the interaction between the catalyst and $NaBH_4$. Raising the temperature exhibited increasing in the H_2 generation rates by intensifying the interaction between the reaction materials, making the reaction faster and more challenging to control. Additionally, increasing the catalyst amount increases the efficiency of both catalysts. A kinetic study was made for H_2 generation from hydrolysis of $NaBH_4$. The activation energies were found as 22.33 and 18.9 kJ/mol for PdRu/MWCNT-GNP and PdRu/MWCNT, respectively. The highest H_2 generation rate for PdRu/MWCNT-GNP was 79.2 mmol/min.g_{cat} and a TOF value 97.5 mol_{H2}/mol_{cat}.min at 0.2 M $NaBH_4$ and 45°C. The highest H_2 generation rate for PdRu/MWCNT was 54.3 mmol/min.g_{cat} and the TOF value was 62.1 mol_{H2}/mol_{cat}.min also at 0.2 M $NaBH_4$ and 45°C. PdRu/MWCNT-GNP presented higher catalytic activity than PdRu/MWCNT, and this may be attributed to the higher surface area that MWCNT-GNP possesses, meaning more active sites and enhancing the activity of the metal catalyst.

A reusability test was executed with PdRu/MWCNT-GNP catalyst powder and supported on GDL examining the reproducibility of H_2 generation. PdRu/MWCNT-GNP supported on GDL showed an excellent ability to retain its efficiency of 89 % even after the 4^{th} use, probably due to the lower catalytic loss compared to the powder catalyst.

TGA indicated that the two catalysts exhibited good thermal stability. XRD analysis was made to evaluate the crystallite size and crystallite structure for both catalysts. XRD results confirmed that PdRu/MWCNT-GNP has a crystallite size of 1.55 nm, smaller than the crystallite size of PdRu/MWCNT whic is equal to 2.01 nm.

CV measurements were used to establish the ECSA of the catalysts. CV showed that PdRu/MWCNT-GNP catalyst possesses a higher ECSA than that of the PdRu/MWCNT catalyst, PdRu/MWCNT-GNP also showed a slightly higher ECSA loss after 1000 cycles. However, the final ECSA for PdRu/MWCNT-GNP is higher than the initial ECSA for PdRu/MWCNT, confirming high stability and durability. The SSA was also calculated for both catalysts and showed that PdRu/MWCNT-GNP possesses a higher SSA than the SSA of PdRu/MWCNT. Consequently, PdRu/MWCNT-GNP seems to have a better electrocatalytic activity because of the synergistic interaction between Pd and Ru particles on MWCNT-GNP support.

PEMFC performance test of the $NaBH_4$ based H_2 generation system integrated to the PEMFC with pure H_2 to compare the H_2 supply from developed solid $NaBH_4$ system at an operating temperature of 65°C. The maximum power density was determined as 0.33 W/cm^2 at 0.82 A/cm^2 current density. When the $NaBH_4$ hydrolysis system was integrated into PEMFC, the same performance was obtained as pure H_2 PEMFC performance.

To sum up everything that has been stated so far, PdRu/MWCNT-GNP bimetallic catalyst is a more suitable catalyst for hydrolysis of $NaBH_4$ and applications of PEMFC due to the high catalytic activity, durability, high efficiency, owing to the synergistic effect of the bimetallic catalyst and the improved hybrid structure of MWCNT-GNP.

REFERENCES

[1] A.H. Awad and T. N. Veziroğlu, "Hydrogen versus synthetic fossil fuels," *International journal of hydrogen energy*, vol. 9, no. 5, pp. 355–366, 1984.

[2] J. M. Ogden, "Prospects for building a hydrogen energy infrastructure," *Annu. Rev. Energy Environ.*, vol. 24, pp. 227–279, 1999.

[3] J. Zhang, T. S. Fisher, J. P. Gore, D. Hazra and P. V. Ramachandran, "Heat of reaction measurements of sodium borohydride alcoholysis and hydrolysis," *International journal of hydrogen energy*, vol. 31, no. 15, pp. 2292–2298, 2006.

[4] L. Schlapbach and A. Züttel, "Hydrogen-storage materials for mobile applications," *Nature*, vol. 414, pp. 353–358, 2001.

[5] P. Brack, S. E. Dann and K. W. Wijayantha, "Heterogeneous and homogenous catalysts for hydrogen generation by hydrolysis of aqueous sodium borohydride ($NaBH_4$) solutions," *Energy Science & Engineering*, vol. 3, no. 3, pp. 174–188, 2015.

[6] D. Mori and K. Hirose, "Recent challenges of hydrogen storage technologies for fuel cell vehicles," *Int. J. Hydrogen Energy*, vol. 34, no. 10, pp. 4569–4574, 2009.

[7] J. Zhang, T. S. Fisher, P. V. Ramachandran, J. P. Gore and I. Mudawar, "A review of heat transfer issues in hydrogen storage technologies," *J. Heat Transfer*, vol. 127, no. 12, pp. 1391–1399, 2005.

[8] C. Yang, J. M. Ogden, R. Hwang and D. Sperling, California's Energy Future: Transportation Energy Use in California, California: California Council on Science and Technology, California, 2011.

[9] U. B. Demirci and P. Miele, "Sodium tetrahydroborate as energy/hydrogen carrier, its history," *Comptes Rendus Chimie*., vol. 12, no. 9, pp. 943–950, 2009.

[10] T. Sadhasivam, H. T. Kim, S. Jung, S. H. Roh, J. H. Park and H. Y. Jung, "Dimensional effects of nanostructured Mg/MgH_2 for hydrogen storage applications: A review," *Renew. Sustain. Energy Rev.*, vol. 72, pp. 523–534, 2017.

[11] A. M. Murshed, B. Huang and K. Nandakumar, "Estimation and control of solid oxide fuel cell system," *Computers & chemical engineering*, vol. 34, no. 1, pp. 96–111, 2010.

[12] C. K. Dyer, "Fuel cells for portable applications," *Journal of Power Sources*, vol. 106, no. 1–2, pp. 31–34, 2002.

[13] B. H. Liu, Z. P. Li and S. Suda, "Solid sodium borohydride as a hydrogen source for fuel cells," *Journal of Alloys and Compounds*, vol. 468, no. 1–2, pp. 493–

498, 2009.

[14] B. Peng and J. Chen, "Functional materials with high-efficiency energy storage and conversion for batteries and fuel cells," *Coordination Chemistry Reviews*, vol. 253, no. 23–24, pp. 2805–2813. 2009.

[15] K. B. Prater, "Polymer electrolyte fuel cells: a review of recent developments," *Journal of Power Sources.*, vol. 51, no. 1–2, pp. 129–144, 1994.

[16] O. Z. Sharaf and M. F. Orhan, "An overview of fuel cell technology: Fundamentals and applications," *Renew. Sustain. Energy Rev.*, vol. 32, pp. 810–853, 2014.

[17] W. R. Grove, " XXIV. On voltaic series and the combination of gases by platinum ," *London, Edinburgh, Dublin Philos. Mag. J. Sci.*, vol. 14, no. 86–87, pp. 127–130, 1839.

[18] G. Couture, A. Alaaeddine, F. Boschet, and B. Ameduri, "Polymeric materials as anion-exchange membranes for alkaline fuel cells," *Progress in Polymer Science*, vol. 36, no. 11, pp. 1521-1557, 2011.

[19] K. Prater, "The renaissance of the solid polymer fuel cell," *J. Power Sources*, vol. 29, no. 1, pp. 239–250, 1990.

[20] C. A. C. Sequeira P. S. D. Brito, A. F. Mota, J. L. Carvalho, L. F. F. T. T. G. Rodrigues, D. M. F. Santos, D. B. Barrio and D. M. Justo, "Fermentation, gasification and pyrolysis of carbonaceous residues towards usage in fuel cells," *Energy Convers. Manag.*, vol. 48, no. 7, pp. 2203–2220, 2007.

[21] M. Nadal and F. Barbir, "Development of a hybrid fuel cell/battery powered electric vehicle," *Int. J. Hydrogen Energy*, vol. 21, no. 6, pp. 497–505, 1996.

[22] G. Merle, M. Wessling and K. Nijmeijer, "Anion exchange membranes for alkaline fuel cells: A review," *Journal of Membrane Science*, vol. 377, no. 1–2, pp. 1–35, 2011.

[23] J.M. Andújar and F. Segura, "Fuel cells: History and updating. A walk along two centuries," *Renewable and sustainable energy reviews*, vol. 13, no. 9, pp. 2309-2322, 2009.

[24] S. Mekhilef, R. Saidur and A. Safari, "Comparative study of different fuel cell technologies," *Renew. Sustain. Energy Rev.*, vol. 16, no. 1, pp. 981–989, 2012.

[25] G. F. McLean, T. Niet, S. Prince-Richard and N. Djilali, "An assessment of AFC technology," *Int. J. Hydrogen Energy*, vol. 27, pp. 507–526, 2002.

[26] P. Breeze, "The Phosphoric Acid Fuel Cell," in *Fuel Cells*, Massachusetts: Academic Press, pp. 45–51, 2017.

[27] P. Breeze, "Fuel Cells," in *Power Generation Technologies.*, 3rd edition, pp.

145–171, 2019.

[28] J. D. Holladay, J. Hu, D. L. King and Y. Wang, An “overview of hydrogen production technologies,” *Catalysis today*, vol. 139, no. 4, pp. 244–260, 2009.

[29] A. Iwan, M. Malinowski and G. Pasciak, “Polymer fuel cell components modified by graphene: Electrodes, electrolytes and bipolar plates,” *Renew. Sustain. Energy Rev.*, vol. 49, pp. 954–967, 2015.

[30] E. Mancusi, É. Fontana, A. A. Ulson De Souza and S. M. A. Guelli Ulson De Souza, “Numerical study of two-phase flow patterns in the gas channel of PEM fuel cells with tapered flow field design,” *Int. J. Hydrogen Energy*, vol. 39, no. 5, pp. 2261-2273, 2014.

[31] A. B. Stambouli and E. Traversa, “Fuel cells, an alternative to standard sources of energy,” *Renewable and sustainable energy reviews*, vol. 6, no. 3, pp. 295-304, 2002.

[32] M. Khakpour and K. Vafai, “Analysis of transport phenomena within PEM fuel cells - An analytical solution,” *Int. J. Heat Mass Transf.*, vol. 51, no. 15-16, pp. 3712-3723, 2008.

[33] D. Chen, C. Chen, Z. M. Baiyee, Z. Shao and F. Ciucci, “Nonstoichiometric oxides as low-cost and highly-efficient oxygen reduction/evolution catalysts for low-temperature electrochemical devices,” *Chemical reviews*, vol. 115, no. 18, pp. 9869-9921, 2015.

[34] Y. Devrim, A. Albostan, and H. Devrim, “Experimental investigation of CO tolerance in high temperature PEM fuel cells,” *Int. J. Hydrogen Energy*, vol. 43, no. 40, pp. 18672–18681, 2018.

[35] N. A. H. Rosli, K. S. Loh, W. Y. Wong, R. M. Yunus, T. K. Lee, A. Ahmad and S. T. Chong, “Review of Chitosan-Based Polymers as Proton Exchange Membranes and Roles of Chitosan-Supported Ionic Liquids,” *Int. J. Mol. Sci.*, vol. 21, pp. 1–632, 2020.

[36] M. M. Nasef, "Radiation-grafted membranes for polymer electrolyte fuel cells: current trends and future directions," *Chemical reviews*, vol. 114, no. 24, pp. 12278-12329, 2014.

[37] F. Barbir, "PEM Fuel Cells," In *Fuel Cell Technology*, London: Springer, 2006, pp. 27-51.

[38] T. Maiyalagan and S. Pasupathi, “Components for PEM fuel cells: An overview,” *Mater. Sci. Forum*, vol. 657, pp. 143–189, 2010.

[39] Y. Devrim and A. Albostan, “Enhancement of PEM fuel cell performance at higher temperatures and lower humidities by high performance membrane electrode assembly based on Nafion/zeolite membrane,” *Int. J. Hydrogen Energy*, vol. 40, no. 44, pp. 15328–15335, 2015.

[40] Y. Özdemir, N. Özkan and Y. Devrim, "Fabrication and Characterization of Cross-linked Polybenzimidazole Based Membranes for High Temperature PEM Fuel Cells," *Electrochim. Acta*, vol. 245, pp. 1–13, 2017.

[41] R. Zeis, "Materials and characterization techniques for high-temperature polymer electrolyte membrane fuel cells," *Beilstein J. Nanotechnol.*, vol. 6, no. 1, pp. 68–83, 2015.

[42] Y. Devrim, E. D. Arıca, and A. Albostan, "Graphene based catalyst supports for high temperature PEM fuel cell application," *Int. J. Hydrogen Energy*, vol. 43, no. 26, pp. 11820–11829, 2018.

[43] J. L. Jespersen, E. Schaltz and S. K. Kær, "Electrochemical characterization of a polybenzimidazole-based high temperature proton exchange membrane unit cell," *J. Power Sources*, vol. 191, no. 2, pp. 289–296, 2009.

[44] F. Ublekov, H. Penchev, V. Georgiev, I. Radev and V. Sinigersky, "Protonated montmorillonite as a highly effective proton-conductivity enhancer in p-PBI membranes for PEM fuel cells," *Mater. Lett.*, vol. 135, pp. 5–7, 2014.

[45] A. Suzuki, U. Sen, T. Hattori, R. Miura, R. Nagumo, H. Tsuboi, N. Hatakeyama, A. Endou, H. Takaba, M. C. Williams and A. Miyamoto, "Ionomer content in the catalyst layer of polymer electrolyte membrane fuel cell (PEMFC): Effects on diffusion and performance," *International Journal of Hydrogen Energy*, vol. 36, no. 3, pp. 2221–2229, 2011.

[46] M. W. Verbrugge and R. F. Hill, "Ion and Solvent Transport in Ion-Exchange Membranes: I. A Macrohomogeneous Mathematical Model," *J. Electrochem. Soc.*, vol. 137, no. 3, pp. 886–886, 1990.

[47] S. T. Revankar and P. Majumdar, *Fuel cells: Principles, design, and analysis*. CRC press, 2014, pp. 1–748.

[48] A. Hermann, T. Chaudhuri and P. Spagnol, "Bipolar plates for PEM fuel cells: A review," *Int. J. Hydrogen Energy*, vol. 30, no. 12, pp. 1297–1302, 2005.

[49] C. Nah, S. G. Kim, G. S. Shibulal, Y. H. Yoo, B. Mensah, B. H. Jeong and J. H. Ahn, "Effects of curing systems on the mechanical and chemical ageing resistance properties of gasket compounds based on ethylene-propylene-diene-termonomer rubber in a simulated fuel cell environment," *Int. J. Hydrogen Energy*, vol. 40, no. 33, pp. 10627–10635, 2015.

[50] R. E. Rosli, A. B. Sulong, W. R. W. Daud, M.A. Zulkifley, T. Husaini, M. I. Rosli and M. A. Haque, "A review of high-temperature proton exchange membrane fuel cell (HT-PEMFC) system," *Int. J. Hydrogen Energy*, vol. 42, no. 14, pp. 9293–9314, 2017.

[51] R. Islam and B. Shabani, "Prediction of electrical conductivity of TiO_2 water and ethylene glycol-based nanofluids for cooling application in low temperature PEM fuel cells," in *Energy Procedia*, vol. 160, pp. 550-557, 2019.

[52] P. Purnima, and S. Jayanti, "A high-efficiency, auto-thermal system for on-board hydrogen production for low temperature PEM fuel cells using dual reforming of ethanol," *Int. J. Hydrogen Energy*, vol. 41, no. 31, pp. 13800-13810, 2016.

[53] M. V. Lototskyy, M. W. Davids, I. Tolj, Y. V. Klochko, B. S. Sekhar, S. Chidziva and B. G. Pollet, "Metal hydride systems for hydrogen storage and supply for stationary and automotive low temperature PEM fuel cell power modules," in *International Journal of Hydrogen Energy*, vol. 40, no. 35, pp. 11491-11497, 2015.

[54] Y. Shao, G. Yin, Z. Wang, and Y. Gao, "Proton exchange membrane fuel cell from low temperature to high temperature: Material challenges," *J. Power Sources*, vol. 167, no. 2, pp. 235–242, 2007.

[55] J. Wu, X. Z. Yuan, J. J. Martin, H. Wang, J. Zhang, J. Shen and W. Merida, "A review of PEM fuel cell durability: Degradation mechanisms and mitigation strategies," *Journal of Power Sources*, vol. 184, no. 1. pp. 104–119, 2008.

[56] Y. Nalbant, C. O. Colpan and Y. Devrim, "Energy and exergy performance assessments of a high temperature-proton exchange membrane fuel cell based integrated cogeneration system," *Int. J. Hydrogen Energy*, vol. 45, no. 5, pp. 3584–3594, 2020.

[57] K. D. Kreuer, "On the complexity of proton conduction phenomena," *Solid State Ionics*, vol. 136, pp. 149–160, 2000.

[58] A. Bazylak, "Liquid water visualization in PEM fuel cells: A review," *International Journal of Hydrogen Energy*., vol. 34, no. 9, pp. 3845-3857, 2009.

[59] J. Zhang, Z. Xie, J. Zhang, Y. Tang, C. Song, T. Navessin and S. Holdcroft, "High temperature PEM fuel cells, " *Journal of Power Sources*, vol. 160, no. 2, pp. 872–891, 2006.

[60] J. H. Wee, "Applications of proton exchange membrane fuel cell systems," *Renewable and Sustainable Energy Reviews*, vol. 11, no. 8, pp. 1720-1738, 2007.

[61] S. J. Andreasen, J. R. Vang and S. K. Kær, "High temperature PEM fuel cell performance characterisation with CO and CO_2 using electrochemical impedance spectroscopy," *Int. J. Hydrogen Energy*., vol. 36, no. 16, pp. 9815-9830, 2011.

[62] R. Devanathan, "Recent developments in proton exchange membranes for fuel cells," *Energy Environ. Sci.*, vol. 1, no. 1, pp. 101-119, 2008.

[63] S. Pasupathi, J. C. C. Gomez, H. Su, H. Reddy, P. Bujlo and C. Sita, *Recent Advances in High-Temperature PEM Fuel Cells*. Academic Press, pp. 1-86, 2016.

[64] A. B. Bozkurt, G. Özer and A.Yurtcan, "Development of Effective Catalysts for Hydrogen Generation from Sodium Borohydride: Ru, Pt, Pd Nanoparticles Supported on Co_3O_4," *Energy*, vol. 180, pp. 702–713, 2019.

[65] J. H. Kim, K. T. Kim, Y. M. Kang, H. S. Kim, M. S. Song, Y. J. Lee, and J. Y. Lee, "Study on degradation of filamentary Ni catalyst on hydrolysis of sodium borohydride," *J. Alloys Compd.*, vol. 379, no. 1–2, pp. 222–227, 2004.

[66] W. Ye, H. Zhang, D. Xu, L. Ma and B. Yi, "Hydrogen generation utilizing alkaline sodium borohydride solution and supported cobalt catalyst," *J. Power Sources*, vol. 164, no. 2, pp. 544–548, 2007.

[67] H. C. Brown and C. A. Brown, "New, Highly Active Metal Catalysts for the Hydrolysis of Borohydride," *J. Am. Chem. Soc.*, vol. 84, no. 8, pp. 1493–1494, 1962.

[68] S. Akbayrak and S. Özkar, "Ruthenium(0) nanoparticles supported on multiwalled carbon nanotube as highly active catalyst for hydrogen generation from ammonia-borane," *ACS Appl. Mater. Interfaces*, vol. 4, no. 11, pp. 6302–6310, 2012.

[69] A. Wang, X. Y. Liu, C. Y. Mou and T. Zhang, "Understanding the synergistic effects of gold bimetallic catalysts," *Journal of catalysis*, vol. 308, pp. 285-271, 2013.

[70] P. Krishnan, T. H. Yang, W. Y. Lee and C. S. Kim, "PtRu-$LiCoO_2$ - An efficient catalyst for hydrogen generation from sodium borohydride solutions," *J. Power Sources*, vol. 143, no. 1–2, pp. 17–23, 2005.

[71] L. Ma, S. Sui and Y. Zhai, "Preparation and characterization of Ir/TiC catalyst for oxygen evolution," *J. Power Sources*, vol. 177, no. 2, pp. 470–477, 2008.

[72] A. Heydari and H. Gharibi, "Fabrication of electrocatalyst based on nitrogen doped graphene as highly efficient and durable support for using in polymer electrolyte fuel cell," *J. Power Sources*, vol. 325, pp. 808–815, 2016.

[73] A. A. Mikhaylova, E. K. Tusseeva, N. A. Mayorova, A. Y. Rychagov, Y. M. Volfkovich, A. V. Krestinin and O. A. Khazova, "Single-walled carbon nanotubes and their composites with polyaniline. Structure, catalytic and capacitive properties as applied to fuel cells and supercapacitors," in *Electrochimica Acta*, vol. 56, no. 10, pp. 3656–3665, 2011.

[74] A. Morozan, B. Jousselme and S. Palacin, "Low-platinum and platinum-free catalysts for the oxygen reduction reaction at fuel cell cathodes," *Energy and Environmental Science*, vol. 4, no. 4. pp. 1238–1254, 2011.

[75] W. Zhang, P. Sherrell, A. I. Minett, J. M. Razal and J. Chen, "Carbon nanotube architectures as catalyst supports for proton exchange membrane fuel cells," *Energy Environ. Sci.*, vol. 3, no. 9, pp. 1286–1293, 2010.

[76] Y. Shao, G. Yin and Y. Gao, “Understanding and approaches for the durability issues of Pt-based catalysts for PEM fuel cell,” *Journal of Power Sources*, vol. 171, no. 2. pp. 558–566, 2007.

[77] D. R. Kauffman and A. Star, “Graphene versus carbon nanotubes for chemical sensor and fuel cell applications,” *Analyst*, vol. 135, no. 11, pp. 2790–2797, 2010.

[78] Z. Liu, L. M. Gan, L. Hong, W. Chen and J. Y. Lee, “Carbon-supported Pt nanoparticles as catalysts for proton exchange membrane fuel cells,” *J. Power Sources*, vol. 139, no. 1–2, pp. 73–78, 2005.

[79] K. M. Liew, M. F. Kai and L. W. Zhang, “Carbon nanotube reinforced cementitious composites: An overview,” *Compos. Part A Appl. Sci. Manuf.*, vol. 91, pp. 301–323, 2016.

[80] S. J. Chen, F. G. Collins, A. J. N. Macleod, Z. Pan, W. H. Duan and C. M. Wang, “Carbon nanotube-cement composites: A retrospect,” *IES J. Part A Civ. Struct. Eng.*, vol. 4, no. 4, pp. 254–265, 2011.

[81] B. Ribeiro, E. C. Botelho, M. L. Costa and C. F. Bandeira, “Carbon nanotube buckypaper reinforced polymer composites: A review,” *Polimeros*, vol. 27, no. 3, pp. 247–255, 2017.

[82] B. P. Grady, *Carbon Nanotube-Polymer Composites: Manufacture, Properties, and Applications*. John Wiley & Sons, 2011, pp. 1-352.

[83] P. A. Martins-Júnior, C. E. Alcântara, R. R. Resende and A. J. Ferreira, “Carbon nanotubes: Directions and perspectives in oral regenerative medicine,” *J. Dent. Res.*, vol. 92, no. 7, pp. 575–583, 2013.

[84] N. Shaari and S. K. Kamarudin, “Graphene in electrocatalyst and proton conductiong membrane in fuel cell applications: An overview,” *Renew. Sustain. Energy Rev.*, 2017, vol. 69, pp. 862–870, 2016.

[85] N. G. Sahoo, Y. Pan, L. Li and S. H. Chan, “Graphene-based materials for energy conversion,” *Adv. Mater.*, vol. 24, no. 30, pp. 4203–4210, 2012.

[86] E. Quesnel, F. Roux, F. Emieux, P. Faucherand, E. Kymakis, G. Volonakis and V. Pellegrini, “Graphene-based technologies for energy applications, challenges and perspectives,” *2D Mater.*, vol. 2, no. 3, pp. 030204, 2015.

[87] T. Maiyalagan, X. Wang and A. Manthiram, “Highly active Pd and Pd-Au nanoparticles supported on functionalized graphene nanoplatelets for enhanced formic acid oxidation,” *RSC Adv.*, vol. 4, no. 8, pp. 4028–4033, 2014.

[88] D. Chen, L. Tang and J. Li, “Graphene-based materials in electrochemistry,” *Chem. Soc. Rev.*, vol. 39, no. 8, pp. 3157-3180, 2010.

[89] Y. W. Lee, M. Kim, Y. Kim, S. W. Kang, J. H. Lee and S. W. Han, “Synthesis

and electrocatalytic activity of Au-Pd alloy nanodendrites for ethanol oxidation," *J. Phys. Chem. C*, vol. 114, no. 17, pp. 7689–7693, 2010.

[90] M. Rashad, F. Pan, A. Tang, M. Asif and M. Aamir, "Synergetic effect of graphene nanoplatelets (GNPs) and multi-walled carbon nanotube (MW-CNTs) on mechanical properties of pure magnesium," *J. Alloys Compd.*, vol. 603, pp. 111–118, 2014.

[91] H. Zhang, G. Zhang, M. Tang, L. Zhou, J. Li, X. Fan and J. Qin, "Synergistic effect of carbon nanotube and graphene nanoplates on the mechanical, electrical and electromagnetic interference shielding properties of polymer composites and polymer composite foams," *Chem. Eng. J.*, vol. 353, pp. 381–393, 2018.

[92] B. Zhao, S. Wang, C. Zhao, R. Li, S. M. Hamidinejad, Y. Kazemi and C. B. Park, "Synergism between carbon materials and Ni chains in flexible poly(vinylidene fluoride) composite films with high heat dissipation to improve electromagnetic shielding properties," *Carbon N. Y.*, vol. 127, pp. 469–478, 2018.

[93] B. Yazdani, H. Porwal, Y. Xia, H. Yan, M. J. Reece and Y. Zhu, "Role of synthesis method on microstructure and mechanical properties of graphene/carbon nanotube toughened Al_2O_3 nanocomposites," *Ceram. Int.*, vol. 41, no. 8, pp. 9813–9822, 2015.

[94] O. S. Asiq Rahman, M. Sribalaji, B. Mukherjee, T. Laha and A. K. Keshri, "Synergistic effect of hybrid carbon nanotube and graphene nanoplatelets reinforcement on processing, microstructure, interfacial stress and mechanical properties of Al_2O_3 nanocomposites," *Ceram. Int.*, vol. 44, no. 2, pp. 2109–2122, 2018.

[95] K. Qian, J. Fang, W. Huang, B. He, Z. Jiang, Y. Ma and S. Wei, "Understanding the deposition–precipitation process for the preparation of supported Au catalysts," *Journal of Molecular Catalysis A: Chemical*, vol. 320, no. 1–2, , pp. 97–105, 2010.

[96] R. L. Augustine, *Heterogeneous catalysis for the synthetic chemist*. CRC Press, 1995, pp. 1–672.

[97] B. Delmon, J. Haber and J. H. Block, "Manual of methods and procedures for catalyst characterization (Technical Report)," *Pure Appl. Chem.*, vol. 67, no. 8–9, pp. 1257–1306, 1995.

[98] J. P. Brunelle, "Preparation of catalysts by metallic complex adsorption on mineral oxides," *Pure Appl. Chem.*, vol. 50, no. 9–10, pp. 1211–1229, 1978.

[99] J. Venter, M. Kaminsky, G. L. Geoffroy and M. A. Vannice, "Carbon-supported FeMn and KFeMn clusters for the synthesis of C_2C_4 olefins from CO and H_2. I. Chemisorption and catalytic behavior," *J. Catal.*, vol. 103, pp. 450-465, 1987.

[100] C. O. Bennett and M. Che, "Some geometric aspects of structure sensitivity," *J.*

Catal., vol. 120, no. , pp. 293-302, 1989.

[101] J. H. Park, Y. Sohn, D. H. Jung, P. Kim and J. B. Joo, "Pt deposited Pt-Pd/C electrocatalysts with the enhanced oxygen reduction activity," *J. Ind. Eng. Chem.*, vol. 36, pp. 109–115, 2016.

[102] A. A. Fedotov, S. A. Grigoriev, P. Millet and V. N. Fateev, "Plasma-assisted Pt and Pt-Pd nano-particles deposition on carbon carriers for application in PEM electrochemical cells," *Int. J. Hydrogen Energy*, vol. 38, no. 20, pp. 8568–8574, 2013.

[103] H. R. Cho and J. R. Regalbuto, "The rational synthesis of Pt-Pd bimetallic catalysts by electrostatic adsorption," *Catal. Today*, vol. 246, pp. 143–153, 2015.

[104] M. Blosi, S. Ortelli, A. L. Costa, M. Dondi, A. Lolli, S. Andreoli and S. Albonetti, "Bimetallic nanoparticles as efficient catalysts: Facile and green microwave synthesis," *Materials (Basel).*, vol. 9, no. 7, pp. 1–25, 2016.

[105] K. J. Sreeram, M. Nidhin and B. U. Nair, "Microwave assisted template synthesis of silver nanoparticles," *Bulletin of Materials Science*, vol. 31, no. 7, pp. 937–942, 2008.

[106] H. El-Deeb and M. Bron, "Microwave-assisted polyol synthesis of PtCu/carbon nanotube catalysts for electrocatalytic oxygen reduction," *J. Power Sources*, vol. 275, pp. 893–900, 2015.

[107] Y. T. Li, X. L. Zhang, Z. K. Peng, P. Liu and X. C. Zheng, "Highly efficient hydrolysis of ammonia borane using ultrafine bimetallic RuPd nanoalloys encapsulated in porous g-C3N4," *Fuel*, vol. 277, pp. 118243–118243, 2020.

[108] M. Rakap, "Hydrolysis of Sodium Borohydride and Ammonia Borane for Hydrogen Generation Using Highly Efficient Poly(N-Vinyl-2-Pyrrolidone)-Stabilized Ru-Pd Nanoparticles as Catalysts," *Int. J. Green Energy*, vol. 12, no. 12, pp. 1288–1300, 2015.

[109] M. Tang, S. Mao, M. Li, Z. Wei, F. Xu, H. Li and Y. Wang, "RuPd alloy nanoparticles supported on N-doped carbon as an efficient and stable catalyst for benzoic acid hydrogenation," *ACS Catal.*, vol. 5, no. 5, pp. 3100–3107, 2015.

[110] X. Xiong, W. Chen, W. Wang, J. Li, and S. Chen, "Pt-Pd nanodendrites as oxygen reduction catalyst in polymer-electrolyte-membrane fuel cell," *Int. J. Hydrogen Energy*, vol. 42, no. 40, pp. 25234–25243, 2017.

[111] K. Fu, Y. Wang, L. Mao, X. Yang, J. Jin, S. Yang and G. Li, "Facile morphology controllable synthesis of PtPd nanorods on graphene-multiwalled carbon nanotube hybrid support as efficient electrocatalysts for oxygen reduction reaction," *Mater. Res. Bull.*, vol. 108, pp. 187–194, 2018.

[112] A. Bharti and G. Cheruvally, "Surfactant assisted synthesis of Pt-Pd/MWCNT and evaluation as cathode catalyst for proton exchange membrane fuel cell," *Int.*

J. Hydrogen Energy, vol. 43, no. 31, pp. 14729–14741, 2018.

[113] J. R. Zapata-Fernández, Y. Gochi-Ponce, M. I. Salazar-Gastélum, E. A. Reynoso-Soto, F. Paraguay-Delgado, S. W. Lin and R. M. Félix-Navarro, "Ultrasonic-assisted galvanic displacement synthesis of Pt–Pd/MWCNT for enhanced oxygen reduction reaction: Effect of Pt concentration," *Int. J. Hydrogen Energy*, vol. 42, no. 15, pp. 9806–9815, 2017.

[114] J. Chai, F. Li, Y. Hu, Q. Zhang, D. Han and L. Niu, "Hollow flower-like AuPd alloy nanoparticles: One step synthesis, self-assembly on ionic liquid-functionalized graphene, and electrooxidation of formic acid," *J. Mater. Chem.*, vol. 21, no. 44, pp. 17922–17929, 2011.

[115] M. Liu, Y. Lu and W. Chen, "PdAg nanorings supported on graphene nanosheets: Highly methanol-tolerant cathode electrocatalyst for alkaline fuel cells," *Adv. Funct. Mater.*, vol. 23, no. 10, pp. 1289–1296, 2013.

[116] R. Awasthi and R. N. Singh, "Optimization of the Pd-Sn-GNS nanocomposite for enhanced electrooxidation of methanol," *Int. J. Hydrogen Energy*, vol. 37, no. 3, pp. 2103–2110, 2012.

[117] Q. Zheng, X. Cheng, T. C. Jao, F. B. Weng, A. Su and Y. C. Chiang, "Microwave assisted synthesis of high performance Ru85Se 15/MWCNTs cathode catalysts for PEM fuel cell applications," *Int. J. Hydrogen Energy*, vol. 36, no. 22, pp. 14599–14607, 2011.

[118] C. Huff, J. M. Long, A. Heyman and T. M. Abdel-Fattah, "Palladium Nanoparticle Multiwalled Carbon Nanotube Composite as Catalyst for Hydrogen Production by the Hydrolysis of Sodium Borohydride," *ACS Appl. Energy Mater.*, vol. 1, no. 9, pp. 4635–4640, 2018.

[119] R. Kiyani, S. Rowshanzamir, and M. J. Parnian, "Multi-walled carbon nanotubes supported palladium nanoparticles: Synthesis, characterization and catalytic activity towards methanol electro oxidation in alkaline media," *Iranian Journal of Hydrogen & Fuel Cell*, vol. 2, no. 2, pp. 67–74, 2015.

[120] M. H. Seo, S. M. Choi, H. J. Kim and W. B. Kim, "The graphene-supported Pd and Pt catalysts for highly active oxygen reduction reaction in an alkaline condition," *Electrochem. commun.*, vol. 13, no. 2, pp. 182–185, 2011.

[121] Y. Liang, H. Bin Dai, L. P. Ma, P. Wang, and H. M. Cheng, "Hydrogen generation from sodium borohydride solution using a ruthenium supported on graphite catalyst," *Int. J. Hydrogen Energy*, vol. 35, no. 7, pp. 3023–3028, 2010.

[122] J. Shen, B. Yan, M. Shi, H. Ma, N. Li and M. Ye, "Fast and facile preparation of reduced graphene oxide supported Pt-Co electrocatalyst for methanol oxidation," *Mater. Res. Bull.*, vol. 47, no. 6, pp. 1486–1493, 2012.

[123] H. Pawar, and A. Lali, "DICAT-2: Solid Acid Catalyst with a Protagonist Backbone for Microwave Assisted Synthesis of 5-Hydroxymethylfurfural in

Isopropyl Alcohol," *Ind. Eng. Chem. Res.*, vol. 57, no. 43, pp. 14428–14439, 2018.

[124] S. H. Hsieh, M. C. Hsu, W. L. Liu and W. J. Chen, "Study of Pt catalyst on graphene and its application to fuel cell," *Appl. Surf. Sci.*, vol. 277, pp. 223–230, 2013.

[125] Y. Y. Chu, Z. B. Wang, D. M. Gu and G. P. Yin, "Performance of Pt/C catalysts prepared by microwave-assisted polyol process for methanol electrooxidation," *J. Power Sources*, vol. 195, no. 7, pp. 1799–1804, 2010.

[126] Y. Devrim and E. D. Arıca, "Multi-walled carbon nanotubes decorated by platinum catalyst for high temperature PEM fuel cell," *Int. J. Hydrogen Energy*, vol. 44, no. 34, pp. 18951–18966, 2019.

[127] Y. Devrim and E. D. Arıca, "Investigation of the effect of graphitized carbon nanotube catalyst support for high temperature PEM fuel cells," *Int. J. Hydrogen Energy*, vol. 45, no. 5, pp. 3609–3617, 2020.

[128] T. Athar, "Smart precursors for smart nanoparticles," In *Emerging Nanotechnologies for Manufacturing*, 2nd edition, William Andrew Publishing, 2015, pp. 444-538.

[129] A. Orfanidi, M. K. Daletou and S. G. Neophytides, "Preparation and characterization of Pt on modified multi-wall carbon nanotubes to be used as electrocatalysts for high temperature fuel cell applications," *Appl. Catal. B Environ.*, vol. 106, no. 3–4, pp. 379–389, 2011.

[130] A. Pozio, M. De Francesco, A. Cemmi, F. Cardellini and L. Giorgi, "Comparison of high surface Pt/C catalysts by cyclic voltammetry," *J. Power Sources*, vol. 105, no. 1, pp. 13–19, 2002.

[131] E. S. Şayin, A. Bayrakçeken and I. Eroğlu, "Durability of PEM fuel cell electrocatalysts prepared by microwave irradiation technique," *Int. J. Hydrogen Energy*, vol. 37, no. 21, pp. 16663–16672, 2012.

[132] Y. Devrim, "Fabrication and performance evaluation of hybrid membrane based on a sulfonated polyphenyl sulfone/phosphotungstic acid/silica for proton exchange membrane fuel cell at low humidity conditions," *Electrochim. Acta*, vol. 146, pp. 741–751, 2014.

[133] H. Pang, X. Wang, G. Zhang, H. Chen, G. Lv and S. Yang, "Characterization of diamond-like carbon films by SEM, XRD and Raman spectroscopy," *Appl. Surf. Sci.*, vol. 256, no. 21, pp. 6403-6407, 2010.

[134] Z. Liu, X. Zhang and S. W. Tay, "Nanostructured PdRu/C catalysts for formic acid oxidation," *J. Solid State Electrochem.*, vol. 16, no. 2, pp. 545–550, 2012.

[135] H. Acidereli, K. Cellat, M. H. Calimli and F. Sen, "Palladium/ruthenium supported on graphene oxide (PdRu@GO) as an efficient, stable and rapid

catalyst for hydrogen production from DMAB under room conditions," *Renew. Energy*, vol. 161, pp. 200-206, 2020.

[136] Q. Huang, W. Yu, F. Lu, R. Lu, X. Si, J. Gao and J. Xu, "Fabrication of highly dispersed Ru nanoparticles stabilized in coated carbon shell via one-pot co-synthesis strategy for aqueous hydrogenation of bio-based itaconic acid," *Catal. Today*, vol. 319, pp. 197-205, 2019.

[137] A. L. Patterson, "The scherrer formula for X-ray particle size determination," *Phys. Rev.*, vol. 56, no. 10, pp. 978–982, 1939.

[138] L. Ma, H. He, A. Hsu and R. Chen, "PdRu/C catalysts for ethanol oxidation in anion-exchange membrane direct ethanol fuel cells," *J. Power Sources*, vol. 241, pp. 696–702, 2013.

[139] L. Li and Y. Xing, "Pt-Ru nanoparticles supported on carbon nanotubes as methanol fuel cell catalysts," *J. Phys. Chem. C*, vol. 111, no. 6, pp. 2803–2808, 2007.

[140] K. Hermann, "Appendix E: Parameter Tables of Crystals," in *Crystallography and Surface Structure*, John Wiley & Sons, 2011, pp. 265–266.

[141] J. Zhang, K. Gao, S. Wang, W. Li and Y. Han, "Performance of bimetallic PdRu catalysts supported on gamma alumina for 2-ethylanthraquinone hydrogenation," *RSC Adv.*, vol. 7, no. 11, pp. 6447–6456, 2017.

[142] X. Zhou, J. Qiao, L. Yang and J. Zhang, "A review of graphene-based nanostructural materials for both catalyst supports and metal-free catalysts in PEM fuel cell oxygen reduction reactions," *Adv. Energy Mater.*, vol. 4, no. 8, pp. 1–25, 2014.

[143] M. G. H. Al-Tememy and Y. Devrim, "Development of effective bimetallic catalyst for high-temperature PEM fuel cell to improve CO tolerance," *Int. J. Energy Res.*, vol. 45, no. 2, pp. 3343-3357, 2020.

[144] S. Tymen, A. Undisz, M. Rettenmayr and A. Ignaszak, "Pt-Pd catalytic nanoflowers: Synthesis, characterization, and the activity toward electrochemical oxygen reduction," *J. Mater. Res.*, vol. 30, no. 15, pp. 2327–2339, 2015.

[145] R. Pattabiraman, "Electrochemical investigations on carbon supported palladium catalysts," *Appl. Catal. A Gen.*, vol. 153, no. 1-2, pp. 9-20, 1997.

[146] I. Takahashi and S. S. Kocha, "Examination of the activity and durability of PEMFC catalysts in liquid electrolytes," *J. Power Sources*, vol. 195, no. 19, pp. 6312–6322, 2010.

[147] T. Vidaković, M. Christov and K. Sundmacher, "A method for rough estimation of the catalyst surface area in a fuel cell," *J. Appl. Electrochem.*, vol. 39, no. 2, pp. 213–225, 2009.

[148] A. Uzundurukan and Y. Devrim, “Hydrogen generation from sodium borohydride hydrolysis by multi-walled carbon nanotube supported platinum catalyst: A kinetic study,” *Int. J. Hydrogen Energy*, vol. 44, no. 33, pp. 17586–17594, 2019.

[149] S. Yolcular and S. Karaoglu, “HYDROGEN GENERATION FROM SODIUM BOROHYDRIDE WITH COBALT BORIDE CATALYSTS,” *ALKÜ Fen Bilimleri Dergisi*, vol. 2, no. 2, pp. 84–96, 2020.

[150] R. Retnamma, C. M. Rangel, A. Q. Novais and M. A. Matthews, “Kinetics of Sodium Borohydride Hydrolysis in Aqueous-Basic Solutions,” in *IV Iberian Symposium on Hydrogen, Fuel Cells and Advanced Batteries*, 2013, pp. 26–29.

[151] A. Uzundurukan and Y. Devrim, “Carbon nanotube-graphene hybrid supported platinum as an effective catalyst for hydrogen generation from hydrolysis of ammonia borane,” *Int. J. Hydrogen Energy*, vol. 44, no. 49, pp. 26773–26782, 2019.

[152] Ö. ŞAHİN, E. ONAT, S. HOROZ, and M. S. İZGİ, “Effect of Co-B Catalyst Synthesized in Methanol on the Hydrolysis of Sodium Borohydride,” *J. Inst. Sci. Technol.*, vol. 7, no. 4, pp. 151–160, 2017.

[153] A. Didehban, M. Zabihi and J. R. Shahrouzi, “Experimental studies on the catalytic behavior of alloy and core-shell supported Co-Ni bimetallic nano-catalysts for hydrogen generation by hydrolysis of sodium borohydride,” *Int. J. Hydrogen Energy*, vol. 43, no. 45, pp. 20645–20660, 2018.

[154] R. Retnamma, L. Yu, C. M. Rangel, A. Q. Novais, K. Johnson and M. A. Matthews, “Kinetics of self-hydrolysis of concentrated sodium borohydride solutions at high temperatures,” *Energy Transp. Process. - Core Program. Top. 2011 AIChE Annu. Meet.*, 2011, pp. 341–348.

[155] E. Antolini, “Graphene as a new carbon support for low-temperature fuel cell catalysts,” *Applied Catalysis B: Environmental*, vol. 123–124. pp. 52–68, 2012.

[156] C. Wu, J. Guo, J. Zhang, Y. Zhao, J. Tian, T. T. Isimjan and X. Yang, “Palladium nanoclusters decorated partially decomposed porous ZIF-67 polyhedron with ultrahigh catalytic activity and stability on hydrogen generation,” *Renew. Energy*, vol. 136, pp. 1064–1070, 2019.

[157] Y. Zou, Y. Yin, Y. Gao, C. Xiang, H. Chu, S. Qiu and L. Sun, “Chitosan-mediated Co–Ce–B nanoparticles for catalyzing the hydrolysis of sodium borohydride,” *Int. J. Hydrogen Energy*, vol. 43, no. 10, pp. 4912–4921, 2018.

[158] N. Sahiner, F. Seven and H. Al-Lohedan, “Super-fast hydrogen generation via super porous Q-P(VI)-M cryogel catalyst systems from hydrolysis of $NaBH_4$,” *Int. J. Hydrogen Energy*, vol. 40, no. 13, pp. 4605–4616, 2015.

[159] S. Özkar and M. Zahmakiran, “Hydrogen generation from hydrolysis of sodium borohydride using Ru(0) nanoclusters as catalyst,” *J. Alloys Compd.*, vol. 404–

406, pp. 728–731, 2005.

[160] Ö. Metin and S. Özkar, "Synthesis and characterization of poly(N-vinyl-2-pyrrolidone)-stabilized water-soluble nickel(0) nanoclusters as catalyst for hydrogen generation from the hydrolysis of sodium borohydride," *J. Mol. Catal. A Chem.*, vol. 295, no. 1-2, pp. 39-46, 2008.

[161] S. Akbayrak and S. Özkar, "Inverse relation between the catalytic activity and catalyst concentration for the ruthenium(0) nanoparticles supported on xonotlite nanowire in hydrogen generation from the hydrolysis of sodium borohydride," *J. Mol. Catal. A Chem.*, vol. 424, pp. 254–260, 2016.

[162] Y. Chen, Y. Shi and Y. Wang, "Preparation of hollow poly(vinylidene fluoride) capsules containing nickel catalyst for hydrogen storage and production," *Int. J. Energy Res.*, vol. 39, no. 5, pp. 634-642, 2015.

[163] M. Rakap, "PVP-Protected Pt-Ru Nanoparticles as Highly Efficient Catalysts for Hydrogen Generation from Hydrolysis of Sodium Borohydride," *Gen. Chem.*, vol. 6, no. 4, pp. 200003-200003, 2020.

[164] F. Seven and N. Sahiner, "Superporous P(2-hydroxyethyl methacrylate) cryogel-M (M:Co, Ni, Cu) composites as highly effective catalysts in H_2 generation from hydrolysis of $NaBH_4$ and NH_3BH_3," *Int. J. Hydrogen Energy*, vol. 39, no. 28, pp. 15455–15463, 2014.

[165] Ö. Şahin, A. Bozkurt, M. Yayla, H. Ç. Kazıcı and M. S. İzgi, "As a highly efficient reduced graphene oxide-supported ternary catalysts for the fast hydrogen release from $NaBH_4$," *Graphene Technology*, vol. 5, no. 3–4, pp. 103–111, 2020.

[166] S. Duman and S. Özkar, "Ceria supported manganese(0) nanoparticle catalysts for hydrogen generation from the hydrolysis of sodium borohydride," *Int. J. Hydrogen Energy*, vol. 43, no. 32, pp. 15262–15274, 2018.

[167] L. Cui, X. Sun, Y. Xu, W. Yang and J. Liu, "Cobalt Carbonate Hydroxide Nanowire Array on Ti Mesh: An Efficient and Robust 3D Catalyst for On-Demand Hydrogen Generation from Alkaline $NaBH_4$ Solution," *Chem. - A Eur. J.*, vol. 22, no. 42, pp. 14831–14835, 2016.